January 2018

Ethanol Autoignition Modeling And Validation At Wide Ranges Of Mixture Temperatures, Pressures, And Equivalence Ratios

Antowan Zyada
Wayne State University, an.zyada@gmail.com

ETHANOL AUTOIGNITION MODELING AND VALIDATION AT WIDE RANGES OF MIXTURE TEMPERATURES, PRESSURES, AND EQUIVALENCE RATIOS

by

ANTOWAN ZYADA

DISSERTATION

Submitted to the Graduate School

of Wayne State University,

Detroit, Michigan

in partial fulfillment of the requirements

for the degree of

DOCTOR OF PHILOSOPHY

2019

MAJOR: MECHANICAL ENGINEERING

Approved By:

_____

Advisor Date

_____

_____

_____

DEDICATION

To my wife, Helen,

for your endless love and presence in my life

To my parents, Issa and Nawal,

for everything you have given me to be successful

To my siblings, Evelyn, Ghassan, and Elias,

for being close despite our distances

To my uncle, Ghassan, and his family

for your support and encouragement

In memory of my uncle, Nabil,

for all of his encouragement to seek my PhD degree

ACKNOWLEDGEMENTS

Life is a journey full of challenges and opportunities. We must decide what path to take to reach our goals. Personally, seeking my PhD degree has not been so easy as I have gone through ups and downs to accomplish my goal. However, I always assured myself to beat every challenge and difficulty that crossed my way. Thus, this resulted in accomplishing my goal as I'm now ready to start the next chapter of my life.

Many people have attributed to my success; first, I would like to thank Dr. Omid Samimi-Abianeh for giving me the opportunity to be part of his group. It was a thought-provoking learning process to work and set up the new rapid compression machine in the Combustion Physics Lab (CPL). Further, Dr. Samimi made sure to keep me in touch with the combustion community. Dr. Samimi is a detail-oriented individual who taught me how to be extra precise in writing lab reports. His help was an essential component in my success.

In addition, I would like to acknowledge my professors in the mechanical engineering department. They are such great professors. I am also grateful for the wise advice I received from the department chairman, Dr. Nabil Chalhoub. Thank you Dr. Chalhoub.

My long journey of studying has been impossible without the support of my family and friends. I grew up in a family that focused on education. I cannot thank my parents enough for their love and prayers. My family encouraged me to go abroad and pursue my Ph.D. Thus, I traveled to Germany and conducted some research. However, my ambition did not stop there; with the support and encouragement from my uncle Ghassan and his family, I came to the United States, and this is where my dream came true. I gratefully appreciate their continued love as they always made me feel like a member of their family.

Mid-way through my PhD degree, I met my wife, Helen. She has filled my life all over again with joy, happiness, and love. Helen has made me feel as I am home again. I am very grateful for her support and always being by my side encouraging me to reach my goals.

Although life has some challenges, it also has its own unique taste of beauty that makes us stronger, learn more, and be successful.

Many thanks to all professors, colleagues, family, and friends who I know and met in Syria, Germany and in the U.S. I did it!

TABLE OF CONTENTS

LIST OF TABLES

LIST OF FIGURES

LIST OF SYMBOLS

Φ	Equivalence ratio
T_c	Compressed gas temperature
T_i	Initial gas temperature
P_i	Initial gas pressure
P_c	Compressed gas pressure
γ	Specific heat ratio
V_{eff}	Effective volume
V_c	Volume at the end of compression
γ_c	Specific heat ratio of the mixture at the end of compression
P_{eff}	Effective compressed gas pressure
P_{min}	Minimum pressure after the end of compression and before the autoignition
T_{eff}	Effective gas temperature
T_{ave}	Average gas temperature
τ_{ig}	Ignition delay time
t_{term}	Termination criteria of the reaction time in RMG modeling
X_{term}	Termination criteria of the species conversion fraction in RMG modeling
R_i	Rate of production of species i (flux)
ε	Error tolerance for RMG modeling
R_{char}	Characteristic flux
C_i	Concentration of species i
X_i	Mole fraction of species i

ABBREVIATIONS

CPL	Combustion Physics Laboratory
PM	Particulate matter
EPA	Environmental Protection Agency
SIDI	Gasoline spark-ignited direct-injection engine
GDCI	Gasoline direct-injection compression ignition engine
PFI-SI	Port fuel injected spark-ignited engine
CFD	Computational fluid dynamics
RCM	Rapid compression machine
SI	Spark ignited
VPFR	Variable pressure flow reactor
RMG	Reaction mechanism generator
SOC	Start of compression
EOC	End of compression
GUI	Graphical user interface
RSM	Rapid sampling machine
GC	Gas chromatographer
NTC	Negative temperature coefficient
HHG	Hierarchical-hydrocarbon-group

CHAPTER 1: INTRODUCTION

1.1. Overview

A clean environment with less pollution is a big concern for the world. One of the sources of air pollution is vehicles that emit carbon dioxide (CO_2), nitrogen oxides (NO_x) and particulate matter (PM). To regulate the amount of these emissions, the Environmental Protection Agency (EPA) issues standards for the U.S. auto industry by setting fuel economy targets and emission reduction plans. These raise attentions toward gasoline spark-ignited direct-injection engines (SIDI) and gasoline direct-injection compression ignition engines (GDCI) due to higher fuel economy compared to conventional port fuel injected spark-ignited engines (PFI-SI). To expedite the engine development process, the scientific community is moving toward combustion modeling of these types of engines with high fidelity numerical models. This computational approach requires numerical models that describe the chemical kinetics of the fuel components. However, with the present computational capabilities, it is a challenge to generate predictive kinetic mechanisms for each individual component or hydrocarbon group while maintaining a mechanism size suitable for computational fluid dynamics (CFD) applications. To solve this problem, researchers use a fuel surrogate with a smaller number of components that mimics only physical properties (e.g., evaporation and distillation) [1-2], or only chemical properties (e.g., combustion, ignition delay and laminar flame speed) [3], or both characteristics of gasoline fuel, e.g., Samimi Abianeh et al. 2015 [4]. For oxygenated gasoline fuel, ethanol kinetics should be considered, and this is the focus of this research.

Globally, the United States is the top producing country of ethanol [5], and it is one of the major components of gasoline in the United States. Some properties of ethanol are shown in Table 1.1. Its concentration in fuel varies from 10% (called E10) to 85% (called E85) by volume to satisfy the U.S. Renewable Fuel Standard Program. Ethanol has a high research octane

number of 108.6 as shown in Table 1.1, which adds desirable combustion characteristics to gasoline, e.g., increasing the knock resistance. In addition, ethanol can be produced from renewable sources (corn and other plant materials), which encourages the use of alternative fuels to combat climate change.

Table 1.1. Ethanol fuel vs. gasoline properties [6].

Fuel	Gasoline	Ethanol
Hydrocarbons	C_4 - C_{12}	C_2H_5OH
Density [kg/m^3]	720-780	789
Molecular weight [g/mol]	100-105	46.07
H/C	1.85	3
Stoichiometric air-fuel ratio [-]	~ 14.5	9
Lower heating value [MJ/kg]	~ 44	26.8
boiling temperature [°C]	~ 150	78.37
RON	91-99	108.6
MON	82-89	89.7
Octane rating AKI= (RON+MON)/2	87-96	99.15
Octane sensitivity= (RON-MON)	2-14	18.9

1.2. Background

Ethanol combustion processes have been studied by researchers due to its increasing use in gasoline fuel. There are ethanol combustion measurements using rapid compression machines (RCM) [7-9], shock tubes [7, 10-14], counter-flow twin-flames [15-16], perforated plate burners [17] and constant volume chambers (bomb) [18-22] as summarized in Tables 1.2 and 1.3. In addition to experimental research in these areas, there have been some kinetic model development studies as shown in Table 1.4. Some of the major ethanol studies, mentioned in Tables 1.2 to 1.4, emphasizing kinetic model development are discussed in the following sections to highlight the contribution of these studies.

Table 1.2. Summary of the laminar flame speed measurements for ethanol. CVC, CF, and PPB represent constant volume chamber, counter-flow, and perforated plate burner, respectively.

Author	Ref.	Instrument	pressure [bar]	Temperature [K]	Φ
Gülder	[18]	CVC	1-8	300-500	0.7-1.4
Egolfopoulos et al.	[15]	CF	1	363-453	0.6-1.8
Hara and Tanoue	[19]	CVC	1	325	0.8-1.5
Liao et al.	[20]	CVC	1	358	0.7-1.4
Veloo et al.	[16]	CF	1	343	0.7-1.5
Van Lipzig et al.	[17]	PPB	1	298, 338	0.65-1.55
Beeckmann et al.	[21]	CVC	10	373	0.7-1.3
Hinton et al.	[22]	CVC	2	380, 450	0.7-1.4

1.2.1. Ethanol Laminar Flame Speed Measurement

Laminar flame speed is an important combustion characteristic of a fuel and oxidizer mixture. Laminar flame speed can be used to drive fuel high temperature reactions and is the back bone of turbulent flame speed modeling, which is widely used for the combustion modeling of spark ignited (SI) engines.

Gülder [18] measured the laminar flame speeds of methanol, ethanol, and isooctane using a constant volume chamber at a pressure range of 1 to 8 bar and temperature range of 300 to 500 K. The maximum burning velocity of ethanol occurs at the equivalence ratio of 1.075.

Egolfopoulos et al. [15] used the counter-flow twin-flame technique to measure the laminar flame speeds of ethanol and air mixture at the pressure of 1 bar and initial temperature range of 363 to 453 K. The flame speed results showed a linear increase with temperature at a given equivalence ratio; therefore, the data can be extrapolated to other temperatures.

Hara and Tanoue [19] measured the laminar flame speeds of ethanol, iso-octane and n-heptane at the equivalence ratio range of 0.8 to 1.5, pressure of 1 bar, and temperature of 325 K using a spherical vessel combustion chamber. The measured laminar flame speeds are in

agreement with the previous measured data of [18] and [15] except at the equivalence ratio range of 1.0 to 1.2. The difference could be due to the device and technique used.

Most recently, Veloo et al. [16] measured different alcohol fuels and their connected n-alkane counterpart fuels' laminar flame speeds using a counter-flow configuration at a temperature of 343 K and atmospheric pressure. The flame speeds of ethanol/air and ethane/air are close.

Van Lipzig et al. [17] measured the laminar flame speeds of n-heptane, iso-octane and ethanol in a perforated plate burner using the heat flux method at atmospheric pressure and initial gas temperatures of 298 and 338 K. They validated the measurements against the data of [18] and [15] at a temperature of 298 K and found a small difference due to the measurement method.

Beeckmann et al. [21] studied methanol, ethanol, n-propanol, and n-butanol laminar flame speeds in a spherical combustion vessel at higher pressure than previous works of 10 bar and mixture temperature of 373 K. Laminar flame speed measurements are summarized and shown in Table 1.2.

1.2.2. Ethanol Ignition Delay Time Measurement and Modeling

RCMs and shock tubes are widely used facilities for measuring ignition delay times. Their typical working conditions are shown in Fig. 1.2. Ignition delays up to 100 ms can be measured accurately using RCMs since the core gas inside the RCM combustion chamber up to that range is not affected by the flow vortex [23, 24]. The shock tube ignition delay is usually limited to 3 ms, depending on the length and diameter of the shock tube.

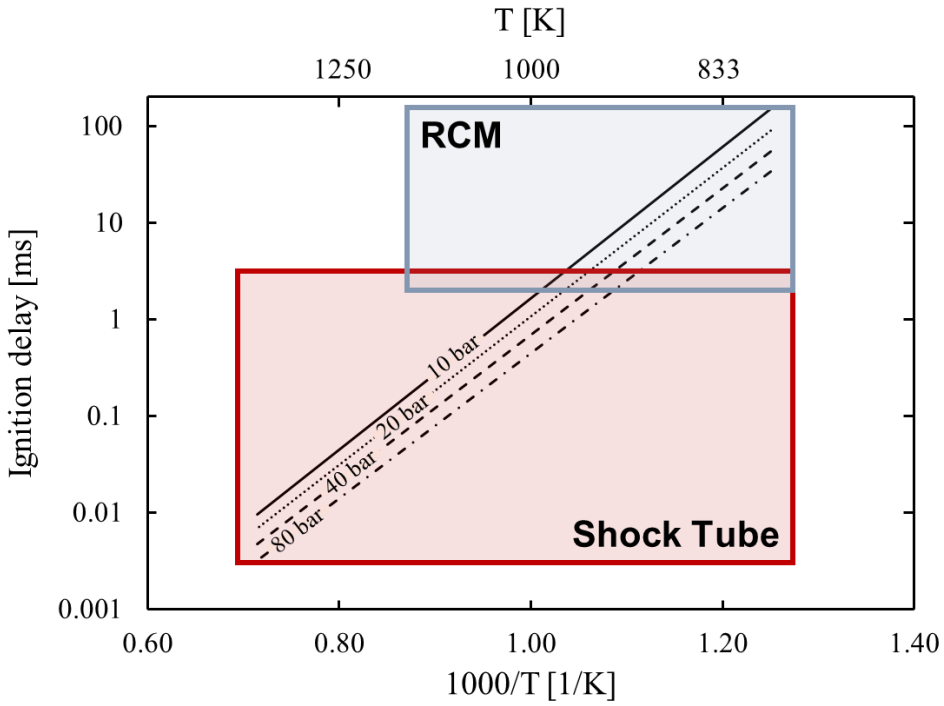

Fig. 1.2. Ethanol ignition delay measurement boundaries using a rapid compression machine (RCM) and shock tube. For the illustration, the modeled kinetic mechanism in this research is included to represent the ignition delay time at four different compressed gas pressures and a wide range of compressed gas temperatures.

Dunphy et al. [25] developed a kinetic model of ethanol with 30 species and 97 reactions. It was assembled from the detailed methanol mechanism model of [26] by adding reactions to account for ethanol combustion. The model is in good agreement with the experimental shock tube data of Dunphy and Simmie [11] at high temperatures and in the pressure range of 2 to 3.4 bar. Further, the ignition delay experiments by [11] showed a decrease of ignition delay by increasing the concentration of the reactant species in ethanol/air mixture.

Marinov [27] developed a kinetic model of ethanol oxidation by assembling the sub-mechanisms of hydrogen, methane, ethylene, ethane, and propane oxidation found in the literature. The model was validated using a variety of experimental measurements at a temperature range of 1000 to 1700 K and a pressure range of 1 to 4.5 atm. The model predictions are in fair agreement with the measured data.

Saxena and Williams [28] extended methane, methanol, ethane, ethylene, acetylene, propane, propene, propyne, allene, hydrogen and carbon monoxide sub-mechanisms to develop an ethanol detailed kinetic model. They validated the mechanism using measured species profiles in a counter-flow burner. The model was further validated against the published laminar flame speed data of [15] and the ignition delay times of [10-11] at near atmospheric pressures.

Li et al. [30] measured stable species profiles using a variable pressure flow reactor (VPFR) at an initial temperature range from 800 to 950 K and a pressure range from 3 to 12 atm. In a different study, Li et al. [31] used the data of [30] to validate their newly developed detailed ethanol kinetic model.

Cancino et al. [12] developed an ethanol detailed kinetic model with 136 species based on the sub-mechanisms of ethanol from [27] and the C_3 reactions from [31]. They validated the model against ignition delay times at a temperature range from 750 to 1200 K and pressures of 10, 30, and 50 bar using a shock tube. The model overpredicts the ignition delay for stoichiometric mixtures (at a pressure of 10 bar and temperatures lower than 900 K) and for lean mixtures (at a pressure of 30 bar).

Lee et al. [7] developed a model for ethanol oxidation based on the kinetic model of [31] by updating the rate coefficients from the literature. They validated the mechanism using the measured ignition delay times using a stoichiometric mixture and at 80 bar by using a shock tube as well as at 37 bar by using an RCM. Further validation was performed using the shock tube ignition delay data from [13] and [14] at pressures from 13 to 75 bar. The model predicts the measured data well at high pressure and low to intermediate temperatures but poorly predicts the measured data at high temperature.

Metcalfe et al. [32] developed a new mechanism for C_1-C_2 hydrocarbons and oxygenated hydrocarbons which covers methane, ethane, ethylene, acetylene, methanol, acetaldehyde, and ethanol. Later, this model was further evaluated and modified [32-38]

Mittal et al. [8] refined the model of [32] and added the hydrogen/oxygen sub-mechanism from [33]. They validated the model against ignition delay data which showed a better prediction for the measured data than other models in the literature.

Barraza-Botet et al. [9] measured ethanol's ignition delay using RCM for stoichiometric mixtures in the pressure range of 3 to 10 bar and temperature range of 880 to 1150 K. They also measured concentrations of some of the species during autoignition.

Table 1.3. Summary of the measured ignition delay times of ethanol. ST stands for shock tube.

Author	Ref.	Instrument	Pressure [bar]	Temperature [K]	Φ	Diluent/O_2
Dunphy and Simmie 1991	[11]	ST	2-5	1080 -1660	0.25-2	12-55
Cancino et al. 2010	[12]	ST	10, 30, 50	750-1200	1	3.88
			30		0.3	
Heufer and Olivier 2010	[13]	ST	13, 19, 40	800 – 1400	1	3.88
Heufer at al. 2011	[14]	ST	75	770 – 1300	1	3.88
Lee et al. 2012	[7]	ST	80	775-1330	1	3.77
		RCM	37	705-910	1	3.77
Mittal et al. 2014	[8]	RCM	10, 25, 50	825-985	0.3	3.77
			10, 25	825-985	0.5	
			10	860-925	1	
Barraza-Botet et al. 2016	[9]	RCM	3-10	880-1150	1	8.27
This research	-	RCM	15, 30	850-1000	0.5-2	12
			20	825-950	1	7.6

Table 1.4. Summary of the kinetic models of ethanol oxidation.

Author	Ref.	Number of Species	Number of Reactions
Dunphy et al. 1991	[25]	30	97
Marinov 1999	[27]	56	351
Saxena and Williams 2007	[28]	57	288
Li et al. 2009	[30]	39	238
Cancino et al. 2010	[12]	136	1136
Lee et al. 2012	[7]	44	279
Metcalf et al. 2013	[32]	124	766
Olm et al. 2016	[39]	49	251
This research	-	107	1795

1.3. Research Objective and Scope

The main objective of the current work is to systematically develop and validate a detailed kinetic model of ethanol using the reaction mechanism generator (RMG) with superior predictive capability with respect to currently available kinetic models in the literature. This was achieved by validating the model against the newly measured ignition delay data of the current work using RCM and available measured data in the literature. The developed detailed mechanism was validated against the measured ignition delay, laminar flame speed and time-resolved species concentration data from various combustion tools such as an RCM, shock tube, constant volume combustion chamber, and flow reactor.

1.4. Structure of the Dissertation

The dissertation includes 5 chapters, and the project abstract is discussed at the end. Chapter 1 above presented an overview and motivation for this work. It also covered a brief literature review of previous research on ethanol combustion characteristics measurements including laminar flame speed and ignition delay measurements, and kinetic model development. The detailed description of the utilized experimental setup for ignition delay measurement is

discussed in Chapter 2. Test methodologies, procedures, and test conditions are briefly described in this chapter. Numerical modeling and kinetic model development are discussed in Chapter 3. The results of kinetic model development and measurements are discussed in Chapter 4, followed by the conclusion and summary of the research project in Chapter 5.

CHAPTER 2: EXPERIMENTAL SETUP

2.1. Rapid Compression Machine

A rapid compression machine is a device that mimics the compression stroke of a single cylinder within an internal combustion engine. It consists mainly of a piston that compresses gases inside the combustion chamber as shown in Fig. 2.1. RCM allows for the exploration of the combustion behavior without creating complexity to the system, such as fuel mixing and evaporation. Therefore, it is a powerful tool for validating chemical kinetics. RCM can be operated at low to intermediate temperatures and various pressures, which are typical conditions of running an internal combustion engine. Typically, RCM has an optical access to allow the entire test volume to be imaged using flame spectrometry and high-speed imaging during autoignition to better understand the excited radicals produced during oxidation and the combustion process. The pressure inside the chamber can be measured, and a typical pressure-time history during the test of reactive mixture is shown in Fig. 2.1. In the figure, the RCM piston and the combustion chamber are presented schematically filled with a mixture of fuel, oxidizer and diluent gases. The rapid compression process begins when the piston is at rest and is as follows:

- Compression event (from A to B) with a duration of 15 to 50 ms: It starts from the predetermined initial conditions of mixture pressure and temperature at point A, called the start of compression (SOC), and ends at point B, called the end of compression (EOC). During the compression period, the initial volume of the mixture decreases sharply, while the temperature and pressure increase.
- Constant volume or post-compression event (B to E): The piston is stopped at the end of compression to provide a constant volume condition for studying the combustion process under a controlled environment.

After the end of compression at point B, the temperature decreases slightly due to the heat transfer from the compressed gas mixture to the chamber wall. This is shown in Fig 2.1 as a pressure drop with respect to time from point B to point C.

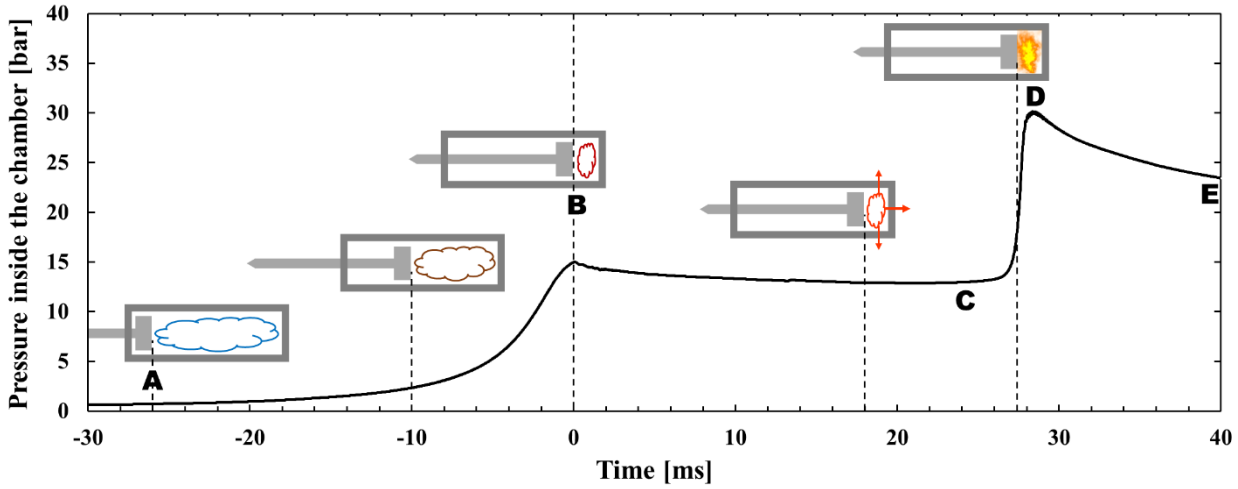

Fig. 2.1. RCM operation process. The time at the end of compression is set to zero as a reference.

The present RCM of the Combustion Physics Laboratory (CPL, cpl.eng.wayne.edu) at Wayne State University is pneumatically driven and hydraulically stopped as shown in Figs. 2.2 and 2.3. Autoignition tests were carried out in the RCM's 2-inch diameter combustion chamber by compressing the fuel/oxidizer/diluent charge while continuously monitoring the pressure inside the chamber by utilizing a pressure sensor. The RCM combustion piston has a crevice to eliminate the production of rolled-up vortices during the compression. The design of the piston crevice is based on the work of Mittal and Sung [23]. As shown in Fig. 2.2, the RCM piston within the combustion chamber is connected via a rod with the hydraulic and pneumatic pistons (pistons-rod set). Various gas temperatures and pressures can be reached at the end of compression by changing the initial gas conditions (i.e. temperature or pressure) or by changing the compression ratio of the RCM.

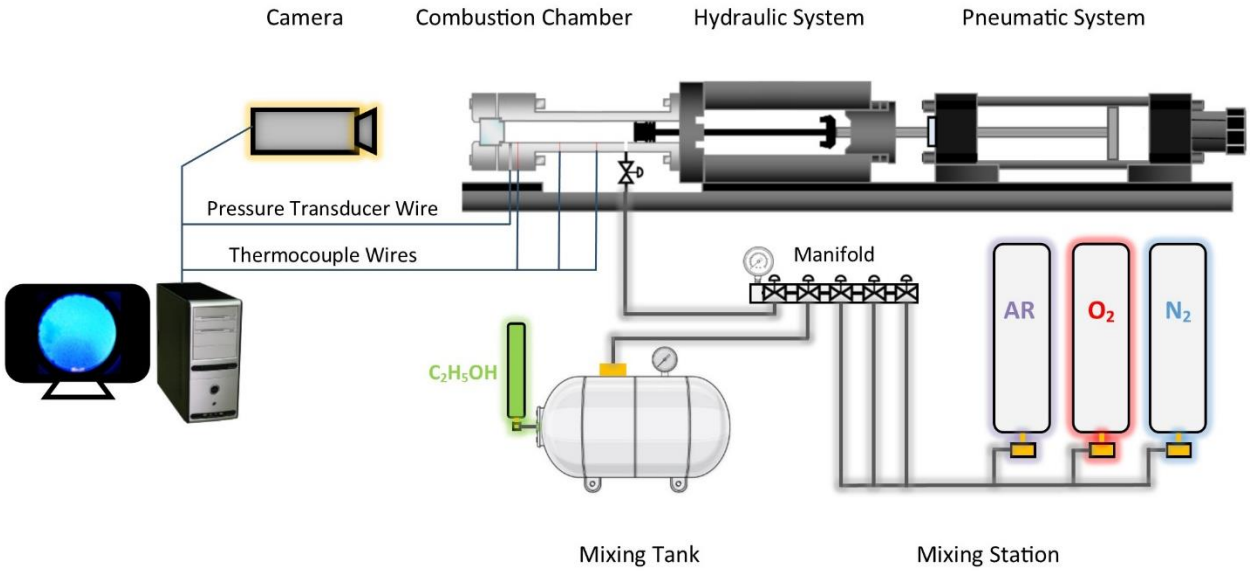

Fig. 2.2. Schematic of RCM and camera setups

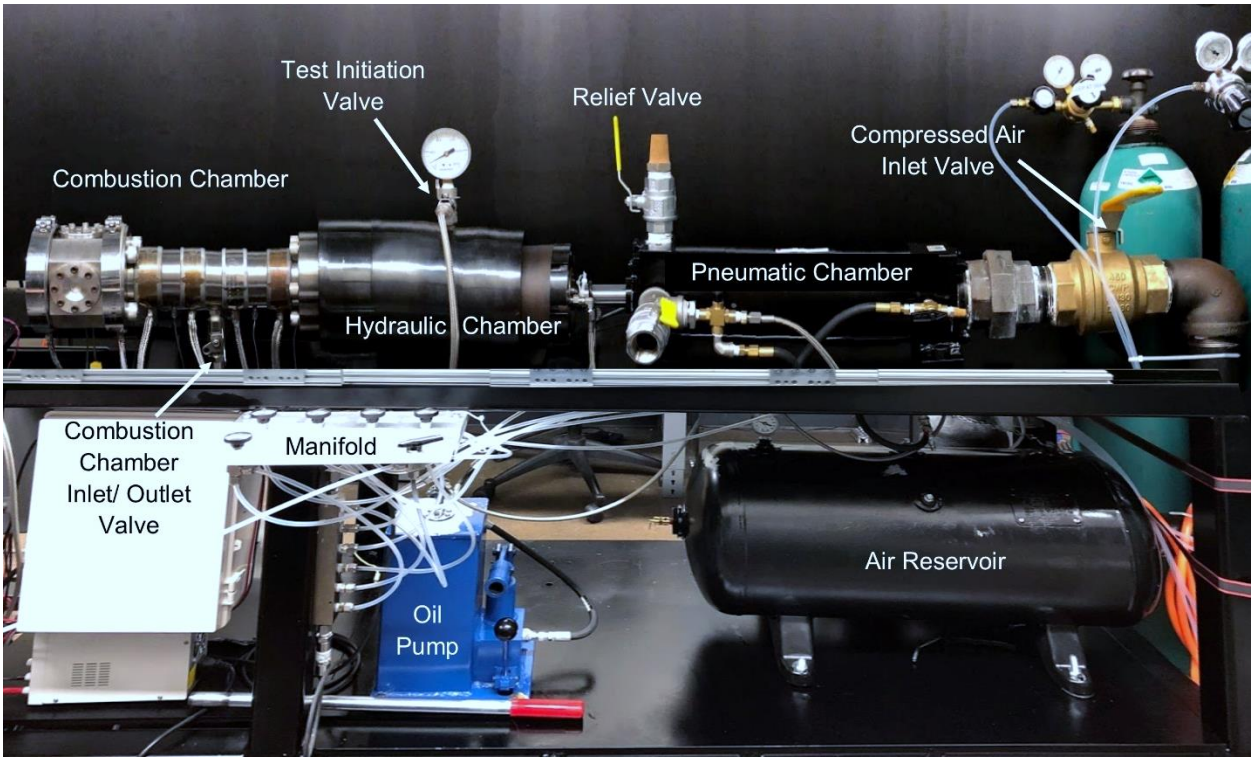

Fig. 2.3. RCM setup

A Phantom VEO 410L high speed camera with a fast 50-mm lens (f/0.95, Navitar) is used to capture combustion images along the axis of the test section. The imaging data can provide qualitative and quantitative indications of the ignition homogeneity and combustion modes. In the following sub sections, various parts of the RCM are briefly described.

2.1.1. Pneumatic System

The pneumatic system consists of a 20-gallon air reservoir connected through a valve to a 5-inch diameter chamber containing the pneumatic piston as shown in Figs. 2.2 and 2.3. The RCM schematic displaying the pneumatic chamber is shown in Fig. 2.4.

The air reservoir pressure can be adjusted between 60 to 150 psi to produce various piston speeds. The pressure inside the reservoir governs the compression time during the test by changing the applied driving pressure on the pneumatic piston. At the end of the chamber there are three relief valves to release the air and avoid any resistance opposing the piston motion.

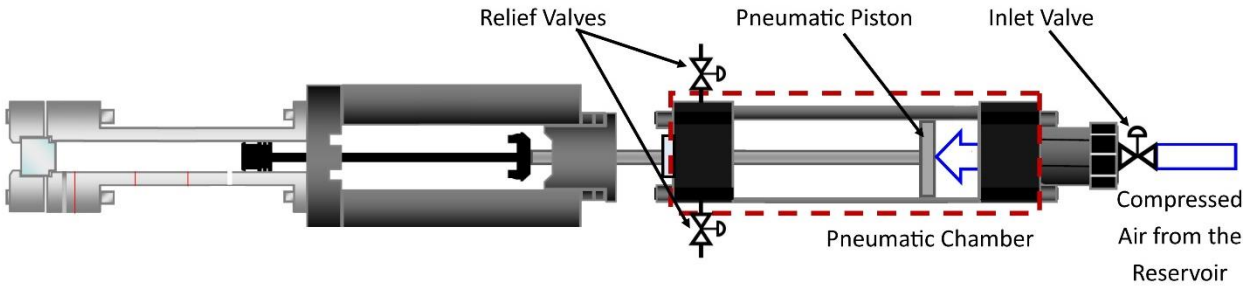

Fig. 2.4. The pneumatic system schematic in RCM (two out of three relief valves are shown)

2.1.2. Hydraulic System

The hydraulic system consists of the oil pump, a chamber and a piston as shown schematically in Fig. 2.5. The hydraulic system has three main applications. First, it resists any movement of the pistons-rod set when the pressured air is applied on the pneumatic piston. For this purpose, the oil pump pressurizes the hydraulic chamber up to 1000 psi. Second, the test is initiated by releasing the compressed oil in front of the hydraulic piston. Third, it stops the hydraulic

piston at the end of the compression period. The length of the hydraulic chamber can be adjusted by changing the number of installed 1-inch thick shims at the back of the hydraulic chamber; as a result, the RCM stroke length can be changed between 8, 9, and 10 inches.

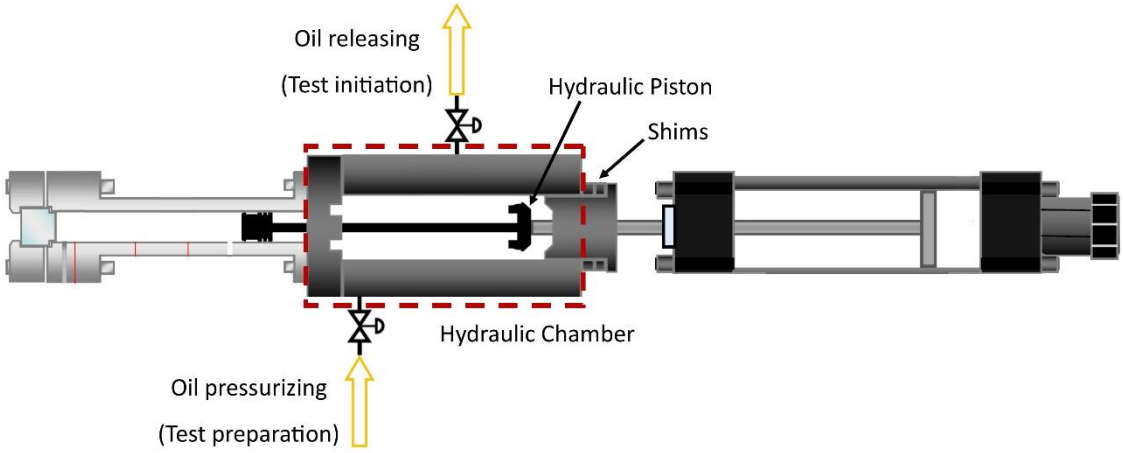

Fig. 2.5. The hydraulic system schematic in RCM

2.1.3. Combustion Chamber

The combustion chamber consists of a 2-inch diameter chamber and the piston. The chamber is made of stainless steel and coated with a thin layer of chrome. The piston is made of aluminum and coated with anodized black powder. Both coatings improve surface hardness and wear resistance. The dimensions of the piston are shown in Fig. 2.6.

The RCM schematic displaying the combustion chamber with the piston placed at the start of compression (SOC) is shown in Fig. 2.7. An inlet/outlet valve is connected to the combustion chamber from one side and to the manifold from the other side. The valve can be opened to either vacuum the gases and residuals from the chamber, or to introduce a fresh mixture. In Fig. 2.7, several heating bands on the RCM chamber are shown.

A	49.80	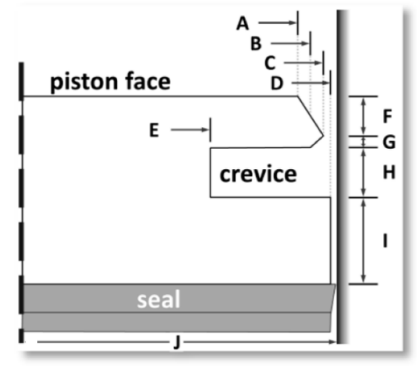		F	4.00
B	50.15			G	n/a
C	50.50			H	20.00
D	50.65			I	3.00
E	47.80			J	50.8

Fig. 2.6. The creviced piston dimensions. All of the values are in mm

A sapphire optical window, approximately 2 inches in diameter with a thickness of 0.75 inches, is seated at the end wall of the RCM. The optical window can withstand pressures up to 320 bar.

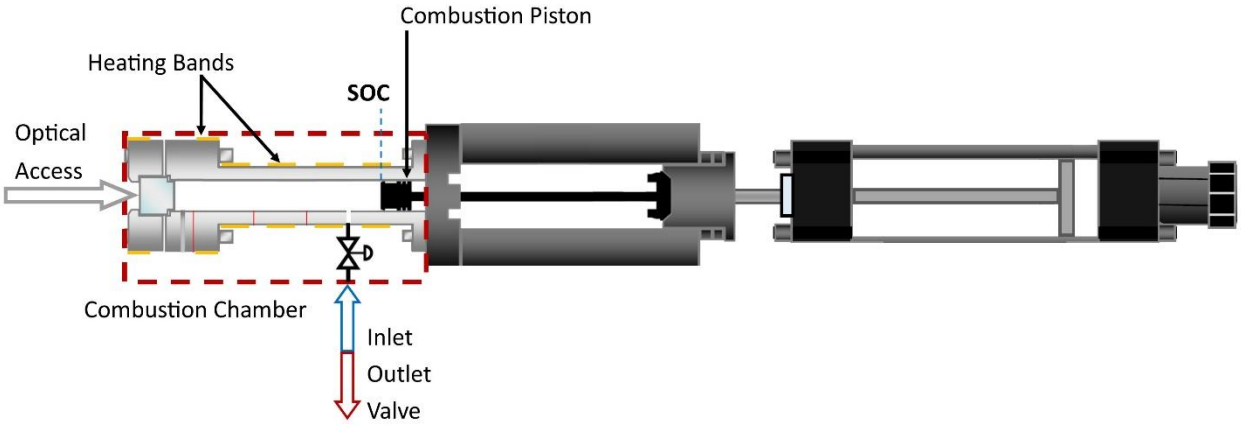

Fig. 2.7. The combustion chamber schematic in RCM. The combustion piston is placed at the end of the chamber (SOC).

Altering the clearance at the end of the compression (top dead center) can be performed in two ways: first, by adding 1/16 inch shims between the hydraulic chamber and the combustion chamber, or extending the piston rod length by 1/4 inch spacers set at the back of the combustion piston. Combined with changing the stroke length, this gives a total change of the compression ratio between 8 and 12.3. The RCM schematic displaying the shims and spacers is shown in Fig. 2.8.

This RCM was built based on the design of [23]; further explanation about the specification can also be found in [40].

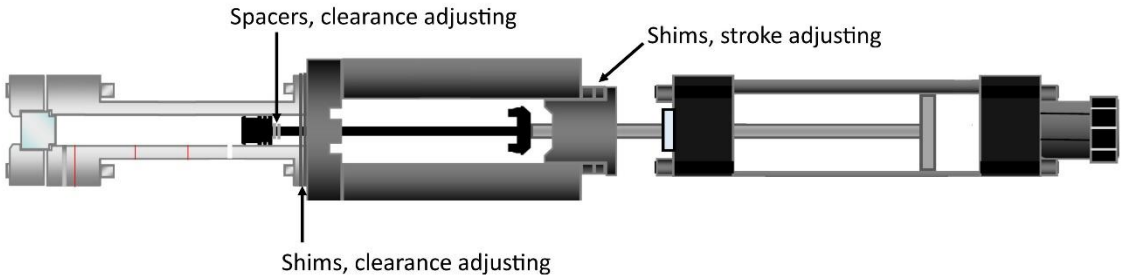

Fig. 2.8. The shim and spacer schematic in the RCM

2.2. Measurement and Control Instrumentations

2.2.1. Temperature and Pressure Measurements

The graphical user interface (GUI) of LabVIEW employed for reading the measurements is shown in Figure 2.9. The initial gas and wall temperatures are measured using several thermocouples (Omega KMQSS-125G-6) embedded within the combustion chamber wall. The initial mixture pressure inside the RCM combustion chamber is measured using a static pressure transducer (Omega PX409). The pressure–time data histories are measured using a piezoelectric transducer (Kistler 6045A) coupled with a charge amplifier (Kistler 5018). The data acquisition system uses NI's LabVIEW program to record the measured pressure as a voltage signal. The piezoelectric pressure sensor is calibrated prior to the experiments and undergoes re-calibration every six months.

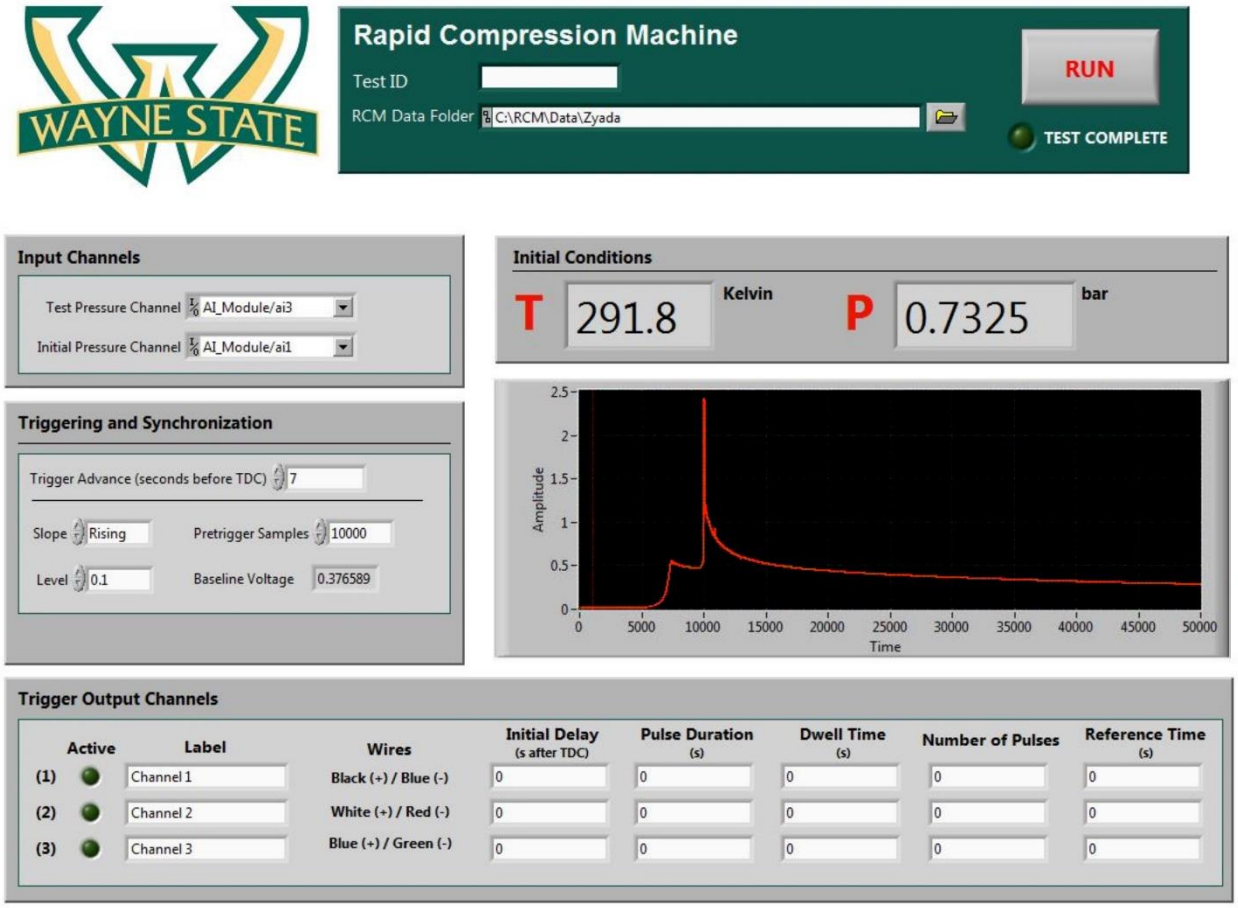

Fig. 2.9. The graphical user interface (GUI) of LabVIEW used to monitor the initial gas temperature and pressure and the time-resolved pressure during the experiment. The pressure-time history signal is shown by the red line.

2.2.2. Initial Temperature Control

Six heating bands are mounted along the RCM chamber wall and used to increase the temperature of the wall and mixture inside the combustion chamber. The electric heating bands are shown in Figs. 2.7 and 2.10. The data acquisition system uses NI's LabVIEW program to control the heating bands and receives feedback from the six thermocouples along the combustion chamber. To control the combustion chamber temperature, the chamber has an insulation jacket as shown in Fig. 2.11. The jacket should be used when the initial temperature is higher than the laboratory temperature. The graphical user interface (GUI) of the heater control

of LabVIEW is shown in Figure 2.10. On the right side of the figure, the schematic arrangements of the thermocouples and the heating bands on the RCM combustion chamber are shown. The set point temperature of the initial mixture and the combustion chamber can be set, and the temperature of each thermocouple can be seen. On the other side of the figure, the PID controller to regulate the temperature of each heating band separately is shown. The temperature of the individual thermocouples can be measured in real time as feedback to the controller and can be monitored on the GUI.

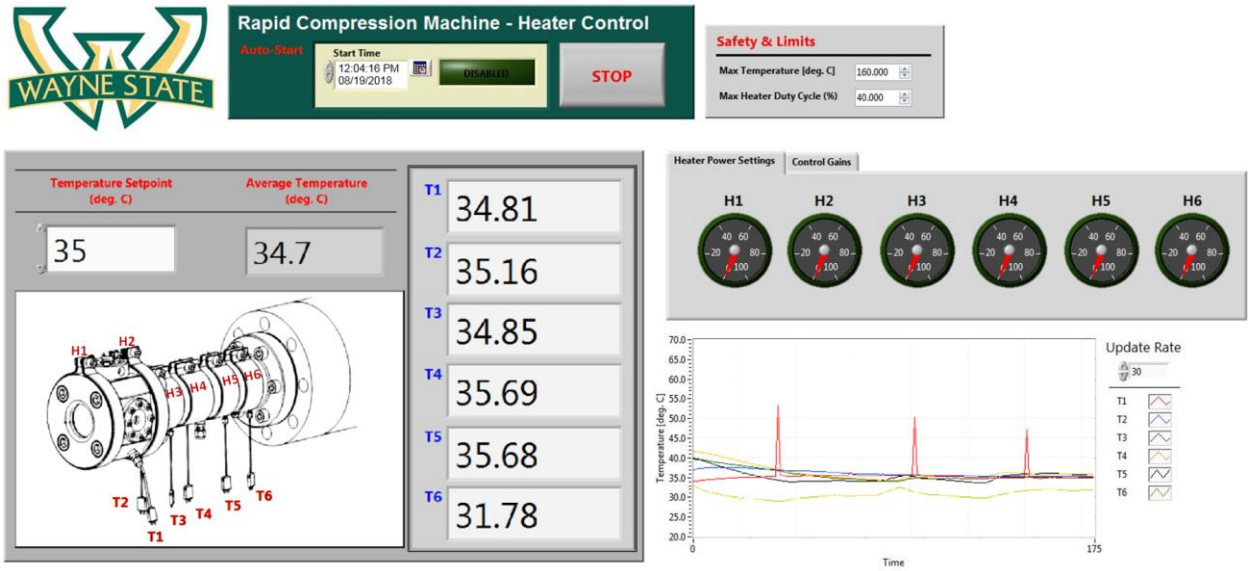

Fig. 2.10. The GUI in Labview that controls the heat of the chamber and the temperature of the mixture. The schematic of the RCM combustion chamber is shown along with the arrangements of thermocouples, denoted by T, and heating bands, denoted by H. The temperature set point is 35 C in this figure. On the right bottom corner of the figure, the graph shows the thermocouple temperature feedback with respect to time. The red peaks are the instant increase in temperature of thermocouple 1 (T1) for three consecutive ignition delay experiments due to combustion.

Fig. 2.11. The insulation jacket on the RCM combustion chamber

2.3. Tests Methodologies

In the following subsections, the mixture preparation and ignition delay measurements are discussed briefly.

2.3.1. Mixture Preparation

The rapid compression machine at CPL was designed initially with an integrated injector on top of the combustion chamber to spray the tested fuel directly inside the chamber. The fuel injector is controlled with an injector driver box and a LabView VI for accuracy and repeatability in injection pulses. Initially, the methodology was to mix the reactants inside the combustion chamber by injecting the liquid fuel into the mixture of the oxidizer and diluent. After two to four minutes, the fuel goes to the vapor phase and creates a homogenous mixture, as suggested by [40]. For this current work, experimental trials were employed to check the homogeneity of the mixture. After injecting the fuel inside the RCM combustion chamber, samples were collected directly from the mixture at various times using a rapid sampling machine (RSM) and were examined using a gas chromatographer (GC). It was found that there was no change in the samples' concentration after approximately 7 hours, which is a long waiting time for performing a single test. Hence, the injector was integrated in a 5-gallon stainless steel vessel through a

custom-made plug. Liquid fuel was injected into the mixture of oxidizer and diluents inside the vessel and left overnight (at least 7 hours) to have a fully homogenous mixture and to perform a series of tests with the same mixture. The mixture in the vessel was enough to perform 15 to 30 tests depending on initial pressure.

The mixtures of ethanol (Decon Laboratories, INC., 200 proof), oxygen (ultra-high purity, 99.994, Airgas), argon (research plus grade with purity of 99.9999, Airgas) and nitrogen (ultra-high purity, 99.999, Airgas) were prepared manometrically in the vessel as follows.

1. The vessel is evacuated using the vacuum pump to reach a pressure of 0.0005 to 0.0010 bar.
2. Half of the diluent (e.g. argon) concentration is introduced into the vessel. Since the diluent has the maximum concentration among the species in the mixture, it is selected as the first component to include the uncertainty of the static pressure sensor at a very low initial pressure of approximately 0.0005 bar in the vessel. In addition, the rest of the diluent is introduced at the end of mixing to push the remaining reactants in the mixing manifold into the vessel. This error of the remaining diluent inside the manifold is approximately 0.4% as calculated by the volume of the manifold divided by the total volume of the diluent.
3. The ethanol fuel is directly injected into the vessel. Approximately 1 ml of ethanol is injected into the chamber at each injection period to avoid wall wetting and provide enough time (approximately 5 minutes) between injection pulses for evaporation.
4. The oxygen is added into the mixture.
5. If available, the second diluent, such as nitrogen gas, is added to the mixture.
6. Finally, the other half of first diluent is added to the mixture.

7. The vessel valve is closed to isolate the mixture and left for at least 7 hours to have a fully homogenous mixture.

In all of the performed tests in this dissertation, argon was used as the first diluent and nitrogen was used as the second diluent if necessary. The specific heat ratio of nitrogen (1.4) is smaller than argon (1.66); thus, the final compressed gas temperature is lower using the mixture with nitrogen content.

Table 2.1. Average mixture compositions

Mixture	Φ	Mixture partial pressure [%]			
		C_2H_5OH	O_2	N_2	AR
1	0.5000	1.2500	7.5000	0.0000	91.2500
2	0.5005	1.2520	7.5046	24.9572	66.2862
3	0.5001	1.2512	7.5053	34.5793	56.6643
4	0.9971	2.5054	7.5379	0.0000	89.9567
5	1.0003	2.5035	7.5080	7.9850	82.0035
6	1.0000	2.4962	7.4885	25.5606	64.4548
7	2.0020	4.9309	7.3892	0.0000	87.6799
8	1.9875	5.0587	7.6358	8.0543	79.2511
9	1.9976	4.7915	7.1960	12.9279	75.0847
10	1.0120	3.7863	11.2250	0.0000	84.9888

The components were mixed in the vessel while their partial pressures were used to accurately determine the species concentration. The partial pressure was measured using the static pressure transducer (Omega PX409). The partial pressure of ethanol in the mixture was kept below its saturated vapor pressure at the laboratory temperature to avoid condensation. Ten different mixtures at varying equivalence ratios were prepared as shown in Table 2.1. Some of them were prepared several times to cover the entire gas temperature range of approximately 850 to 1000 K. The equivalence ratios of these mixtures was approximately 0.5, 1.0, and 2.0

based on the ratio of ethanol to oxygen partial pressure respect to stoichiometric conditions. The total pressure of the vessel is limited to 2.8 bar due to the static pressure sensor limitation. Mixtures 7 to 10 of Table 2.1 were made at lower total pressure to avoid ethanol condensation.

2.3.2. Ignition Delay Test Protocol

The following order was considered for ignition delay measurements.

1. The RCM combustion piston should be moved and placed at the end of the chamber, at the SOC, as shown in Fig. 2.7.
2. The combustion chamber is evacuated to reach the pressure of approximately 0.0002 to 0.0006 bar.
3. The combustion chamber is filled with the premixed mixture to reach the initial pressure.
4. The predetermined initial temperature is achieved by using the heating bands. The system should be left for 30 to 60 minutes to reach a steady and uniform temperature throughout the mixture and chamber walls.
5. The hydraulic chamber is pressurized to 1000 psi using the oil pump. As shown in Fig. 2.5.
6. The air reservoir is filled with compressed air to the desired driving pressure for the pneumatic chamber. For this work, a pressure of approximately 100 psi was used.
7. The pneumatic chamber is pressurized with air coming from the reservoir by opining the inlet valve as shown in Fig. 2.4.
8. Subsequently, the test can be triggered by releasing the oil in front of the hydraulic piston through a controlled valve. The valve is actuated manually as shown in Fig. 2.5. Thus, the piston compresses the reactants rapidly, and thereby, the temperature and pressure increase.

The camera triggering system is shown in Fig. 2.12. The camera trigger is controlled by a digital delay generator (SRS DG645) connected to a laser (39000 RCR44) and a light diode (CP-TIM-201-1D-650) which is fixed on the RCM rod. The light diode produces a pulse when it is in front of the laser. When the rod moves, the pulse drops to zero, and the pulse generator will send a 5-Volt TTL signal to the camera. The room should be dark for proper operation of the diode.

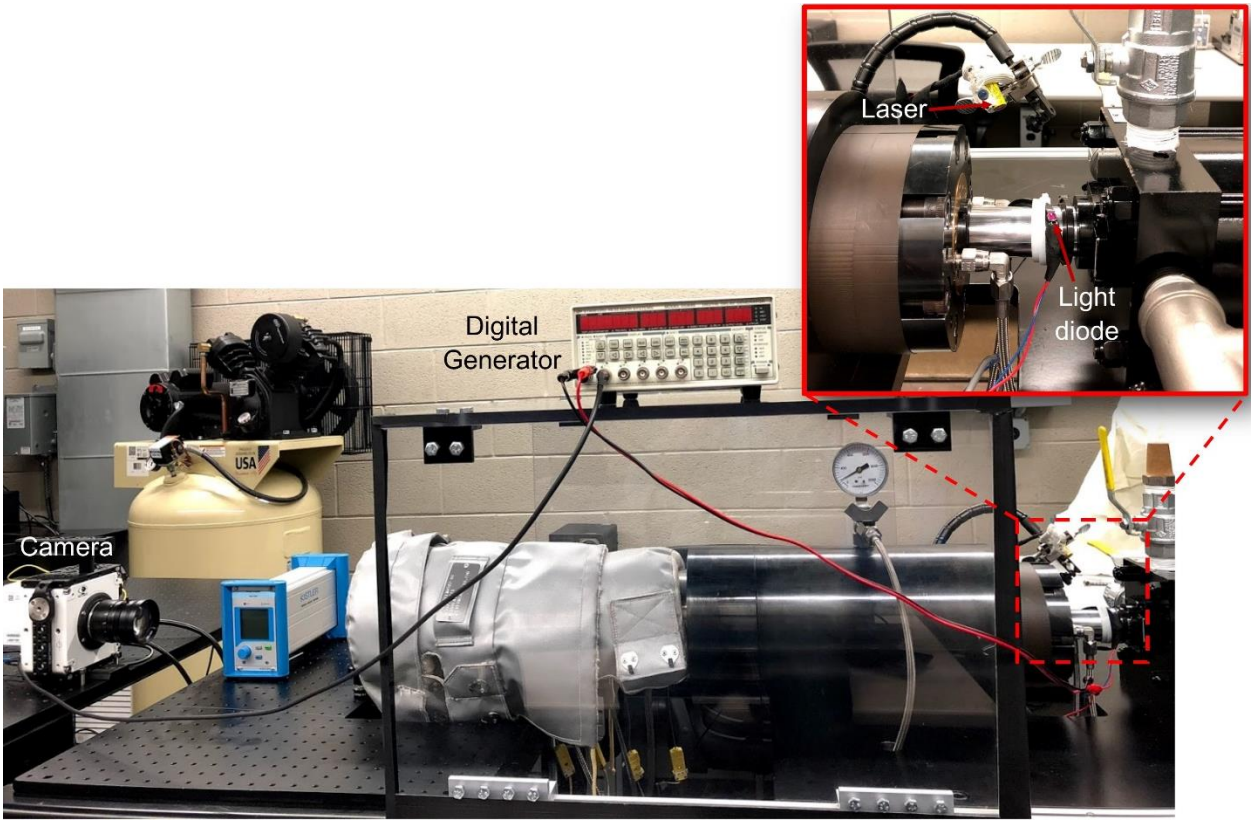

Fig. 2.12. The high speed camera with the triggering system setups

2.4. Experimental Test Conditions

The ethanol fuel tests for ignition delay time measurements were conducted at pressures of 15, 20, and 30 bar, a temperature range of 850 to 1000 K, and equivalence ratios of 0.5, 1.0 and 2.0 using the optically accessible rapid compression machine at CPL. The mixtures were diluted mainly with argon as shown previously in Table 2.1. Nitrogen gas was added to the mixture to reach a lower temperature.

Fig. 2.13 shows different pressures and temperatures at which ethanol ignition delay measurements were investigated in previous studies and in the current research. The experimental tests of the current work were performed at conditions that were not investigated previously using RCMs.

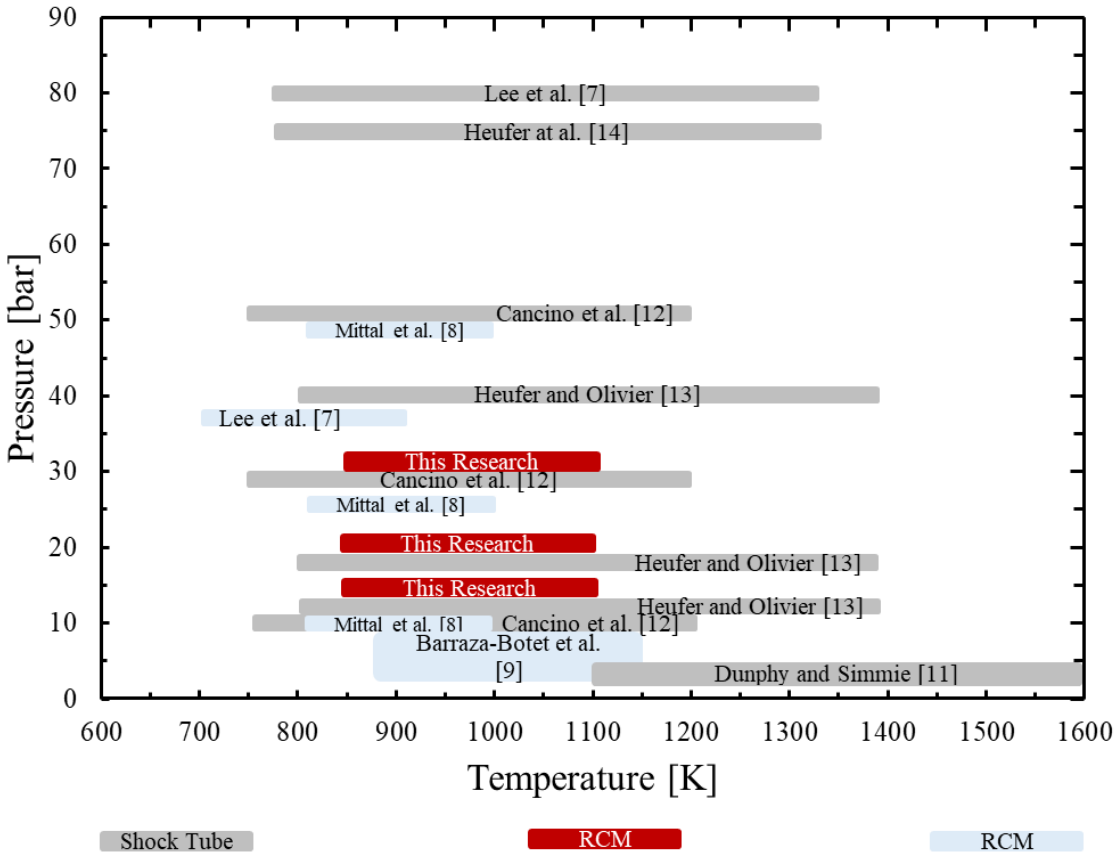

Fig. 2.13. Overview of the test conditions investigated for ethanol ignition delay measurements in this research and previous studies in the literature.

2.5. Data Measurement and Uncertainty Analysis

Initial mixture pressure and temperature inside the RCM were predetermined for each test as mentioned in the previous chapter. Initial gas pressure inside the RCM chamber was measured using the static pressure transducer (Omega PX409) with 0.7% relative uncertainty. The initial gas temperature was measured using thermocouples (Omega KMQSS-125G-6) with 1.5 K absolute uncertainty. To evaluate the compressed mixture at the end of the compression time,

pressure–time data were measured using the piezoelectric pressure transducer (Kistler 6045A) coupled with a charge amplifier (Kistler 5018) with a total of 1.9% relative uncertainty. In addition, the isentropic compression equation was applied, assuming chemistry to be frozen during the compression stroke, to determine the compressed gas temperature, T_c, as follows:

$$ln\left(\frac{P_c}{P_i}\right) = \int_{T_i}^{T_c} \frac{\gamma(T)}{\gamma(T)-1}\frac{dT}{T} \tag{2.1}$$

The compressed gas temperature, T_c, was calculated using the measured initial gas temperature, T_i, initial gas pressure, P_i, compressed gas pressure, P_c, and variable specific heat ratio of the mixture as a function of temperature, $\gamma(T)$. The specific heat ratio has an uncertainty of 0.7% due to the error associated with the static pressure transducer during mixture preparation. These inputs are used to determine the uncertainty in the reported compressed gas temperature by applying the uncertainty propagation approach as described by [41]. The analysis estimates an overall uncertainty from 9 to 13 K for the calculated compressed gas temperature.

The ignition delay time is defined in this research as the time from the end of compression to the local maximum of the derivative of the pressure with respect to time as shown in Fig. 2.14. This definition imposes 5% relative uncertainty in the measured ignition delay time of the current work since the autoignition moment could be defined anywhere between the start of the pressure rise to the peak pressure after the pressure rise due to the combustion.

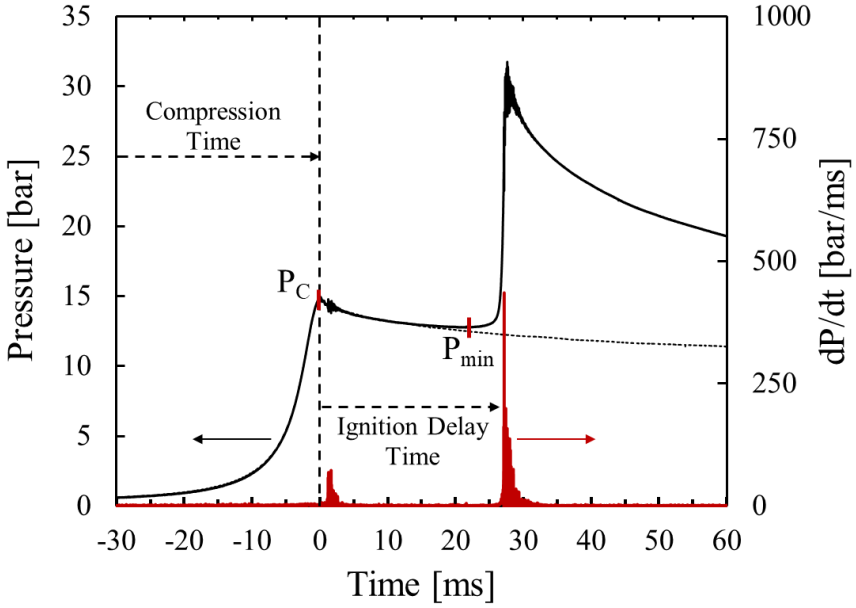

Fig. 2.14. Pressure history of autoignition and inert experiments

CHAPTER 3: NUMERICAL METHODOLOGY

3.1. RCM Modeling Methodology

Different methodologies are available in the literature to include the pressure drop during the autoignition process in the zero-dimensional combustion modeling of RCM. The pressure drop is due to the heat transfer from the hot gas mixture to the chamber wall and is a function of several parameters, such as diluent choice, geometry of the chamber and the compression ratio [42]. There are mainly three methods to account for heat transfer which will be explained briefly in this section. In all of these methods, we assume there is a core gas inside the combustion chamber which follows the isentropic compression process during the compression stroke as discussed by [23]. The difference between them is how the heat transfer is modeled during post compression before the onset of autoignition.

In the first method, both compression and post-compression processes are assumed to be isentropic processes. Hence, to account for the pressure drop, the core gas should expand. The effective volume calculation based on the pressure trace has been explained by [23, 43-44]. The effective volume during the post compression is calculated using the isentropic expansion equation by using the compressed gas pressure and the compressed gas volume at the end of compression:

$$\mathrm{V}_{eff}\ (\mathrm{t}) = V_c \left(\frac{P_c}{P(t)}\right)^{\frac{1}{\gamma_c}} \tag{3.1}$$

The effective volume is calculated in each condition (temperature, pressure and equivalence ratio) by using the inert test. In the inert test, the oxygen in the mixture is replaced by nitrogen and the test is performed without combustion. The *P(t)* in Eq. (3.1) is the time-resolved gas pressure during post compression using the inert mixture. The effective volume is used in a zero-dimensional modeling of RCM to account for the heat transfer.

In the second method, as explained by [45], the effective pressure, P_{eff}, is calculated as the time-averaged integrated pressure from the compressed pressure at the end of compression, P_c, to the minimum pressure, P_{min}, before the pressure rise due to combustion (Fig. 2.14). The effective temperature is calculated according to the gas law as follows:

$$\frac{P_{eff}}{T_{eff}} = \frac{P_c}{T_c} \tag{3.2}$$

In this method, the effective pressure and temperature are used in a zero-dimensional modeling of RCM.

In the third method, as explained by [9, 45-47], the average temperature is calculated according to the isentropic equation:

$$ln\left(\frac{P_{eff}}{P_i}\right) = \int_{T_i}^{T_{avg}} \frac{\gamma(T)}{\gamma(T)-1}\frac{dT}{T} \tag{3.3}$$

In this method, both compression and post-compression processes are assumed to follow the isentropic process. The compressed gas pressure in Eq. (2.1) is replaced by the effective compressed gas pressure as shown in Eq. (3.3) to calculate the average compressed gas temperature for the post-compression period. Desgroux et al. [48] showed that the core gas temperature follows the average temperature for the short ignition delay and follows the effective temperature for a long ignition delay.

The comparisons between the calculated effective and average gas temperatures versus the compressed gas temperature are shown in Figs. 3.1 and 3.2 at two compressed gas pressures. Both effective and average gas temperatures are lower than the compressed gas temperature due to the heat transfer to the chamber wall. In addition, the effective and average gas temperatures are a function of the compressed gas pressure. This is depicted in the developed linear fits to correlate the compressed gas temperature to the effective and average

gas temperatures at each pressure. The developed correlation for predicting the effective and average gas temperature at higher pressure (30 bar) cannot be used to predict the gas temperature at lower pressure (20 bar).

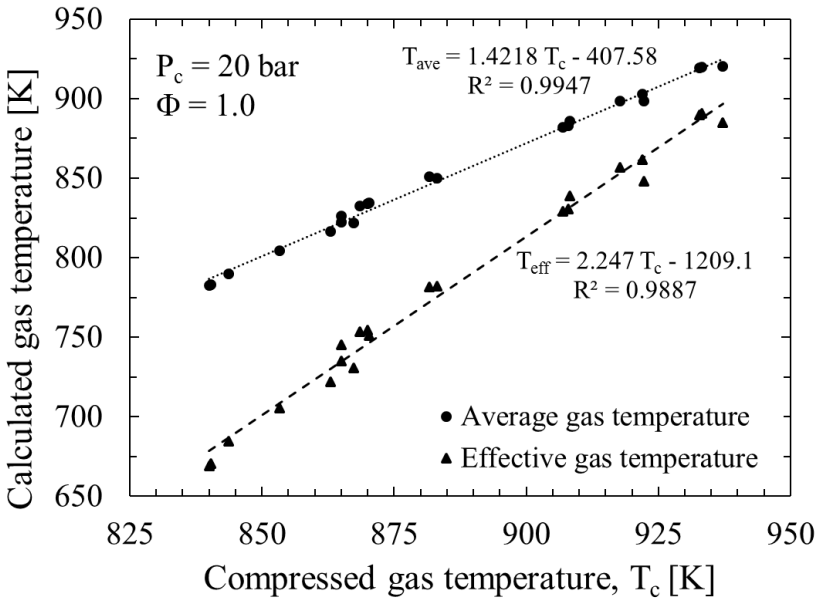

Fig. 3.1. Calculated effective and average gas temperatures at average effective pressure of 17.29 bar with standard deviation of 1.16. The average compressed gas pressure for the data is 20 bar with a standard deviation of 0.08. Mixtures 10 of Table 2.1 is used for measuring the ignition delay at the equivalence ratio of 1.0.

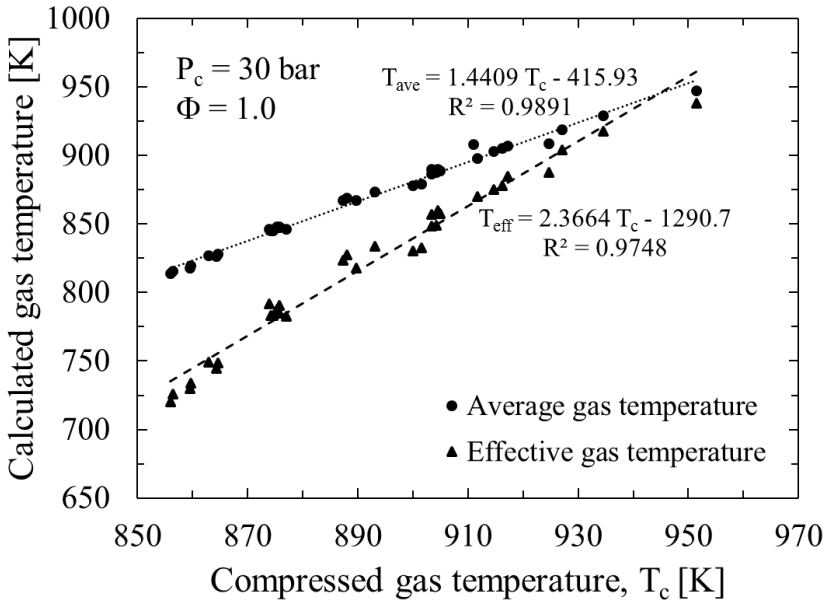

Fig. 3.2. Calculated effective and average gas temperatures at average effective pressure of 26.94 bar with a standard deviation of 1.01. The average compressed gas pressure for the data is 30 bar with a standard deviation of 0.76. Mixtures 4, 5, 6 of Table 2.1 are used for measuring the ignition delay at the equivalence ratio of 1.0.

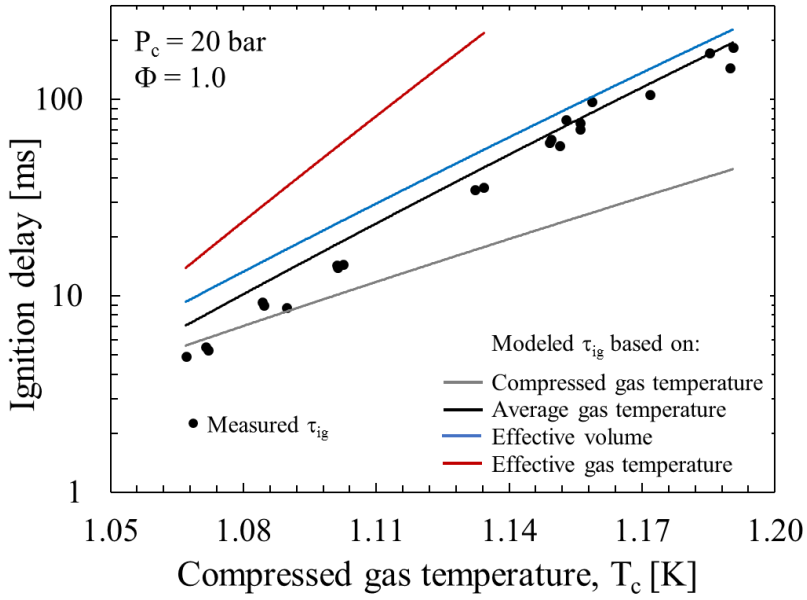

Fig. 3.3. Measured ignition delay times (τ_{ig}) at average compressed pressure of 20 bar, an equivalence ratio of 1 and by using mixture 10 of Table 2.1. Zero-dimensional modeling of ethanol ignition delay by using various numerical methods are also shown in the figure. The detailed final kinetic model of this work was used for simulations.

The measured ignition delay times of ethanol at the equivalence ratio and compressed gas pressure of 1.0 and 20 bar were measured and used to compare all of the discussed modeling methods as shown in Fig. 3.3. The methodology used to calculate temperature (as an input for the zero-dimensional model) affects the modeled ignition delay significantly. The ignition delay of the ethanol mixture is shorter at a higher gas temperature since there is no NTC region. The shortest ignition delay is calculated by using the compressed gas temperature. The modeled ignition delay times using the average gas temperature mimic the measured data very well. Using the method of the effective volume in the modeling mimics the measured data well enough. Finally, the modeling using the effective gas temperature overpredicts the measured ignition delays by far. Average gas temperature method is used for the zero-dimensional modeling of the ignition delay in this research.

3.2. Ignition Delay Modeling

As mentioned in the previous section, the methodology used in the current work is based on using the average gas temperature to include the effect of heat transfer in the temperature calculation. The method uses the isentropic compression process during compression and post-compression events for calculating the average gas temperature as shown above in Eq. (3.3). In conjunction, the effective compressed gas pressure, P_{eff}, is used.

The calculated average compressed gas temperatures (from Eq. (3.3)) were compared to the compressed gas temperatures (from Eq. (2.1)) at the compressed gas pressures of 15 and 30 bar and are shown in Fig. 3.4. The average compressed gas temperature is a function of the compressed gas pressure and is higher at higher gas pressure. At a fixed compressed gas temperature, the ignition delay is shorter at the higher pressure since there is less time for heat transfer to occur within the RCM and the effective pressure is higher. Higher effective pressure

results in a higher average compressed gas temperature, which corroborates the data shown in Fig. 3.4.

A closed homogeneous batch reactor [49] was used to simulate the measured ignition delay times by using CHEMKIN-PRO. To account for heat transfer during the post-compression period, the effective compressed gas pressure and the average compressed gas temperature were used as the initial mixture conditions for the model.

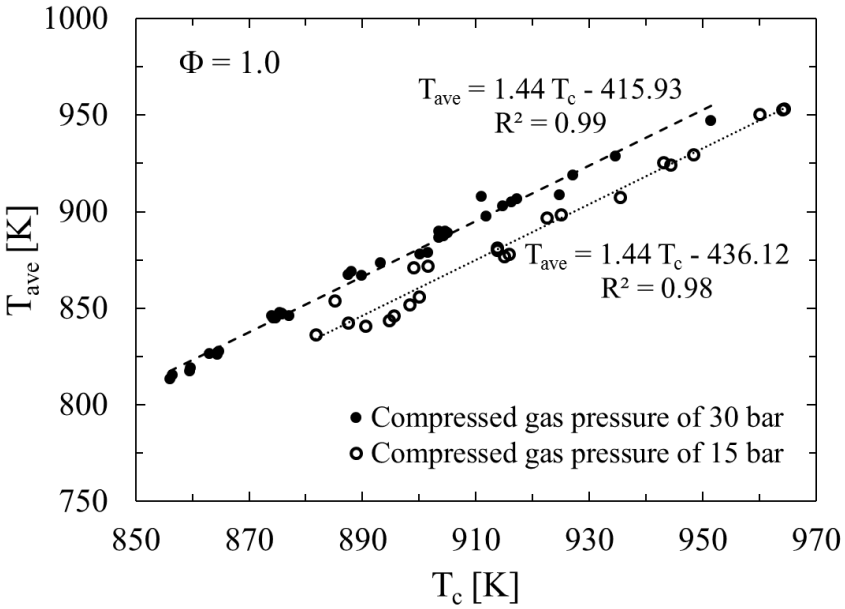

Fig. 3.4. Calculated average compressed gas temperatures for compressed gas pressures of 15 bar (with standard deviation of 0.26 bar) and 30 bar (with standard deviation of 0.76 bar). Mixture 5 was used at a compressed gas pressure of 15 bar, and mixtures 4-6 were used at a compressed gas pressure of 30 bar. The equivalence ratio of all of the tested mixtures is approximately 1.0 as listed in Table 2.1. The dashed lines are linear fits of the measured data with their respective correlations beside them.

3.3. Laminar Flame Speed Modeling

The laminar flame speeds were simulated using the premixed laminar flame speed model of CHEMKIN-PRO [49] at the conditions reported in the literature. Simulations were performed using the conditions from the measured data of [15-19].

A flame speed reactor [49] was used to simulate the laminar flame speeds by using CHEMKIN-PRO.

3.4. Species Concentrations Modeling

To simulate the time-resolved species concentrations reported in [9] by using an RCM and in [29] by using variable flow reactor, a closed zero-dimensional homogeneous batch reactor [49] was used. For the prediction of the stable species in the variable flow reactor, the simulation results were shifted in time to match 50% ethanol consumption as a reference point, as suggested by [29]. The absolute time of the flowing mixture in the flow reactor is experimentally unknown as discussed by [29].

3.5. Kinetic Model Development by using RMG

The automated mechanism generator methodology was used to develop ethanol detailed kinetic model reactions. It is the first time that this methodology has been used for the development of ethanol combustion kinetics. The reaction mechanism generator (RMG) as explained briefly by [50-53], was used to build a kinetic model. The model was constructed step by step by adding the elementary reactions using the theoretical rules of molecules. RMG has several advantages over the hierarchical-hydrocarbon-group (HHG) methodology, e.g., [54-55],

- RMG considers all the possible collisions (reactions) between species.
- The mechanism construction is faster using RMG respect to HHG model.
- RMG can be used for heavy hydrocarbons mechanism development without having the knowledge of smaller hydrocarbons kinetics, therefore, it can predict the kinetics of heavier hydrocarbon molecules (e.g. C_8).

Since the generated mechanism has reaction coefficients made based on known rules, theories, and available libraries, the coefficients could include error. Hence, modification and evaluation of the reactions coefficients are required. RMG also generates the species

thermodynamic information by using Benson-style group additivity [56] or on-the-fly quantum chemistry [57].

The RMG model requires the reactor conditions (i.e., temperature and pressure), initial species concentrations, termination circumstances (i.e., predetermined reaction time, t_{term}, or species conversion fraction X_{term}), and an error tolerance or model accuracy (i.e., the allowable flux for adding new species to the mechanism) to be defined for the reaction rate development. Species' reaction rate coefficients are estimated by using a database of known rate rules and reaction templates. RMG considers all elementary reactions that are possible between the species in the mechanism (hydrogen abstraction, beta scission, bond dissociation, etc.) while generating the mechanism. A seed mechanism can be used to include an entire sub-mechanism in the final model. It is made of a list of species and reactions the user can provide in RMG; then, RMG adds additional important species and reactions by using a rate-based algorithm [58]. The species generation process using RMG is shown in Fig. 3.5. It describes the development progression toward adding new species and reactions to the RMG engine core while constructing the mechanism. The rate-based algorithm with specified reactor conditions and termination circumstances is presented in Fig. 3.6. A new mechanism generation is described as follows:

- The initial species as provided by the user, e.g., ethanol, oxygen, nitrogen and etc., are listed in the mechanism generator engine, called the core.
- Starting from the initial species, RMG estimates all possible reactions and produces new species. The new species are listed in the edge, outside of the core.
- The algorithm will start step by step by checking the flux, R_i, from the core species to each species in the edge until the following criterion is reached:

$$R_i > \varepsilon R_{char} \tag{3.4}$$

$$R_i = \frac{dC_i}{dt} \left[\frac{mol}{cm^3\ s}\right] \tag{3.5}$$

Which *R* is rate of production (flux), ε is the error tolerance specified by the user, and R_{char} is characteristic flux which is the root-sum-squared of the existing species' fluxes in the core.

- The edge species that have the largest flux are added to the core. Subsequently, the corresponding reactions of the newly added species are included to the core.

  If the error tolerance is big, limited numbers of new species along with reactions will be added to the mechanism core. On the other hand, having a small error tolerance would allow more edge species along with their reactions to be added to the core producing a mechanism with more species and reactions.

- The process will stop when the termination criteria are reached and the final mechanism is generated.

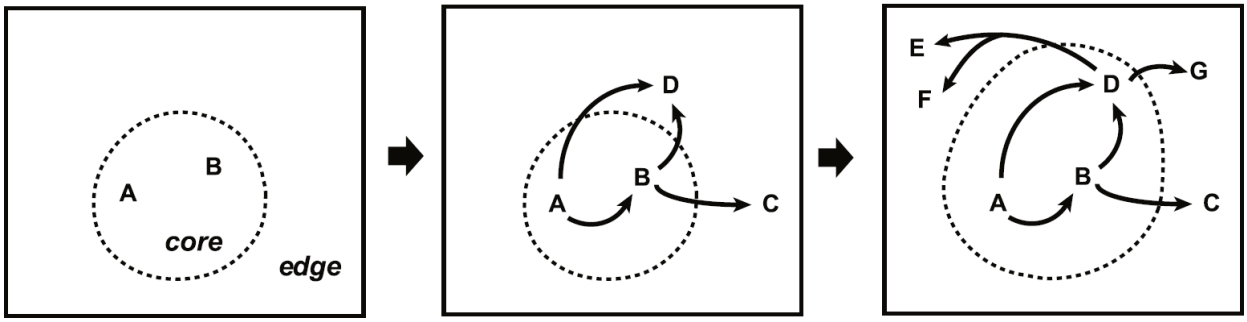

Fig. 3.5. Schematic describing the process RMG uses to build the model. Initially, the core includes the input species (A and B); then RMG estimates the list of possible reactions along with their products and lists these products (species D, C, etc.) in the edge. The figure is adopted from [53].

Forty-five reaction families are used in RMG to estimate the possible elementary reactions between the species in the mechanism as shown in Table 3.1 [53]. They are a set of templates that list the reactive process between certain species and their products.

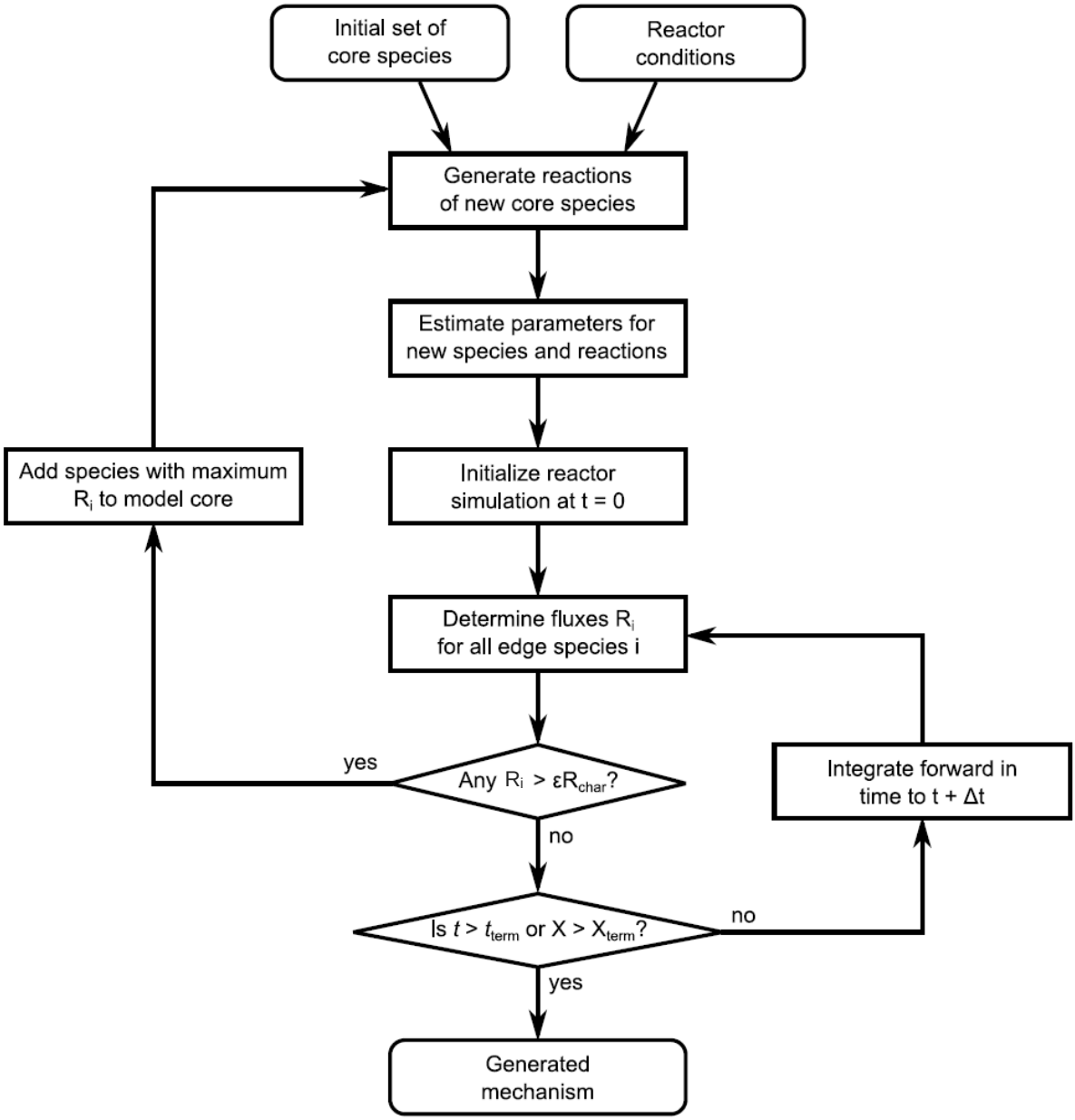

Fig. 3.6. Flowchart of the rate-based algorithm employed in RMG for the model generation process. At time zero, the process starts with the inputs (reactor conditions, fuel species, and seed mechanism) with respect to the specified error tolerance. This step is repeated until the termination circumstances are met, producing the final mechanism. The figure is adopted from [53].

Table 3.1. Reaction families [53]

1+2_Cycloaddition	intra_substitutionS_isomerization
1,2-Birad_to_alkene	Ketoenol
1,2_Insertion_carbene	Korcek_step1
1,2_Insertion_CO	Korcek_step2
1,2_shiftS	lone_electron_pair_bond
1,3_Insertion_CO_2	Oa_R_Recombination
1,3_Insertion_ROR	R_Addition_Com
1,3_Insertion_RSR	R_Addition_CSm
1,4_Cyclic_birad_scission	R_Addition_MultipleBond
1,4_Linear_birad_scission	R_Recombination
2+2_cycloaddition_CCO	Substitution_O
2+2_cycloaddition_Cd	SubstitutionS
Birad_recombination	intra_OH_migration
Diels_alder_addition	Intra_R_Add_Endocyclic
H_shift_ cyclopentadiene	Intra_R_Add_Exocyclic
2+2_cycloaddition_CO	Intra_R_Add_ExoTetCyclic
Cyclic_Ether_Formation	Intra_RH_Add_Endocyclic
Disproportionation	Intra_RH_Add_Exocyclic
H_Abstraction	intra_substitutionCS_cyclization
HO2_Elimination_from_PeroxyRadical	intra_substitutionCS_isomerization
Intra_Diels_alder	intra_substitutionS_cyclization
Intra_Disproportionation	intra_NO2_ONO_conversion
intra_H_migration	

3.6. Ethanol Kinetics Model Development

RMG-Py version 2.0.0 written in Python [53] was used in this work to build the ethanol mechanism. GRI-Mech 3.0 [59] was used as a seed mechanism with 206 reactions and 35 species. RMG added more species and reactions to the seed mechanism to build the final ethanol mechanism. To develop the final model, multiple homogeneous batch reactors were simulated at

various mixture compositions, gas temperatures and pressures. For the current research, the gas temperatures and pressures ranges were set in the range of 850 to 1400 K and 5 to 40 bar to develop the kinetic model. The error tolerance and termination time were defined as 0.1 and 2 s for the simulation. The input file (input.py) for the ethanol mechanism generation written in Python is described in Appendix D. The command prompt for running the input file code is shown in Fig 3.7. The output of RMG modeling is a kinetic model in CHEMKIN format along with the species thermodynamic file, species transport file, and species dictionary.

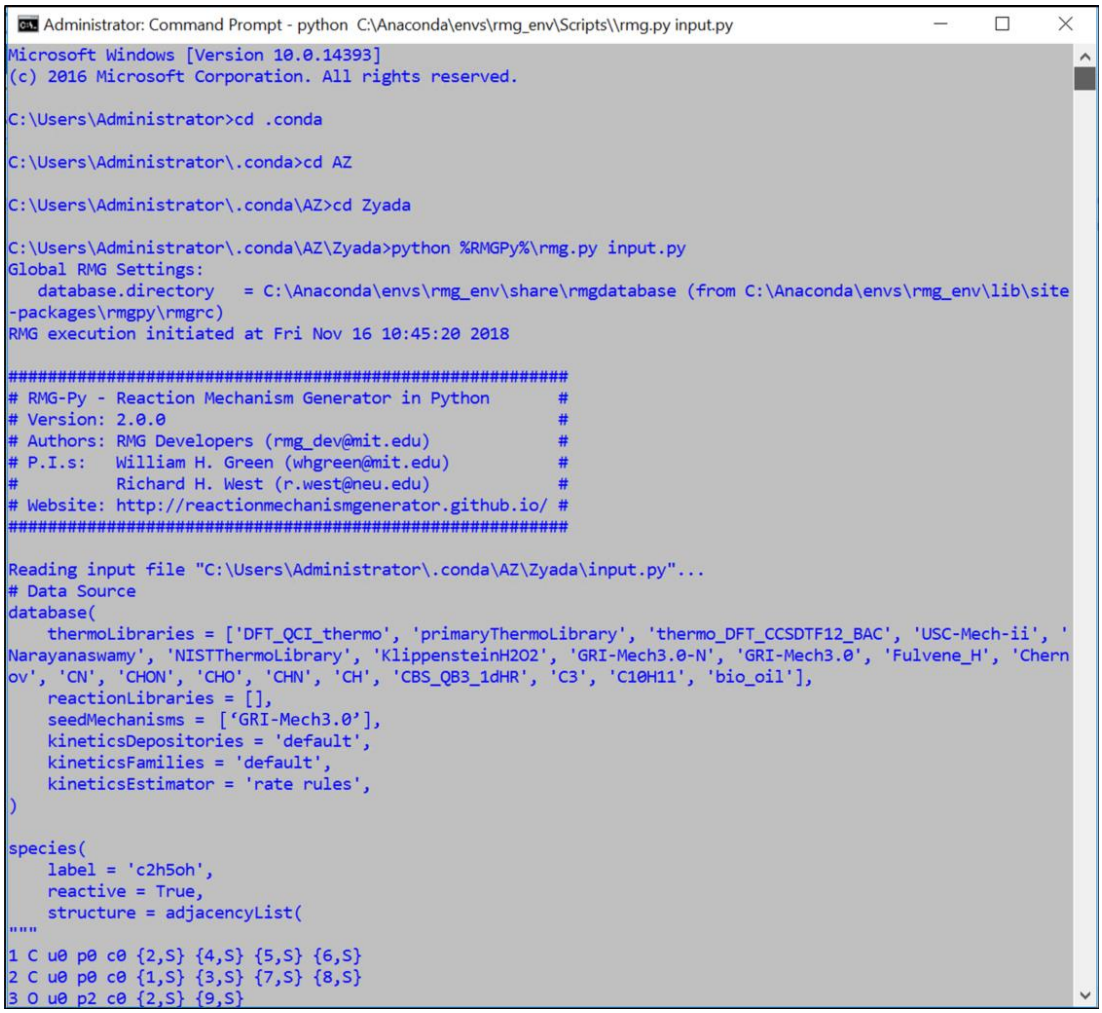

Fig. 3.7. Command Prompt window for running the Python syntax input file

CHAPTER 4: RESULTS AND DISCUSSION

4.1. Ethanol Ignition Delay Measurements by using RCM

Several mixtures were prepared to vary the equivalence ratio and compressed gas temperature as shown in Table 2.1. Note that the equivalence ratio is similar between multiple mixtures, but the diluents have varying concentrations to impact the compressed gas temperature. Mixture 10 in Table 2.1 was used to study the effect of the oxidizer concentration on the measured and modeled ignition delay. The mixtures were used in combustion experiments to measure the ignition delay times at a compressed gas temperature range of 850 to 1000 K, equivalence ratios of approximately 0.5, 1.0 and 2.0, and compressed gas pressures of approximately 15, 20, and 30 bar as shown in Figs. 4.1-4.3. At compressed gas pressure of 20 bar, the ignition delay was measured only at the equivalence ratio of 1.0 using mixture 10 as shown in Fig. 4.2. Each test was performed at least three times under the same conditions to ensure the repeatability of the results. Over 200 experiments were performed to measure the ignition delay times under the aforementioned range of conditions. The details of the tests are reported in Appendix A. As shown in the figures, the ignition delay decreases as the equivalence ratio and compressed gas pressure increase. The ignition delay also shows an inverse relationship with the concentration of the oxidizer. This is true even when the equivalence ratio is held constant. This is seen in Figs. 4.2 and 4.3, where the equivalence ratio is held constant (mixtures 4, 5, 6 and 10) and the ignition delay times are approximately the same despite being at different compressed gas pressures of 20 bar for mixture 10 and 30 bar for the others.

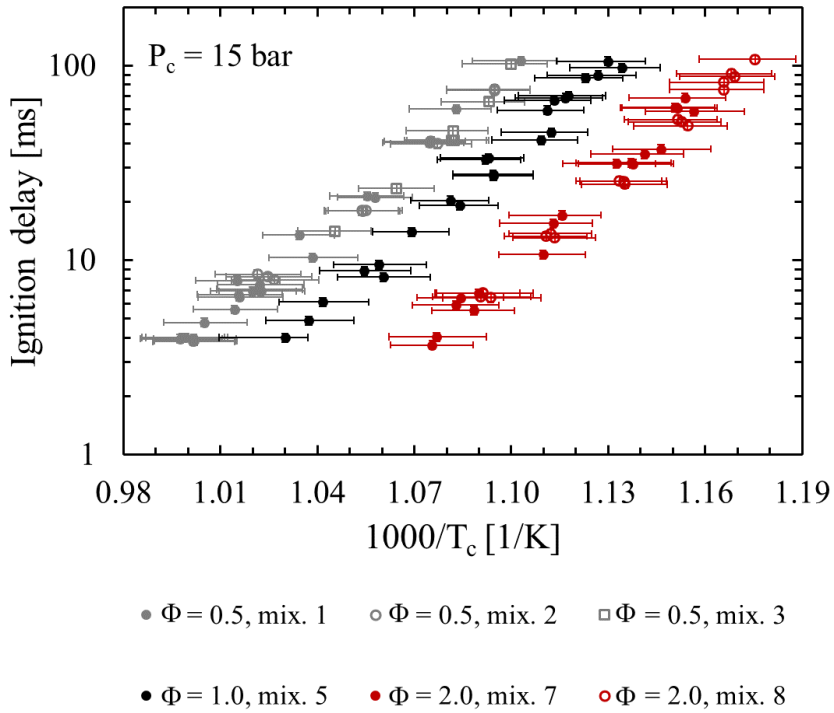

Fig. 4.1. Measured ignition delay times at various equivalence ratios and an average compressed gas pressure of 15 bar with a standard deviation of 0.33 bar. The mixture compositions are shown in Table 2.1.

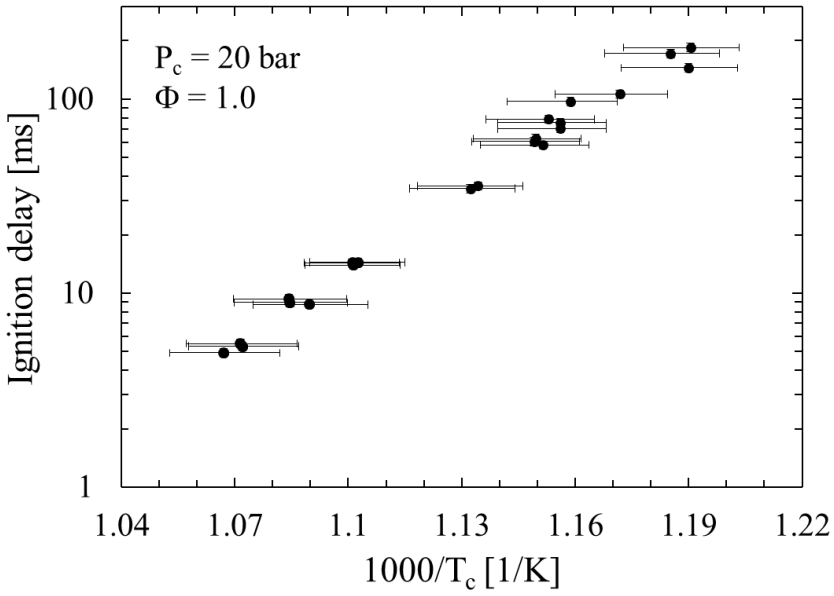

Fig. 4.2. Measured ignition delay times at an equivalence ratio of 1.0 and an average measured compressed gas pressure of 20 bar with a standard deviation of 0.29 bar. Mixture 10 of Table 2.1 was used for the measurements.

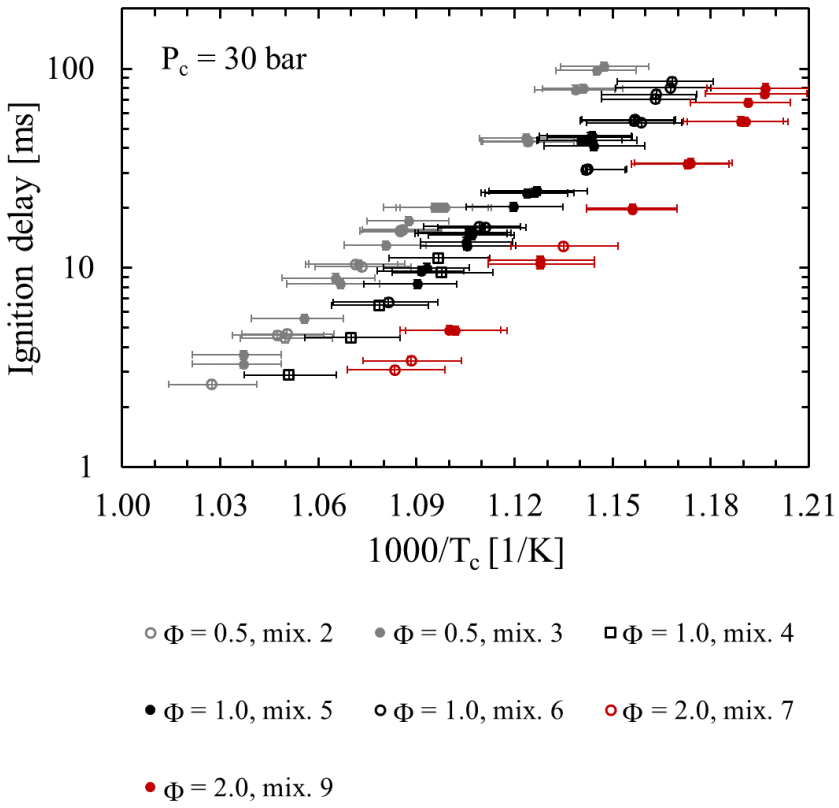

Fig. 4.3. Measured ignition delay times at various equivalence ratios and an average measured compressed gas pressure of 30 bar with a standard deviation of 0.49 bar. Mixtures used for the measurements are in Table 2.1.

An equation in the Arrhenius format was developed to correlate the measured ignition delay data as a function of the compressed gas pressure, temperature, initial ethanol concentration, and equivalence ratio as follows:

$$\tau_{ig} = 6.086 \times 10^{-14}\, P_c^{-1.34}\, \emptyset^{-0.57}\, (X_{ethanol})^{-0.9}\, exp\left(\frac{31000}{T_c}\right);$$

$$15 \leq P \leq 30, 850 \leq T_c \leq 1000, 0.5 \leq \emptyset \leq 2.0 \qquad (4.1)$$

In Eq. (4.1), the ignition delay, ethanol concentration, pressure, and temperature have units of millisecond, mole fraction, bar, and Kelvin, respectively. The coefficient of determination, R^2, of Eq. (4.1) is 0.982, which is indicative that the equation correlates very well with the measured data. The influence of the diluent on the ignition delay was not studied; therefore, the developed

correlation is only valid for the used diluent mixture of nitrogen and argon as reported in Table 2.1.

To visually demonstrate the validity of Eq. (4.1), all of the measured and predicted ignition delay times, at different compressed gas pressures, equivalence ratios and ethanol concentrations, were plotted against their corresponding compressed gas temperatures in Fig. 4.4. As shown, the developed function (Y axis) provides excellent predictability for the range of tested conditions.

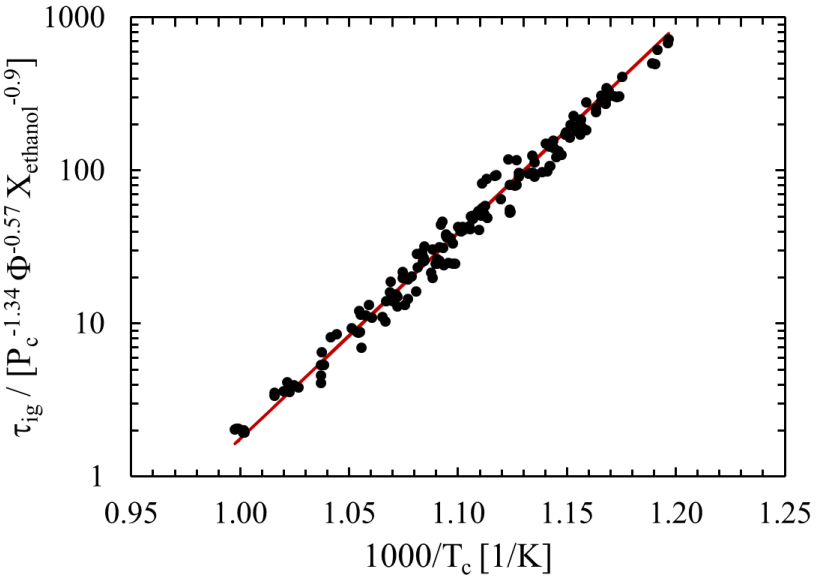

Fig. 4.4. Measured ignition delay data at various equivalence ratios, pressures, temperatures and fuel and oxidizer concentrations.

4.2. Combustion Images Recording and Processing

The combustion images from the high speed camera at a compressed gas pressure of 30 bar and two compressed gas temperatures of 865 and 925 K are shown in Fig. 4.5. Combustion at the lower gas temperature, shown in Fig. 4.5a, is initially characterized by a continuum of low intensity blue background light that fills the combustion chamber (indicative of volumetric combustion). Then, a high intensity blue light (the apparent flame front) propagates from the chamber wall until it gradually permeates the entire combustion chamber. The timing at which the

high intensity blue light completely fills the entire chamber is defined as the onset of combustion as determined by the blue light (or onset of the full-circle blue light). The blue flame speed is faster at the higher compressed gas temperature, e.g., the speed is approximately 257.9 m/s at the compressed gas temperature of 925 K (Fig 4.5b) and is approximately 111.6 m/s at the lower compressed gas temperature of 865 K (Fig 4.5a). The laminar flame speeds at conditions of Figs. 4.5a and 4.5b are approximately 0.08 and 0.1 m/s, respectively. Since the calculated speed of the high intensity blue light is slower than the speed of sound but faster than the laminar flame speed, the combustion modes can be referred to as deflagration. Depending on the compressed gas pressure, temperature and equivalence ratio, the blue light may be succeeded by the white and yellow light as shown in Fig. 4.5b. As shown by the graph in Fig. 4.5, the maximum pressure caused by combustion increases from approximately 60 to 115 bar through increasing the compressed gas temperature by 60 K. The higher combustion pressure causes the mixture inside the RCM's piston crevice, which is at a lower gas temperature than the mixture inside the chamber, to autoignite simultaneously or after the autoignition in the combustion chamber. This autoignition also produces the white light at the periphery of the chamber as shown in Fig. 4.5b at the time of 5.86 ms. The autoignition of the mixture in the crevice is likely the cause of the pressure wave oscillations observed at the time of combustion for the compressed gas temperature of 925 K. Further combustion images at the compressed gas pressure of 15 bar are reported in Appendix B, Fig B.1.

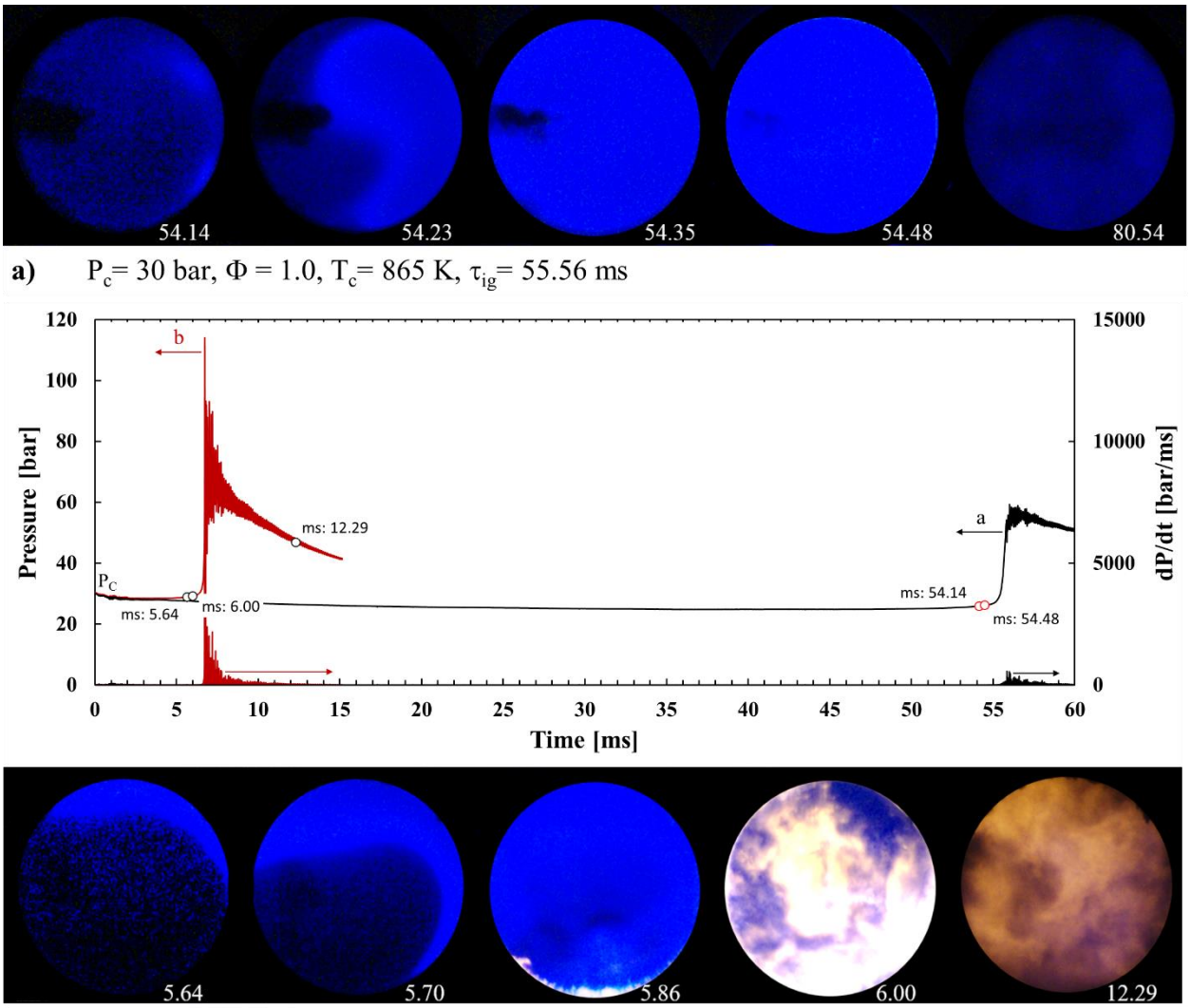

Fig. 4.5. High speed images and pressure traces at a compressed gas pressure of 30 bar and an equivalence ratio of 1. The time after the end of compression is shown in milliseconds at the bottom of each image. a) The compressed gas temperature and ignition delay are 865 K and 55.56 ms. An exposure time of 15.27 μs and camera recording speed of 57,000 fps were used. b) The compressed gas temperature and ignition delay are 925 K and 6.72 ms. An exposure time of 2.73 μs and camera recording speed of 57,000 fps were used.

The effects of the equivalence ratio on the autoignition process were investigated at an average compressed gas pressure of 30 bar and a compressed gas temperature of 925 K, as shown in Fig. 4.6. To ensure optimal picture quality, the images were taken using different exposure times depending on the equivalence ratio. If the exposure time were long, the flame

intensity would saturate the chip of the camera and make it impossible to view the flame propagation and structure. However, the low intensity light cannot be detected by using a short exposure time. Hence, different exposure times are used in Fig. 4.6. As the equivalence ratio was increased from 0.5 to 2.0, the apparent blue flame speed also increased. The apparent flame speeds at equivalence ratios of 0.5, 1 and 2.0 were calculated as 36.29 m/s, 257.86 m/s, and 362.12 m/s, respectively. The high speed camera blue light response is approximately between 375 and 550 nm as shown in Fig. B.2 of appendix B. Due to the wavelength range of blue light recorded by the camera, the origin of the blue light should be the excited radical of carbon dioxide generated by following reactions [60]:

$$CO + O\ (+M) \rightarrow CO_2(^3B_2)(+M) \tag{4.2}$$

$$CO_2(^3B_2) \rightarrow CO_2(^1B_2) \tag{4.3}$$

$$CO_2(^1B_2) \rightarrow CO_2(^1\Sigma_g^+) + h\nu \tag{4.4}$$

$$CO_2(^1B_2)(+M) \rightarrow CO_2(^1\Sigma_g^+)\ (+M) \tag{4.5}$$

As further discussed by [60-61], the intensity of the excited carbon dioxide radical is determined by using:

$$I_{CO_2} = I_0 \times [CO] \times [O] \tag{4.6}$$

where I_0 is the reaction rate coefficient and [CO] and [O] are the concentration of CO and O. Hence, the blue light intensity should be a function of the concentrations of carbon monoxide and atomic oxygen. By increasing the gas temperature, the CO_2 intensity increases as predicted by Eq. (4.6).

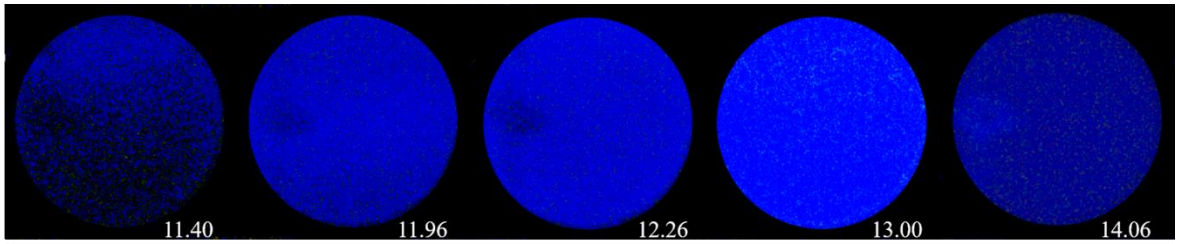

a) P_c= 30 bar, Φ = 0.5, T_c= 925 K, τ_{ig}= 13.00 ms

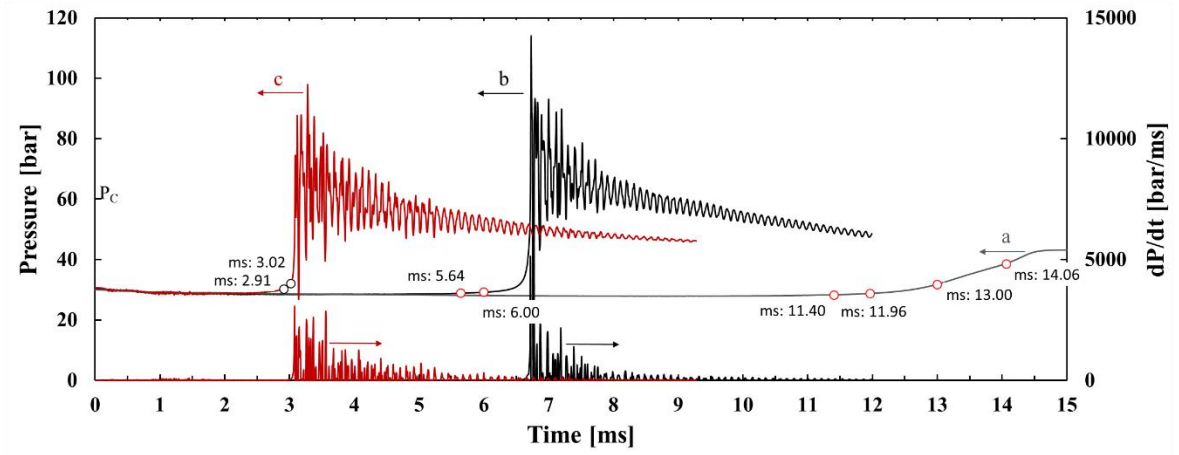

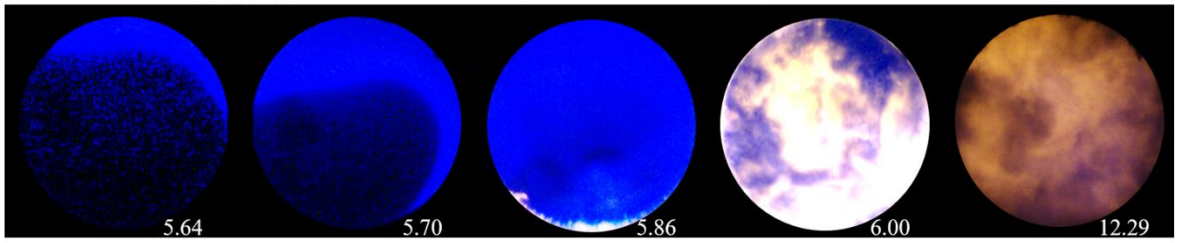

b) P_c= 30 bar, Φ = 1.0, T_c= 925 K, τ_{ig}= 6.72 ms

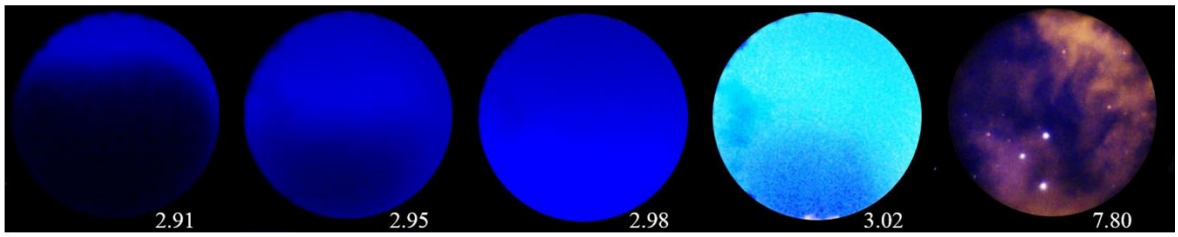

c) P_c= 30 bar, Φ = 2.0, T_c= 925 K, τ_{ig}= 3.08 ms

Fig. 4.6. High speed images and pressure traces at a compressed gas pressure of about 30 bar and a compressed gas temperature of about 925 K. The time after the end of compression is shown in milliseconds at the bottom of each image. a) Equivalence ratio and ignition delay are 0.5 and 13 ms. An exposure time of 44.48 μs and camera recording speed of 57,000 fps were used. dP/dt is relatively small at this scale and is not well depicted. b) Equivalence ratio and ignition delay are 1.0 and 6.72 ms. An exposure time of 2.73 μs with a camera recording speed of 57,000 fps was used. c) Equivalence ratio and ignition delay are 2.0 and 3.08 ms. An exposure time of 15.27 μs and camera recording speed of 57,000 fps were used.

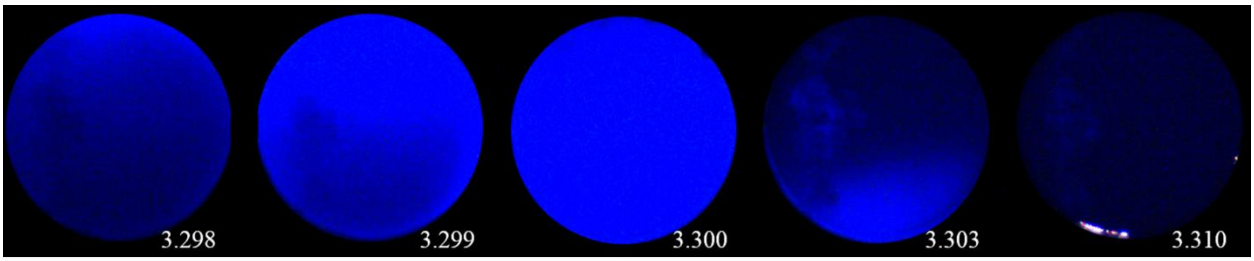

b) P_c= 30 bar, Φ = 0.5, T_c= 964 K, τ_{ig}= 3.30 ms

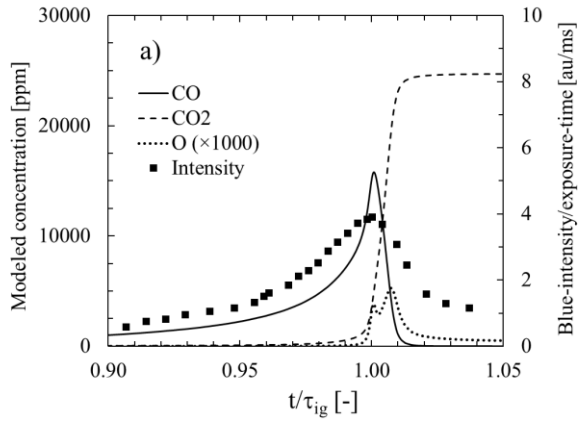

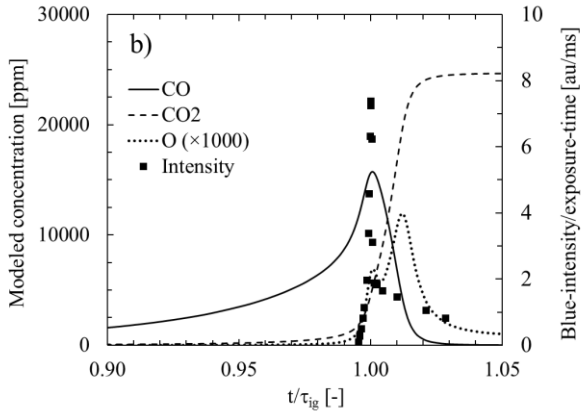

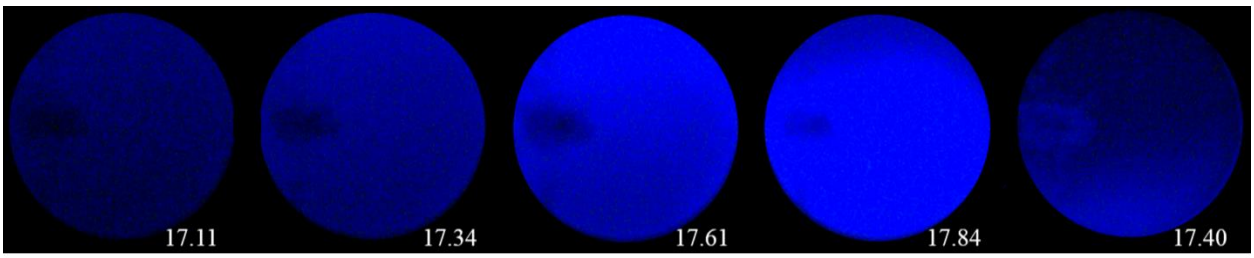

a) P_c= 30 bar, Φ = 0.5, T_c= 920 K, τ_{ig}= 17.17 ms

Fig. 4.7. The high speed images and simulated species concentration at a compressed gas pressure of about 30 bar and an equivalence ratio of 0.5. The time after the end of compression is shown in milliseconds at the bottom of each image as a reference. In the graphs, the camera intensity is calculated as the non-dimensional average of the intense blue light divided by the exposure time. The time is normalized to the timing of the onset of full-circle blue light as an indication of the time of combustion (a: 17.84 ms and b: 3.300). The simulation was performed using the developed mechanism of the current research. The simulation time is normalized to the modeled ignition delay time (a: 21.83 and b: 6.71). a) Compressed gas temperature and measured ignition delay are 920 K and 17.17 ms. An exposure time of 29.2 μs and camera recording speed of 30,000 fps were used. b) Compressed gas temperature and measured ignition delay are 964 K and 3.30 ms. An exposure time of 21.8 μs and camera recording speed of 40,000 fps were used.

Further scrutiny was applied by plotting the measured intensity of the blue light and modeled species concentrations at two different compressed gas temperatures as shown in Fig. 4.7. As shown in the figure, the concentration of carbon monoxide is almost the same for both high and low gas temperatures. The atomic oxygen concentration, however, is approximately two times greater at the higher gas temperature than the lower gas temperature. Hence, the authors think the origin of the high intensity blue light is the same as for the low intensity blue light which is the excited carbon dioxide radical, with the greater intensity produced at the higher gas temperature due to the increased atomic oxygen concentration.

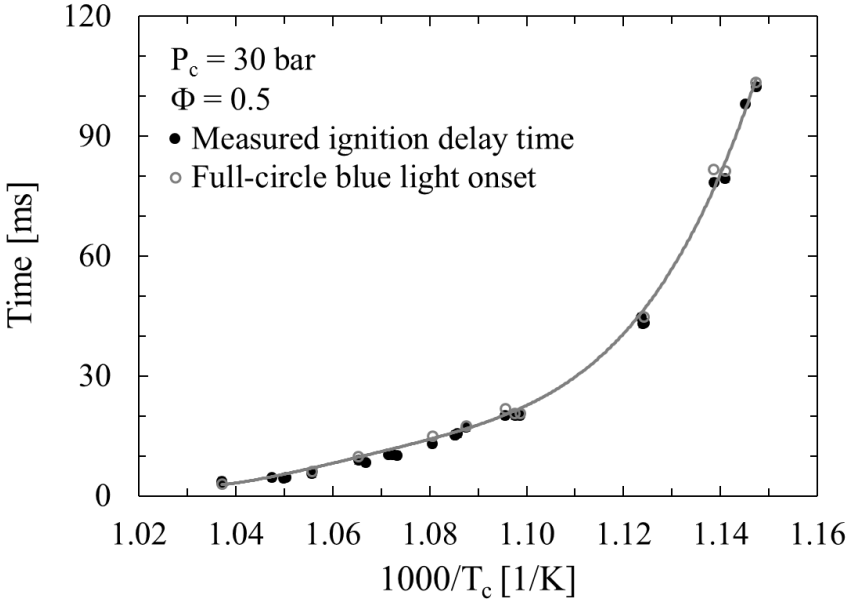

Fig. 4.8. Measured ignition delay times (black circle) and the measured timing of onset of the full-circle high intensity blue light (open gray circles). The line is the trend-line of the measured ignition delay. Data were measured at a compressed gas pressure of 30 bar and an equivalence ratio of 0.5.

The measured ignition delay based on the pressure rise and the onset of the full-circle blue light are compared in Fig. 4.8 at a compressed gas pressure of 30 bar and equivalence ratio of 0.5. The data shows that both methods agree quite well on the time of the ignition delay. The

comparisons between these two methods at other pressure and equivalence ratios are reported in Appendix B, Fig B.3.

4.3. Mechanism Development and Validation

A detailed mechanism of ethanol was developed using the RMG and validated with the experimental data from this research and sources in the literature. The mechanism was compared to the measured ignition delay data at a low to intermediate gas temperature range using the RCM of the current work and ignition delay data at high gas temperature range using shock tube, time-resolved species concentrations, and laminar flame speeds from the literature. The details of the development and validation are discussed in this section.

The kinetic reaction model of this research was developed in three iterations as shown in Table 4.1. Three mechanisms were developed, which are called Mechanism-Alpha, -Beta, and –Gamma, and evaluated versus the measured data. The first mechanism, Mechanism-Alpha, was generated without a seed mechanism. The mechanism was used to simulate the ignition delay of the experimental conditions with unsatisfactory results as shown in Fig. 4.9. To improve the mechanism's prediction, GRI-Mech 3.0 [59] was used as a seed mechanism to develop the next generation, Mechanism-Beta. Mechanism-Beta's ignition delay predictions are in excellent agreement with the measured data as shown in Fig. 4.9. However, the mechanism did not adequately predict the laminar flame speed as shown in Fig. 4.10. Furthermore, Mechanism-Beta was not quite able to fully capture the time-resolved species concentrations as illustrated in Fig. 4.11. While it was able to reasonably predict the measured concentrations, some components (such as CH_4 and C_2H_4) were significantly underpredicted. Sensitivity and reaction path analyses were performed to identify the reactions that were critical in predicting the laminar flame speed and aforementioned species concentrations. The reactions were modified to produce the final iteration of the mechanism: Mechanism-Gamma. The mechanism is in excellent agreement with

the measured data as shown in Figs. 4.9-4.11 and 4.18. A summary of these steps taken to finalize the model and a discussion of the results are described in the following sub-sections.

Table 4.1. Summary of the developed kinetic model

Mechanism	Alpha	Beta	Gamma
Seed mechanism	No	GRI-Mech 3.0	GRI-Mech 3.0
Number of species	250	107	107
Number of reactions	4313	1797	1795

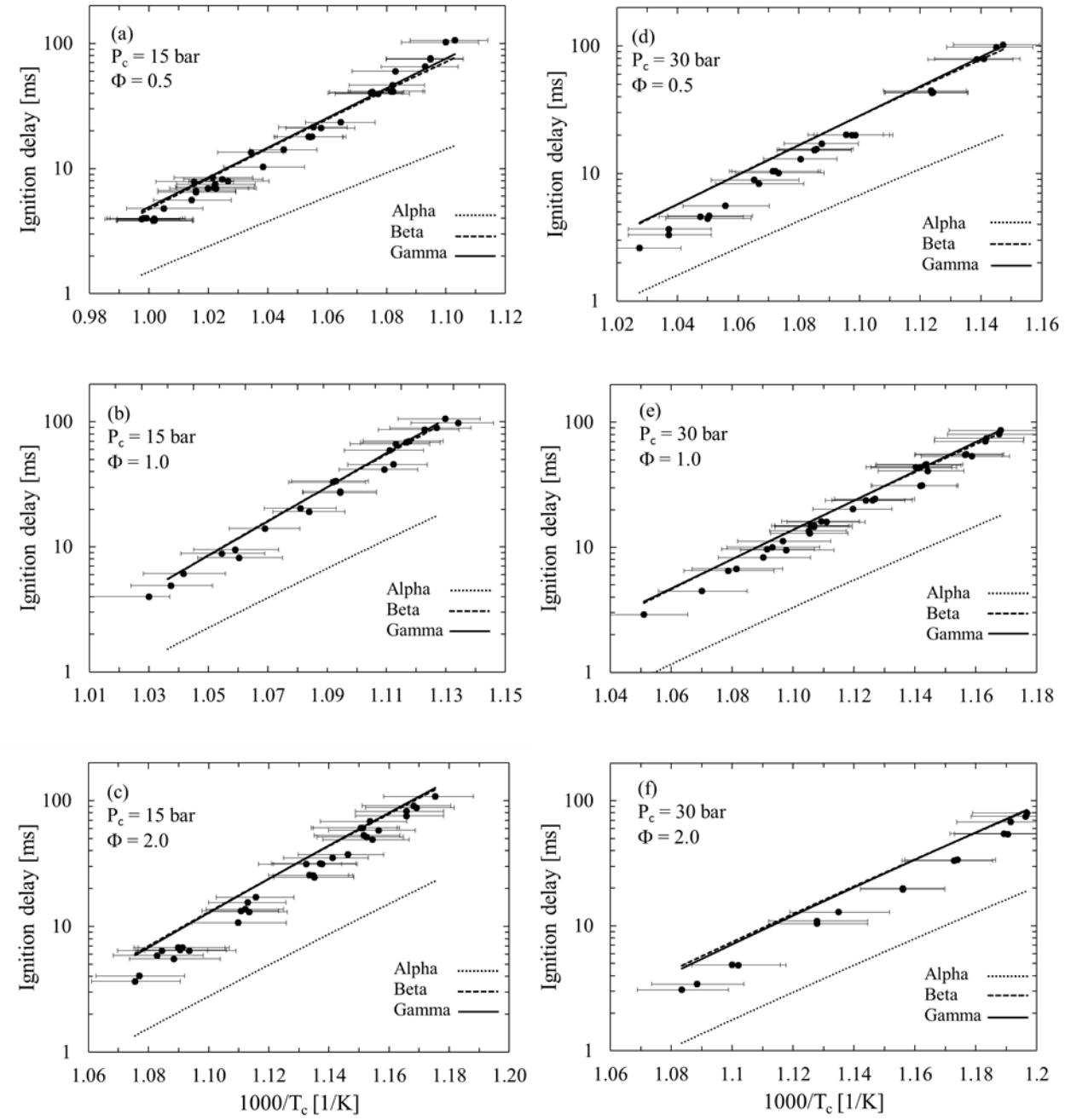

Fig. 4.9. Measured and modeled ignition delay times at average measured compressed gas pressures of 15 and 30 bar and equivalence ratios of 0.5, 1.0, and 2.0.

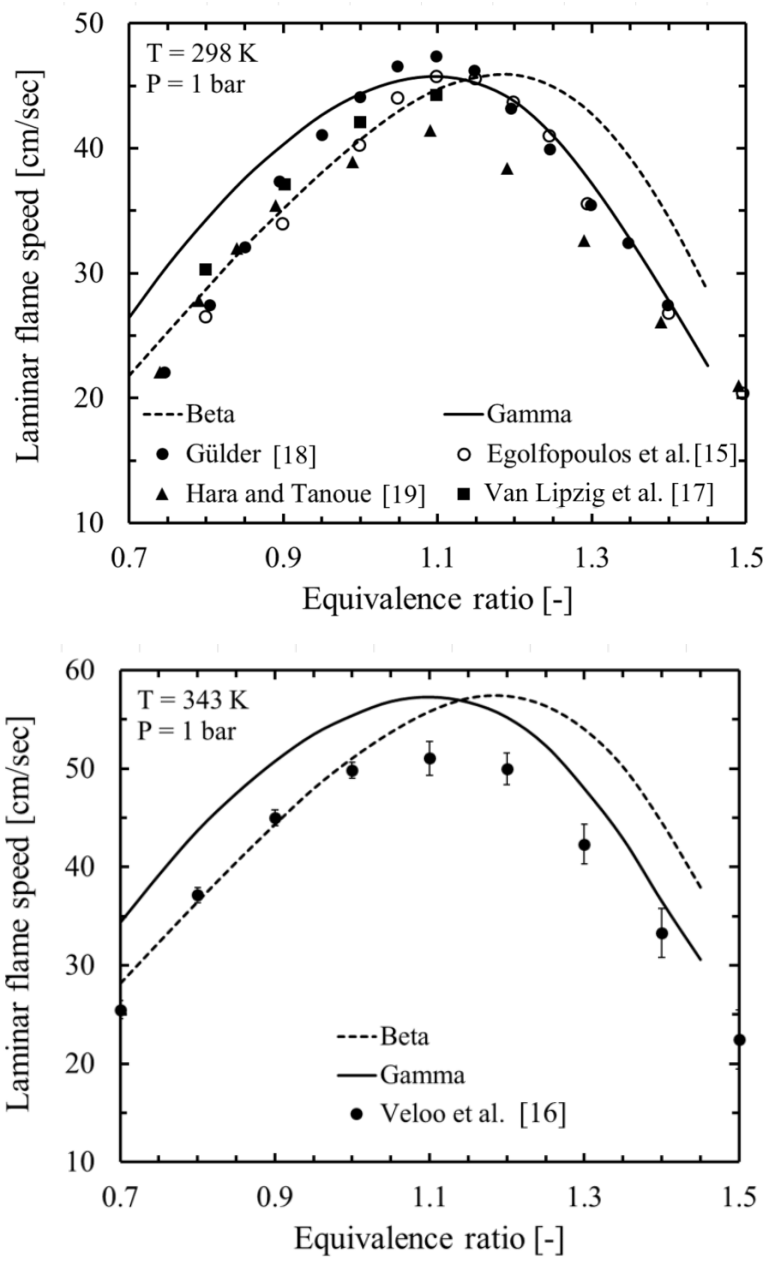

Fig. 4.10. Laminar flame speed of ethanol at atmospheric pressure and gas temperature of 298 and 343 K for mixtures of ethanol and air. The air composition is N_2: 79.5% and O_2: 20.5%, vol/vol. Experiments are shown by the symbols, and the simulations are shown by the lines.

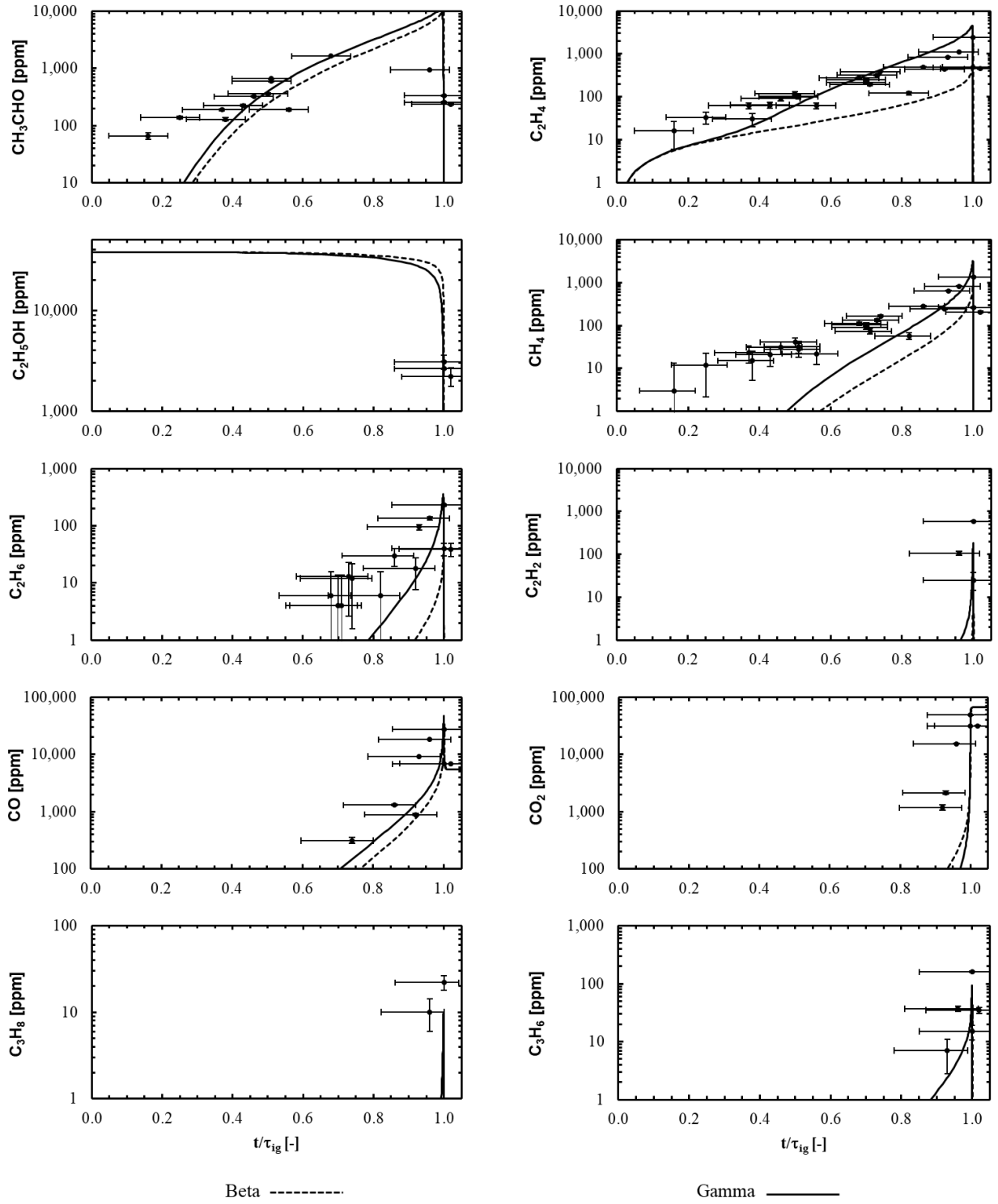

Fig. 4.11. The simulated and measured time-resolved intermediate species of ethanol autoignition. The mixture composition is Ar: 5.31%, C_2H_5OH: 3.75%, N_2: 79.6, O_2: 11.33% (molar basis). The effective compressed gas pressure, average compressed gas temperature, and equivalence ratio are 10.1 atm, 930 K, and 1.0, respectively. The measured data is from [9].

4.3.1. Laminar Flame Speed

Mechanism-Beta shows the peak of laminar flame speed at the equivalence ratio of 1.2, but the measured data shows it at a different equivalence ratio of 1.1 as shown in Fig. 4.10. A sensitivity analysis was performed to identify the major reactions responsible for the laminar flame speed so that the flame speed may show an improved dependency on equivalence ratio. The results of the sensitivity analysis are shown in Table 4.2. The reaction O + OH = HO_2 was found to be responsible for the equivalence ratio at which peak laminar flame speed occurred. The O + OH = HO_2 reaction coefficients were not found in the literature but were generated by the RMG. The reaction was removed from Mechanism-Beta to correct the laminar flame speed peak at the equivalence ratio of 1.1. After this modification, the laminar flame speed peak was correctly predicted at the equivalence ratio of 1.1, but its value was overpredicted with respect to the measured data. The laminar flame speed overprediction was corrected later during the development process by improving the carbon dioxide concentration. As shown later in Fig. 4.18, the mechanism overpredicts carbon dioxide concentration under the conditions of the flow reactor. A reaction path analysis was performed at atmospheric pressure and a temperature of 298 K to understand which reactions were responsible for carbon dioxide concentration. The results produced a hierarchical layout of ethanol consumption pathways along with other species, as shown in Fig. 4.12. The reaction OH + CO_2 = CHO_3 was identified to have a significant effect on laminar flame speed. The excess CO_2 production, as shown in Fig. 4.18, is also caused by this reaction. The reaction is not mentioned in the literature and is generated by the RMG, so the reaction was removed from the mechanism. This step fixed the final mechanism, which has improved laminar flame speed and carbon dioxide predictions when compared to the measured data.

Table 4.2. Important Mechanism-Beta reactions with significant effect on laminar flame speed. A, b, and E_a are coefficients (constants) in the modified Arrhenius equation, $k = A\ T^b \exp(-E_a/RT)$. Units are moles, cm, sec, K and kcal/mole.

Reaction	A	b	E_a	Ref.
$O_2+H=O+OH$	2.65e+16	-0.67	17.04	GRI-Mech 3.0
$OH+CO=H+CO_2$	4.76e+07	1.23	0.07	GRI-Mech 3.0
$O+OH=HO_2$	1.00e+13	0.00	0.00	RMG
$H+HO_2=O_2+H_2$	4.48e+13	0.00	1.07	GRI-Mech 3.0
$H+CH_3(+M)=CH_4(+M)$	1.39e+16	-0.53	0.54	GRI-Mech 3.0
$HO_2+CH_3=OH+CH_3O$	3.78e+13	0.00	0.00	GRI-Mech 3.0 (is updated in Table 4.6)
$H_2+OH=H_2O+H$	2.16e+08	1.51	3.43	GRI-Mech 3.0
$CH_2CO+O=C_2H_2O_2$	1.07e+08	1.60	-1.38	RMG
$H+HO_2=2OH$	8.40e+13	0.00	0.64	GRI-Mech 3.0

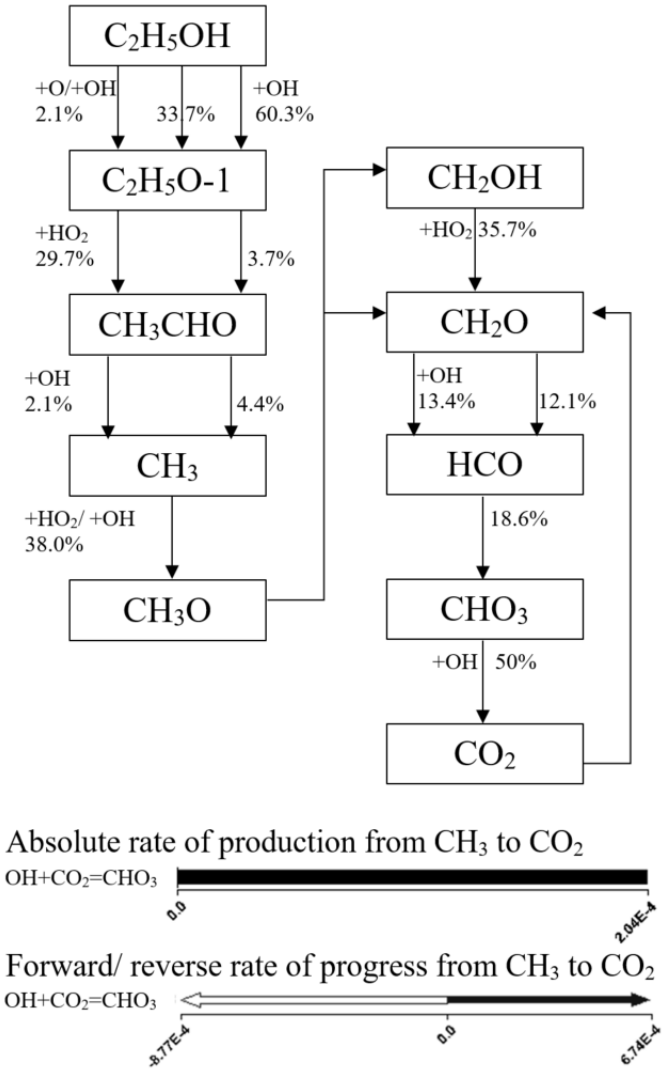

Fig. 4.12. Laminar flame speed reaction pathway analysis for carbon dioxide at atmospheric pressure and a temperature of 298 K. The sensitivity and rate of carbon dioxide production are shown. The shown percentage near the arrows corresponds to the total depletion of the species through the specific reaction. The simulated data are shown at where the gas temperature is 1041 K.

4.3.2. Intermediate Species Modeled and Measured by using RCM

The model was further validated against time-resolved species measurements of [9]. Reported gas pressure and temperature of 10 bar and 930 K in [9] were assumed to be the effective compressed gas pressure and average compressed gas temperature. The measured and modeled time-resolved ethanol intermediate species concentrations during autoignition are

shown in Fig. 4.11. Mechanism-Beta underpredicted certain species concentrations, e.g., CH_3CHO, C_2H_4, CH_4, and C_2H_6. The major reaction pathways were determined, and the reaction coefficients were compared to the measured data in the literature for each species. Corrections were made to the reaction coefficients to better predict the species concentration. This process is explained in more detailed for the aforementioned species as follows:

CH_3CHO: The CH_3CHO sub-mechanism was updated using the measured data of [32, 62-67] as shown in Table 4.3. CH_3CHO concentrations improved slightly as shown in Fig. 4.11.

Table 4.3. CH_3CHO sub-mechanism reactions. A, b, and E_a are coefficients in the modified Arrhenius equation, $k = A\ T^b \exp(-E_a/RT)$. Units are moles, cm, sec, K and kcal/mole.

Reaction	A	b	E_a	Ref.
$CH_3CHO(+M)=CH_3+HCO(+M)$	2.45E+22	-1.74	86.35	[62]
$CH_3CHO(+M)=CH_4+CO(+M)$	2.72E+21	-1.74	86.35	[62]
$CH_3CHO+O_2=C_2H_3O+HO_2$	3.01E+13	0.00	39.15	[63]
$CH_3CHO+O=C_2H_3O+OH$	5.94E+12	0.00	1.87	[32]
$CH_3CHO+H=C_2H_3O+H_2$	1.31E+05	2.58	1.22	[64]
$CH_3CHO+OH=C_2H_3O+H_2O$	3.37E+12	0.00	-0.62	[65]
$CH_3CHO+HO_2=C_2H_3O+H_2O_2$	3.01E+12	0.00	11.92	[63]
$CH_3CHO+CH_3=C_2H_3O+CH_4$	7.08E-04	4.58	1.97	[66]
$CH_3CHO+H=CH_2CHO+H_2$	2.72E+03	3.10	5.21	[64]
$CH_3CHO+OH=CH_2CHO+H_2O$	1.72E+05	2.40	0.82	[67]

C_2H_4: Reaction pathway analysis was performed for the C_2H_4 species. Several major reactions associated with this species were identified as shown in Fig. 4.13. The reaction coefficients were comparable to those in the literature, so no modification was made. The underprediction of C_2H_4 appears to be a result of an underpredicted concentration of C_2H_5O-2, which is the major contributor to the formation of C_2H_4 as shown Fig. 4.13. An additional sensitivity analysis was performed to determine the major reactions that affect the C_2H_5O-2 concentration as shown in Fig. 4.14. The reaction rates were compared with those available in the literature,

and a discrepancy with the reaction $H_2O + C_2H_5O\text{-}2 = C_2H_5OH + OH$ was determined. The rates were modified by using the measured data of [34] as shown in Table 4.4. The final mechanism predicted the C_2H_4 concentration fairly well as shown in Fig. 4.11.

Table 4.4. Reaction coefficients for Mechanism-Gamma (C_2H_4 production improvement). A, b, and E_a are coefficients (constants) in the modified Arrhenius equation, $k = A\,T^b \exp(-E_a/RT)$. Units are moles, cm, sec, K and kcal/mole.

Reaction	A	b	E_a	Ref.
$H_2O+C_2H_5O\text{-}2 = C_2H_5OH+OH$	3.73E+3	2.78	-1.81	[34]

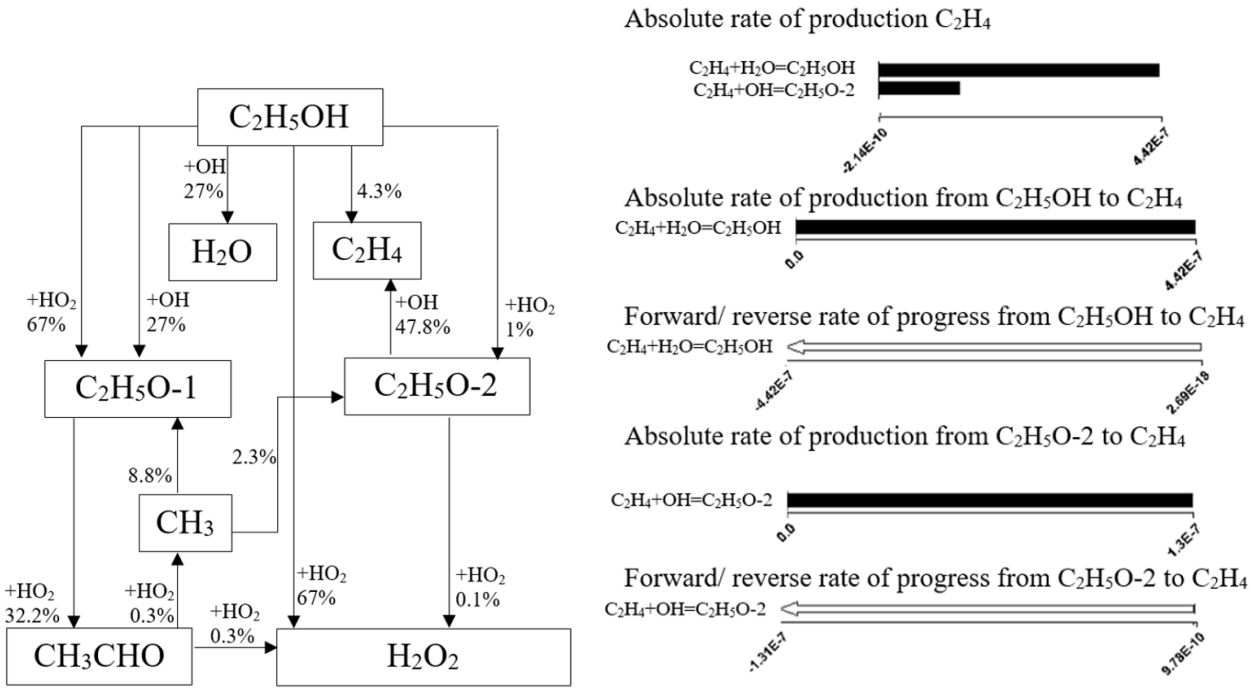

Fig. 4.13. Reaction pathways of C_2H_4 along with its rate of production and sensitivity analysis. The shown percentage near the arrows corresponds to the total depletion of the species through the specific reaction. The simulated data is shown at the timing of 40% of the ignition delay, where the modeled species' concentration starts to deviate from the measured data, as shown in Fig. 4.11.

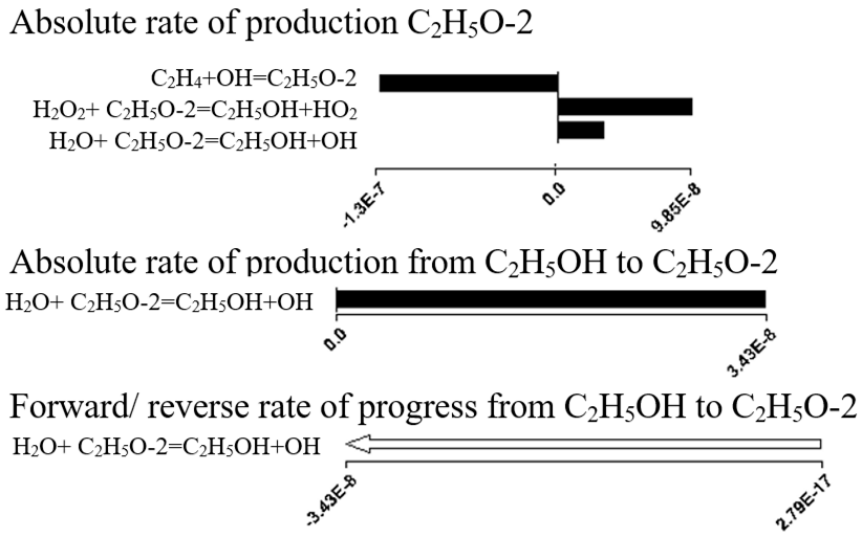

Fig. 4.14. Sensitivity analysis of C_2H_5O-2 along with its rate of production. The modeled data is shown at the timing of 40% of the ignition delay time, where the prediction of this species' concentration starts to deviate from the measured data, as shown in Fig. 4.11.

CH_4: The reaction pathways and major reactions associated with methane production are shown in Fig. 4.15. By updating the $CH_4 + C_2H_5O\text{-}2 = C_2H_5OH + CH_3$ reaction rate with those from [68], the model prediction was improved significantly as shown in Fig. 4.11. The modified reaction rates are shown in Table 4.5.

Table 4.5. Reaction coefficients of Mechanism-Gamma (CH_4 production improvement). A, b, and E_a are coefficients (constants) in the modified Arrhenius equation, $k = A\,T^b \exp(-E_a/RT)$. Units are moles, cm, sec, K and kcal/mole.

Reaction	A	b	E_a	Ref.
$CH_4 + C_2H_5O\text{-}2 = C_2H_5OH + CH_3$	19.93	3.37	7.63	[68]

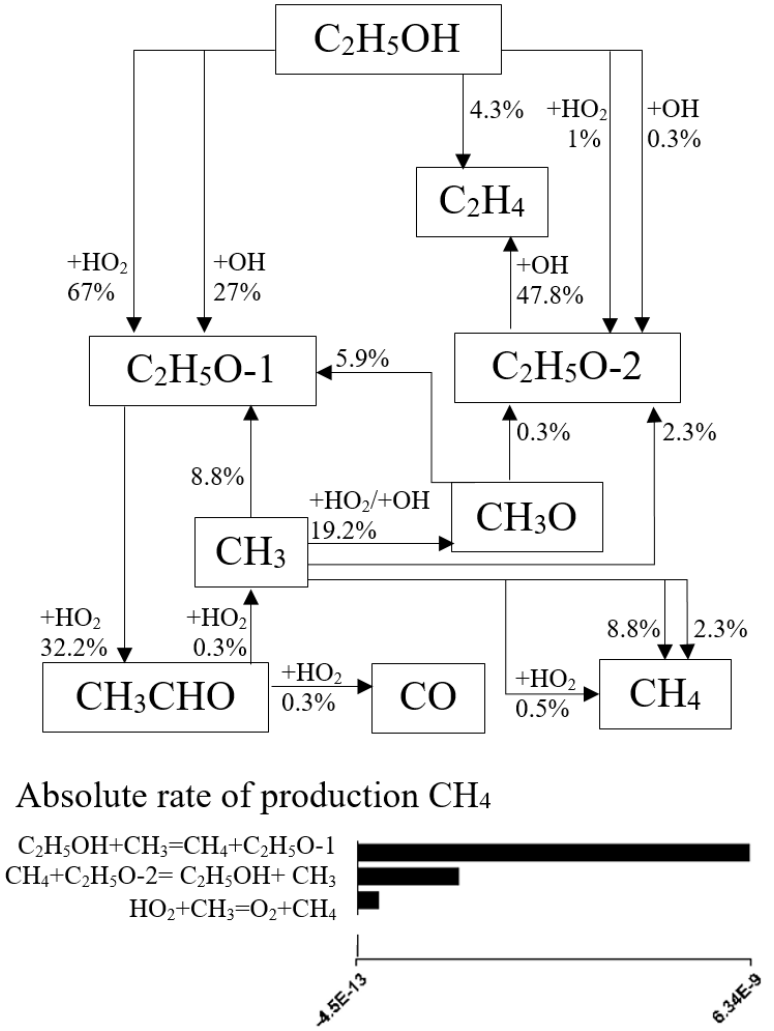

Fig. 4.15. Reaction pathways of CH_4 along with its sensitivity analysis. The shown percentage near the arrows corresponds to the total depletion of the species through the specific reaction. The modeled data is shown at the timing of 40% of the ignition delay time, where the modeled species' concentration is negligible despite available measured data, as shown in Fig. 4.11.

C_2H_6: Fig. 4.16 shows the reaction pathways and the major reaction associated with C_2H_6. The major reaction rate, as reported in Fig. 4.16, was compared with the available measured data with no observed deviation. The concentration of CH_3 as the major species for C_2H_6 production was then analyzed. The analysis showed an error in the reaction rates of $CH_3 + HO_2 = CH_3O + OH$ resulting in excess consumption of CH_3 as shown in Fig. 4.17. The reaction coefficients were

modified using the measured data of [69], which improved the predicted C_2H_6 concentration as shown in Fig. 4.11. The updated reaction coefficients are shown in Table 4.6.

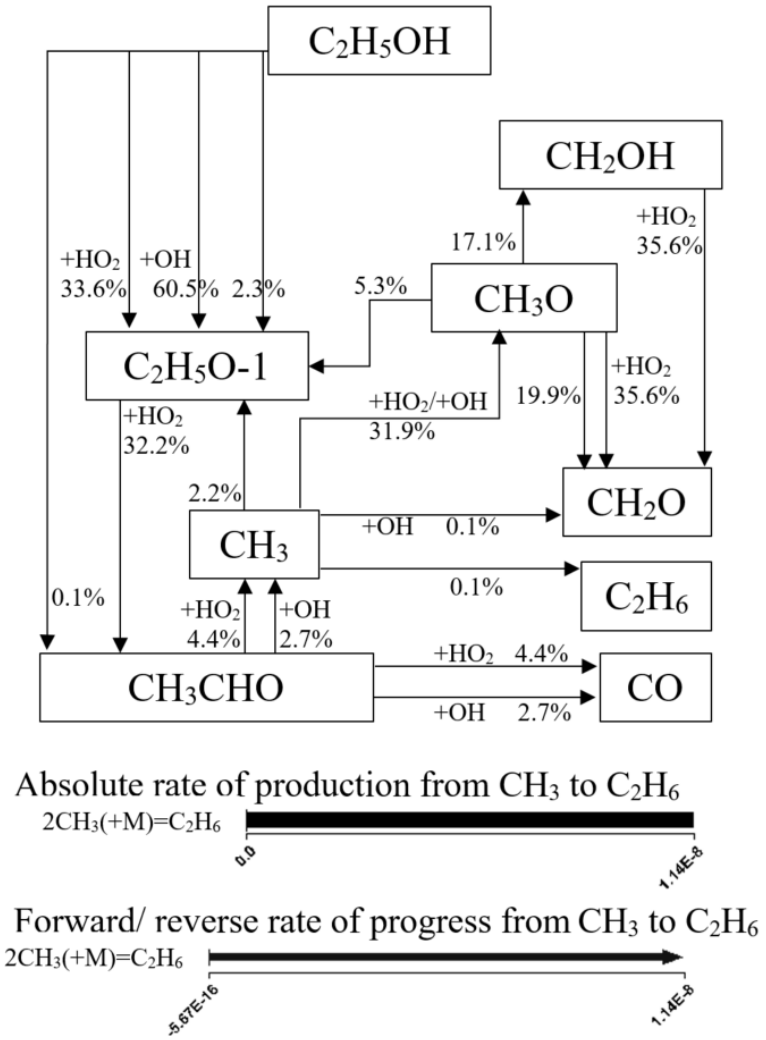

Fig. 4.16. Reaction pathways for C_2H_6 along with its rate of production. The shown percentage near the arrows corresponds to the total depletion of species through the specific reaction. The modeled data is shown at the timing of 75% of the ignition delay, where the modeled species' concentration is negligible despite available measured data, as shown in Fig. 4.11.

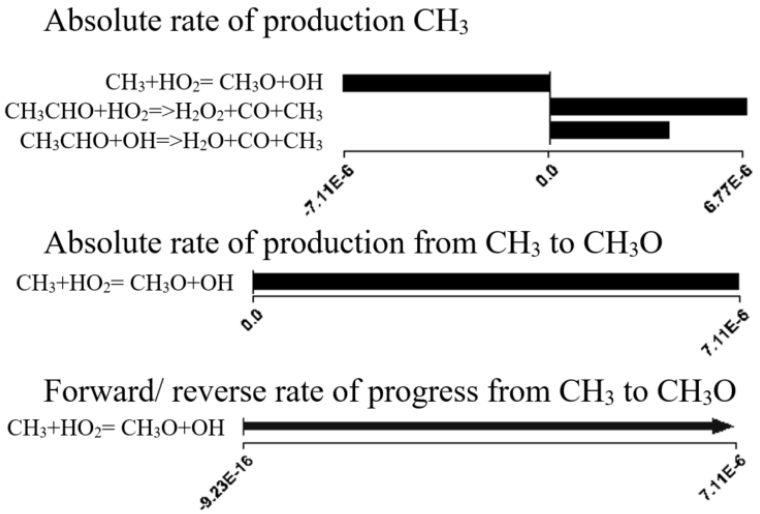

Fig. 4.17. Sensitivity analysis of CH_3 along with its rate of consumption. The modeled data is shown at the timing of 75% of the ignition delay, where the modeled species' concentration starts to deviate from the measured data, as shown in Fig. 4.11.

Table 4.6. Reaction coefficients of Mechanism-Gamma (C_2H_6 production improvement). A, b, and E_a are coefficients (constants) in the modified Arrhenius equation, $k = A\,T^b \exp(-E_a/RT)$. Units are moles, cm, sec, K and kcal/mole.

Reaction	A	b	E_a	Ref.
$CH_3+HO_2=CH_3O+OH$	1E+12	0.27	-0.69	[69]

After these modifications, a fair agreement was achieved between the various modeled and measured species concentrations as shown in Fig. 4.11. To expand the model's validation, the mechanism was again subjected to testing at different pressures, temperatures and equivalence ratios by using the measured data of the variable pressure flow reactor (VPFR) and shock tube. This analysis is described in the following sub-sections.

4.3.3. Intermediate Species Modeled and Measured by using Variable Pressure Flow Reactor

The modeled time-resolved species concentrations were compared with the flow reactor measured data of [29] at an equivalence ratio of 1.0, as shown in Fig. 4.18. Comparison between modeled and measured data at equivalence ratios of 0.6 and 1.2 were also performed and are

reported in Appendix C, Fig C.1 and Fig C.2. The carbon dioxide production using Mechanism-Beta was overpredicted significantly, which was corrected as discussed in section 4.3.1. Most of the intermediate species concentrations histories were predicted very well using the final mechanism.

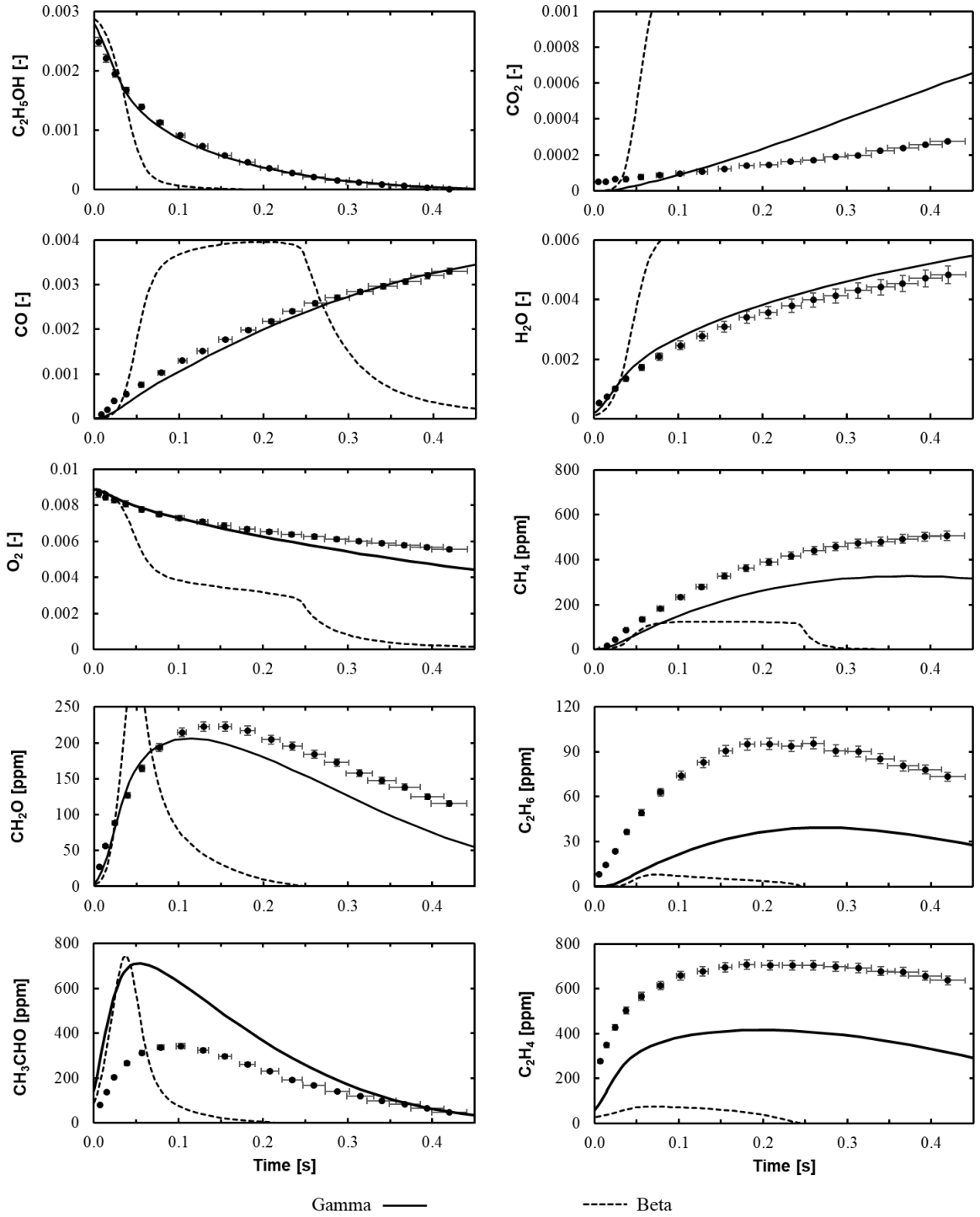

Fig. 4.18. Simulated and measured intermediate species of the ethanol/air mixture (N_2: 98.8%, C_2H_5OH: 0.3%, O_2: 0.9%) at gas pressure of 3 atm, gas temperature of 950 K, and equivalence ratio of 1.0. The mole fraction is shown by non-dimensional unit, [-], e.g., y-axis of O_2. Simulation results were shifted in time to the left by 45 ms to match the modeled and measured ethanol 50% conversion. The measured data is from [29].

4.3.4. Ignition Delay Modeled and Measured by using RCM and Shock Tube

By modifying the reaction rates in the previous steps, the ignition delay was slightly increased with respect to Mechanism-Beta. A temperature sensitivity analysis was performed to identify the most critical reactions to ethanol autoignition as shown in Fig. 4.19. Eight reactions were identified that have a significant effect on the gas temperature (or ignition delay). Of these reactions, the one that dominates the ignition delay is H_2O_2 + C_2H_5O-1 = C_2H_5OH + HO_2. The temperature sensitivity of this reaction is positive, indicating that an increase in the rate of the reaction leads to a higher gas temperature or shorter ignition delay. The reaction rates were updated using the measured data of [34] as shown in Table 4.7. The predicted ignition delay times produced by the final mechanism (Mechanism-Gamma) are in excellent agreement with the measured ignition delay data, as shown previously in Fig. 4.9.

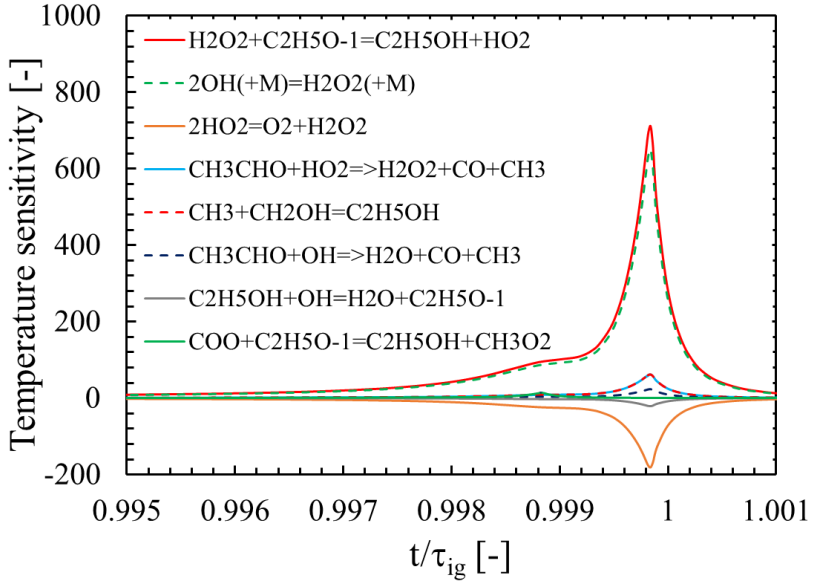

Fig. 4.19. Temperature sensitivity analysis of the Mechanism-Beta at compressed gas pressure of 15 bar, compressed gas temperature of 950 K, and equivalence ratio of 1 by using mixture 5 of Table 2.1. t/τ_{ig} = 0 corresponds to the end of compression, whereas t/τ_{ig} = 1 corresponds to the timing of ignition delay.

Table 4.7. Reaction coefficients of Mechanism-Gamma (Ignitin delay time prediction improvement). A, b, and E_a are coefficients (constants) in the modified Arrhenius equation, $k = A T^b \exp(-E_a/RT)$. Units are moles, cm, sec, K and kcal/mole.

Reaction	A	b	E_a	Ref.
$H_2O_2 + C_2H_5O\text{-}1 = C_2H_5OH + HO_2$	2.45E-5	5.26	7.48	[34]

To evaluate the kinetic model at higher gas temperatures, the final mechanism was tested against the measured shock tube ignition delay data of [14]. The measurements and simulations were performed at a wide range of gas temperatures (from 900 to 1500 K) at pressures of 13, 19, 40 and 75 bar. The mechanism predicts the ignition delays excellently, as shown in Fig. 4.20.

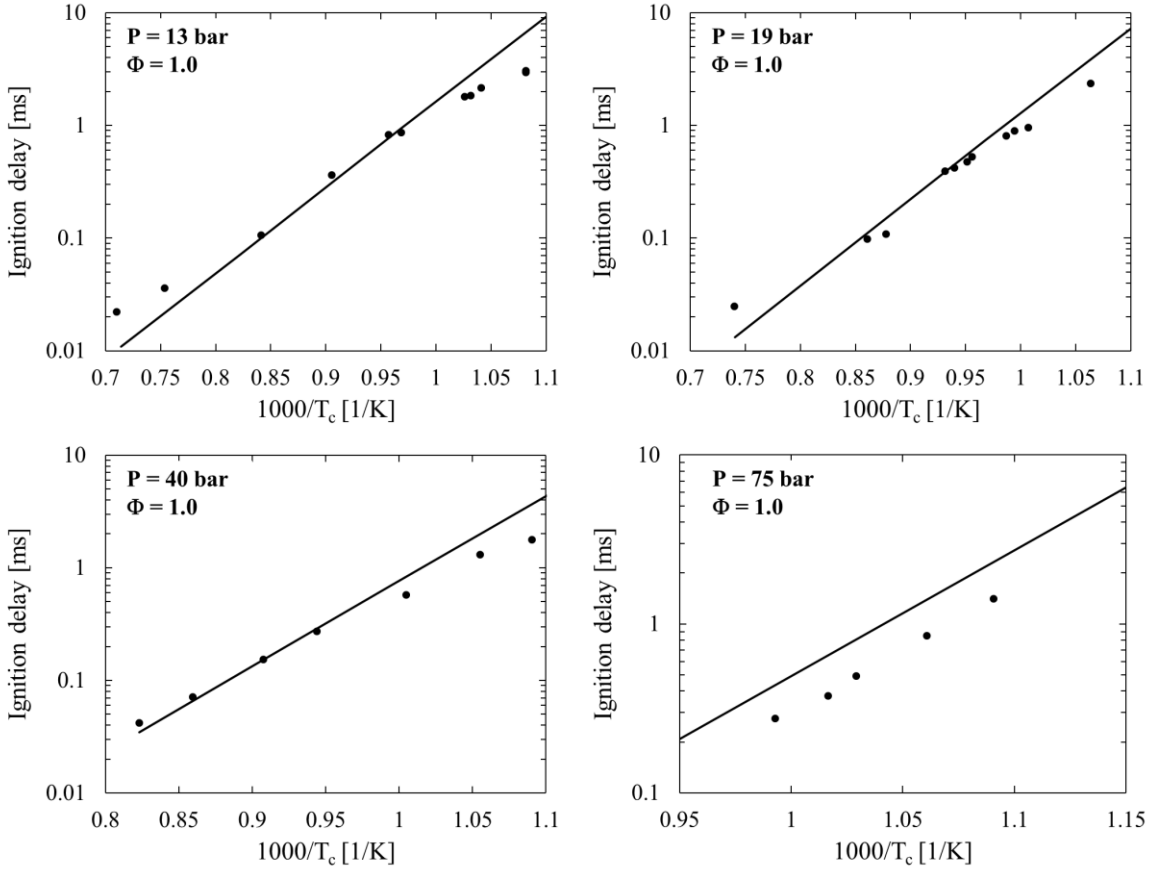

Fig. 4.20. Ignition delay of ethanol at varying pressures using an equivalence ratio of 1. The oxidizer and diluent mixture composition is N_2: 79.5% and O_2: 20.5%, vol/vol. The measured data are shown as dots, while the simulations of Mechanism-Gamma are shown as lines.

CHAPTER 5: CONCLUSIONS AND FUTURE WORK

5.1. Research Summary

The autoignition of ethanol was studied using numerical and experimental frameworks at wide ranges of pressures, temperatures and equivalence ratios. The ignition delays were measured using an optically accessible RCM and used for kinetic model validation. A high speed camera was used to observe the chemiluminescence during autoignition. The images showed that chemiluminescence intensity is dependent on the compressed gas temperature, pressure and equivalence ratio. In addition to the measured data, a detailed chemical kinetic model of ethanol was developed using the reaction mechanism generator. The model was evaluated, modified and validated using measured ignition delays at temperatures ranging from 850 to 1400 K, laminar flame speeds and time-resolved species concentrations. The final kinetic model includes 107 species and 1795 reactions. Overall, the kinetic model predicts the measured data very well at a wide range of combustion conditions.

5.2. Future Work

The final kinetic model (version 1.0) will be improved gradually to more accurately predict the species' concentrations. The uncertainty of the thermodynamic data was not investigated during this research but could be a reason for the poor agreement between a few modeled and measured species concentrations. The thermodynamic data should be more accurately measured and used in kinetic model development.

To participate in quantifying and identifying the facility influence on ignition delay measurements, part of this research was submitted to the RCM Workshop 2nd Characterization Initiative on ethanol fuel. Initial results showed the fidelity of the measured data in this work compared to other data from different facilities. This is an ongoing research project, and a final report will be published when the work is completed.

APPENDIX A

Table A.1. The test conditions are the same as shown in Fig. 4.1. Mixtures composition is shown in Table 2.1. Equivalence ratio is 0.5 and compressed gas pressure is approximately 15 bar.

Mixture	P_c (bar)	T_c (K)	P_{eff} (bar)	T_{ave} (K)	Ignition delay (ms)
1	15.30	998	14.69	984	3.86
1	15.30	998	14.67	983	3.84
1	15.50	1003	14.76	985	3.94
1	15.34	998	14.95	989	3.96
1	15.36	999	14.74	984	3.83
1	15.44	1001	14.93	989	4.01
1	15.48	1002	15.00	991	4.01
1	15.46	986	14.84	971	5.59
1	15.73	984	14.98	967	6.47
1	15.70	981	15.00	965	6.93
1	15.56	979	14.90	964	7.08
1	15.60	978	14.87	961	6.93
1	15.59	978	14.90	963	7.48
1	15.95	985	15.32	971	6.66
1	15.67	963	14.91	946	10.30
1	15.96	948	14.64	919	21.42
1	16.00	945	14.88	921	21.08
1	15.30	967	14.40	947	13.48
1	15.40	985	14.90	974	7.87
1	15.20	995	14.90	988	4.79
2	14.92	913	12.46	863	74.81
2	14.97	913	12.50	862	75.76
2	15.02	930	13.02	889	40.89
2	14.92	928	13.05	890	39.67
2	15.04	931	13.07	890	40.23
2	14.89	949	13.63	922	17.89
2	14.90	948	13.60	921	18.00
2	14.96	949	13.73	924	17.97
2	14.79	976	14.04	960	8.22
2	14.96	979	14.00	959	8.47
2	14.75	974	14.13	961	7.92
3	14.72	924	12.91	883	46.35
3	14.82	924	13.05	884	41.36
3	14.90	925	13.10	884	41.46
3	14.91	939	13.66	910	23.37
3	14.86	957	14.06	936	14.13
3	14.82	909	12.24	853	102.30
3	14.78	915	12.61	867	65.24

Table A.2. The test conditions are the same as shown in Fig. 4.1. Mixture composition is shown in Table 2.1. Equivalence ratio is 1.0 and compressed gas pressure is approximately 15 bar.

Mixture	P_c (bar)	T_c (K)	P_{eff} (bar)	T_{ave} (K)	Ignition delay (ms)
5	15.20	900	12.80	856	59.11
5	14.70	898	12.50	852	66.49
5	14.80	916	13.00	878	32.91
5	15.10	915	13.00	877	33.56
5	15.00	891	12.30	841	86.45
5	14.60	887	12.40	843	89.46
5	14.30	882	12.10	836	97.81
5	14.50	902	13.00	872	41.52
5	14.40	899	13.00	871	45.54
5	14.80	923	13.50	897	19.11
5	15.40	925	13.50	899	20.31
5	14.80	943	13.90	926	8.18
5	15.20	944	13.70	925	9.50
5	15.00	948	14.00	930	8.84
5	14.80	960	14.30	951	6.10
5	14.70	964	14.40	953	4.90
5	14.80	964	14.40	954	4.00
5	14.80	935	14.90	908	14.00
5	14.82	885	12.92	854	105.66
5	14.66	895	12.24	844	70.10
5	14.84	895	12.45	846	68.42
5	14.98	914	13.36	880	27.13
5	15.02	914	13.42	881	27.65

Table A.3. The test conditions are the same as shown in Fig. 4.1. Mixtures composition is shown in Table 2.1. Equivalence ratio is 2.0 and compressed gas pressure is approximately 15 bar.

Mixture	P_c (bar)	T_c (K)	P_{eff} (bar)	T_{ave} (K)	Ignition delay (ms)
7	15.17	867	12.90	825	68.55
7	15.28	869	13.11	840	60.87
7	15.24	869	13.05	829	60.69
7	15.09	879	13.51	850	31.34
7	15.05	879	13.48	851	31.66
7	15.29	883	13.60	852	31.37
7	15.13	899	14.03	878	15.50
7	15.03	896	13.87	875	17.04
7	15.02	923	14.46	913	5.88
7	15.06	922	14.50	912	6.42
7	15.56	901	14.67	903	10.70
7	15.03	918	14.26	921	6.78
7	14.94	919	14.45	930	5.51
7	14.95	930	14.54	940	3.66
7	14.89	929	14.46	938	4.04
7	15.21	865	12.93	840	58.16
7	14.88	872	13.04	855	37.34
7	14.94	876	13.10	857	35.14
8	14.96	851	12.25	802	108.12
8	14.80	858	12.55	817	75.55
8	14.91	858	12.55	812	82.17
8	14.82	855	12.38	811	88.06
8	14.93	856	12.40	819	91.23
8	14.73	866	12.86	832	49.06
8	14.80	868	12.86	832	51.50
8	14.90	868	12.83	831	52.97
8	14.73	881	13.47	858	24.61
8	14.88	882	13.53	858	25.57
8	14.84	881	13.46	856	25.46
8	14.88	898	14.11	884	13.05
8	14.95	899	14.14	885	13.70
8	15.01	900	14.10	884	13.31
8	14.94	917	14.43	908	6.49
8	14.82	914	14.33	905	6.41
8	14.95	916	14.33	905	6.78

Table A.4. The test conditions are the same as shown in Fig. 4.2. Mixture composition is shown in Table 2.1. Equivalence ratio is 1.0 and compressed gas pressure is approximately 20 bar.

Mixture	P_c (bar)	T_c (K)	P_{eff} (bar)	T_{ave} (K)	Ignition delay (ms)
10	19.30	840	15.40	783	145.40
10	19.70	844	16.00	790	172.23
10	19.70	840	15.70	782	184.72
10	19.50	853	16.10	804	106.11
10	19.40	865	16.50	822	75.52
10	19.50	865	16.80	825	70.52
10	19.60	867	16.50	822	78.75
10	19.50	863	16.30	816	97.36
10	19.24	869	16.69	832	58.01
10	19.31	870	16.75	833	62.66
10	19.40	870	16.70	834	60.48
10	19.00	883	16.80	850	34.64
10	18.74	882	16.61	850	35.66
10	19.70	908	18.20	886	14.33
10	19.80	907	18.10	882	14.42
10	19.90	908	18.20	883	13.95
10	19.90	922	18.60	903	8.94
10	19.60	918	18.30	898	8.73
10	19.90	922	18.30	899	9.34
10	19.70	933	18.80	920	5.50
10	19.60	933	18.70	919	5.32
10	19.70	937	18.60	920	4.93

Table A.5. The test conditions are the same as shown in Fig. 4.3. Mixtures composition is shown in Table 2.1. Equivalence ratio is 0.5 and compressed gas pressure is approximately 30 bar.

Mixture	P_c (bar)	T_c (K)	P_{eff} (bar)	T_{ave} (K)	Ignition delay (ms)
2	29.60	973	29.60	973	2.60
2	29.50	921	27.70	904	15.56
2	29.40	922	27.70	904	15.24
2	29.40	922	27.70	904	15.33
2	29.40	933	28.20	921	10.43
2	29.20	932	28.00	920	10.12
2	29.75	953	29.30	948	4.44
2	30.00	955	29.37	948	4.59
2	29.84	952	29.32	947	4.66
3	29.71	872	24.83	825	102.37
3	29.90	873	25.28	829	98.02
3	29.88	876	25.41	834	79.37
3	30.04	878	25.46	835	78.46
3	29.91	890	26.18	854	44.73
3	29.87	890	26.44	857	43.29
3	29.84	890	26.39	857	43.05
3	29.67	910	27.27	887	20.05
3	29.71	911	27.32	888	20.05
3	29.92	939	27.90	919	8.90
3	29.90	937	28.19	921	8.31
3	30.03	933	25.69	880	10.42
3	30.03	947	29.38	934	5.57
3	30.00	964	29.64	951	3.30
3	30.13	964	29.74	951	3.66
3	29.99	913	28.12	885	20.13
3	30.11	920	28.37	893	17.17
3	30.03	925	28.49	901	13.00

Table A.6. The test conditions are the same as shown in Fig. 4.3. Mixtures composition is shown in Table 2.1. Equivalence ratio is 1.0 and compressed gas pressure is approximately 30 bar.

Mixture	P_c (bar)	T_c (K)	P_{eff} (bar)	T_{ave} (K)	Ignition delay (ms)
4	30.50	911	30.20	908	9.49
4	28.50	912	27.20	898	11.21
4	28.00	927	27.30	919	6.49
4	27.90	935	27.40	929	4.47
4	28.40	951	28.00	947	2.90
5	29.80	874	27.00	846	40.93
5	28.80	876	26.00	848	43.70
5	28.50	893	26.60	874	20.23
5	28.40	905	27.00	890	12.94
5	28.33	905	26.85	889	13.51
5	28.20	917	27.20	907	8.30
5	29.70	874	26.60	845	45.99
5	29.60	875	26.50	845	45.36
5	29.80	877	26.60	846	43.77
5	29.60	890	27.20	867	23.73
5	29.20	887	27.10	867	24.31
5	29.20	888	27.20	869	23.85
5	29.50	903	27.70	887	14.99
5	29.50	904	27.70	887	14.88
5	29.30	903	27.80	890	14.57
5	28.90	916	27.70	905	9.66
5	27.80	915	26.60	903	10.02
5	30.55	900	28.19	878	15.95
5	29.08	902	26.85	879	16.14
5	30.00	925	28.79	909	6.72
6	29.81	856	25.02	814	86.24
6	29.82	856	25.21	816	80.18
6	30.01	860	25.48	818	74.35
6	29.89	860	25.52	819	70.37
6	29.87	863	25.92	827	53.53
6	30.03	864	25.86	826	55.56
6	30.06	865	26.03	828	54.79
6	29.90	876	26.80	847	31.10
6	29.76	875	26.78	848	31.26

Table A.7. The test conditions are the same as shown in Fig. 4.3. Mixtures composition is shown in Table 2.1. Equivalence ratio is 2.0 and compressed gas pressure is approximately 30 bar.

Mixture	P_c (bar)	T_c (K)	P_{eff} (bar)	T_{ave} (K)	Ignition delay (ms)
7	30.72	923	29.24	919	3.08
7	29.35	919	28.13	917	3.42
7	28.84	881	26.79	911	12.88
9	29.8	839	25.42	803	67.69
9	29.98	841	26.00	809	54.51
9	29.85	840	25.93	808	54.19
9	29.72	852	26.49	826	33.66
9	29.78	853	26.46	826	33.18
9	29.65	865	26.95	843	19.94
9	29.04	865	26.51	845	19.63
9	29.74	836	25.23	796	79.76
9	29.77	836	25.37	798	75.04
9	29.09	909	27.70	896	4.87
9	29.12	908	27.78	895	4.85
9	29.26	887	27.04	866	10.92
9	28.89	887	26.82	868	10.42

APPENDIX B

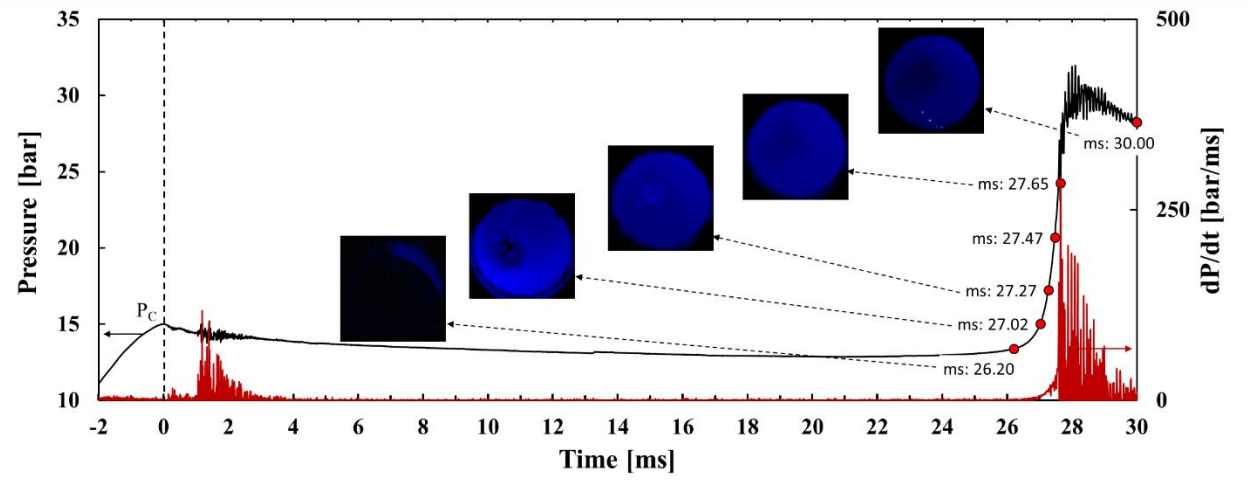

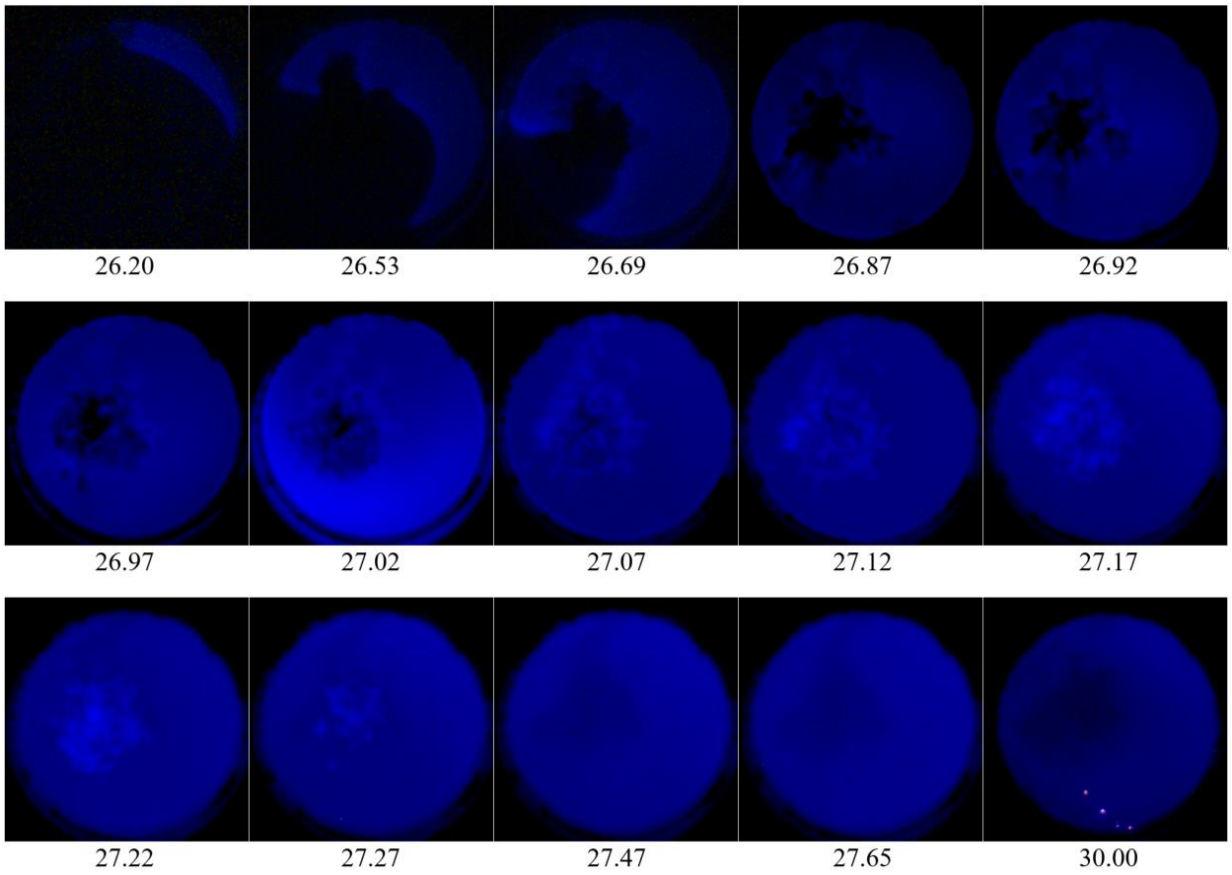

Fig. B.1. High speed images and pressure trace at compressed gas pressure of 15 bar, compressed gas temperature of 914 K, and equivalence ratio of 1. The ignition delay at this condition is 27.05 ms. The time after the end of compression is shown in milliseconds at the bottom of each image. An exposure time of 15.27 μs and camera recording speed of 57,000 fps were used.

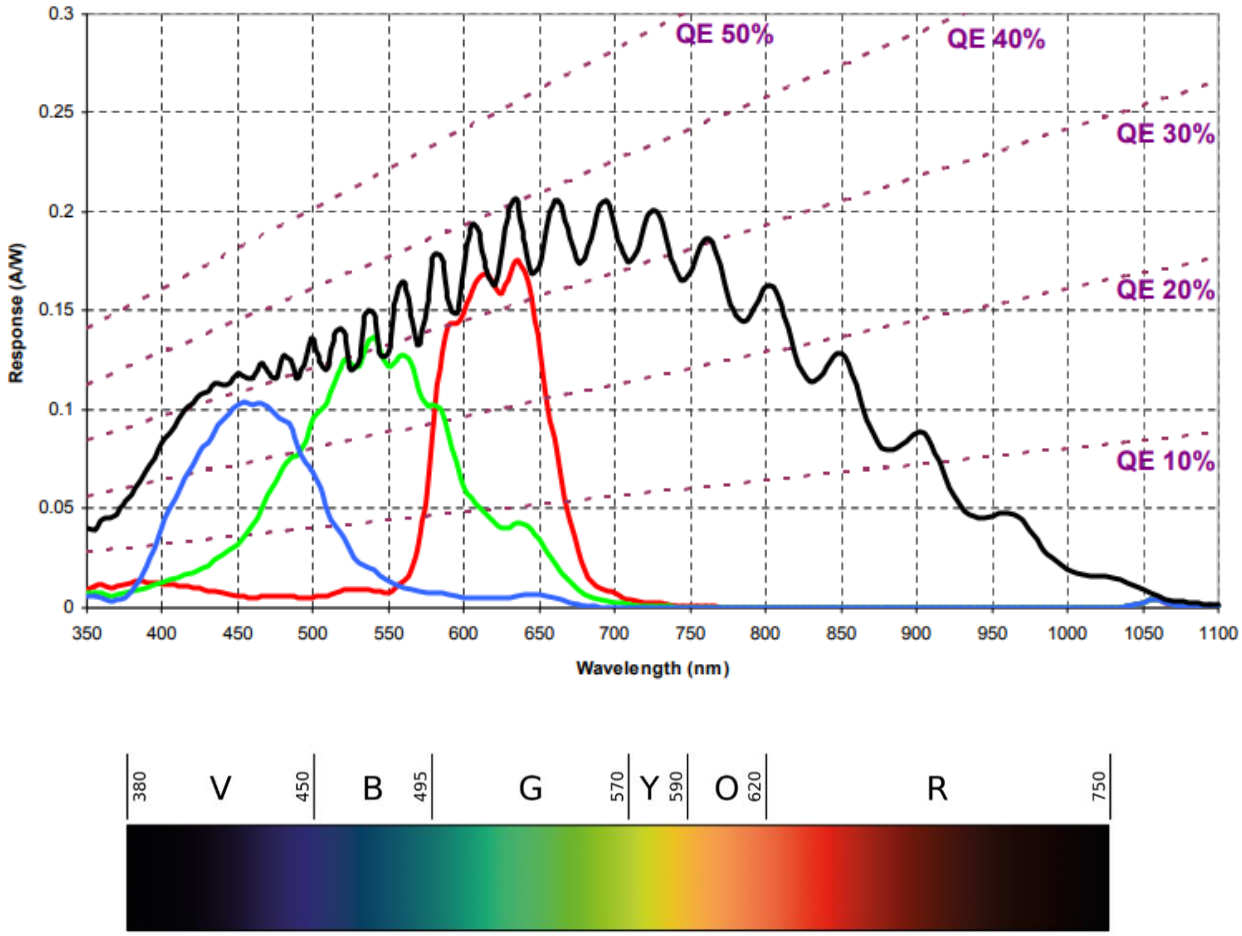

Fig. B.2. Color and spectral response curve of the high speed camera

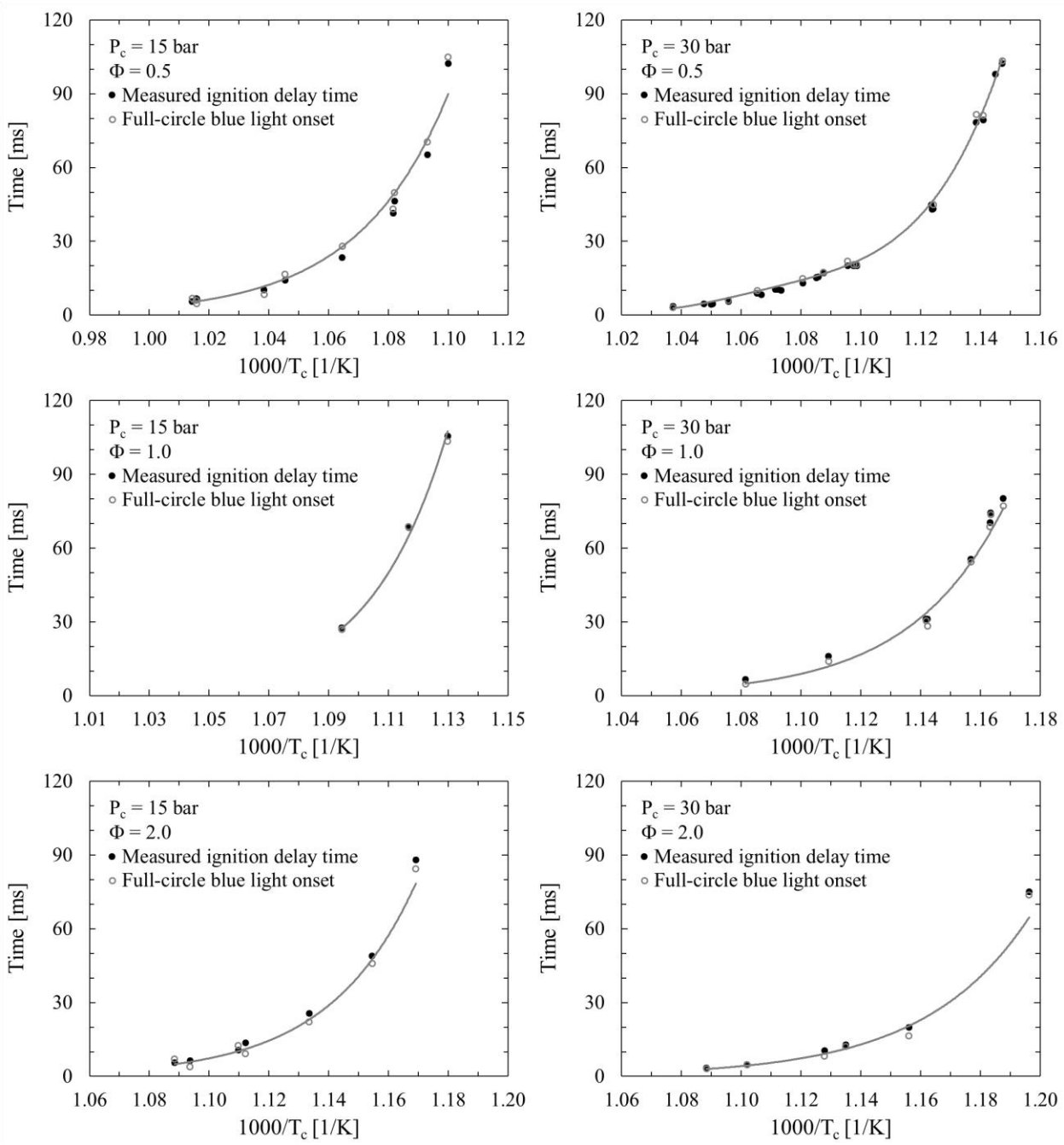

Fig. B.3. Measured ignition delay times (black circle) and the timing of measured onset of high intensity full-circle blue light (open gray circles). The lines are the trend-lines of the measured ignition delays. Data were measured at compressed gas pressures of 15 and 30 bar and equivalence ratios of 0.5, 1.0, and 2.0.

APPENDIX C

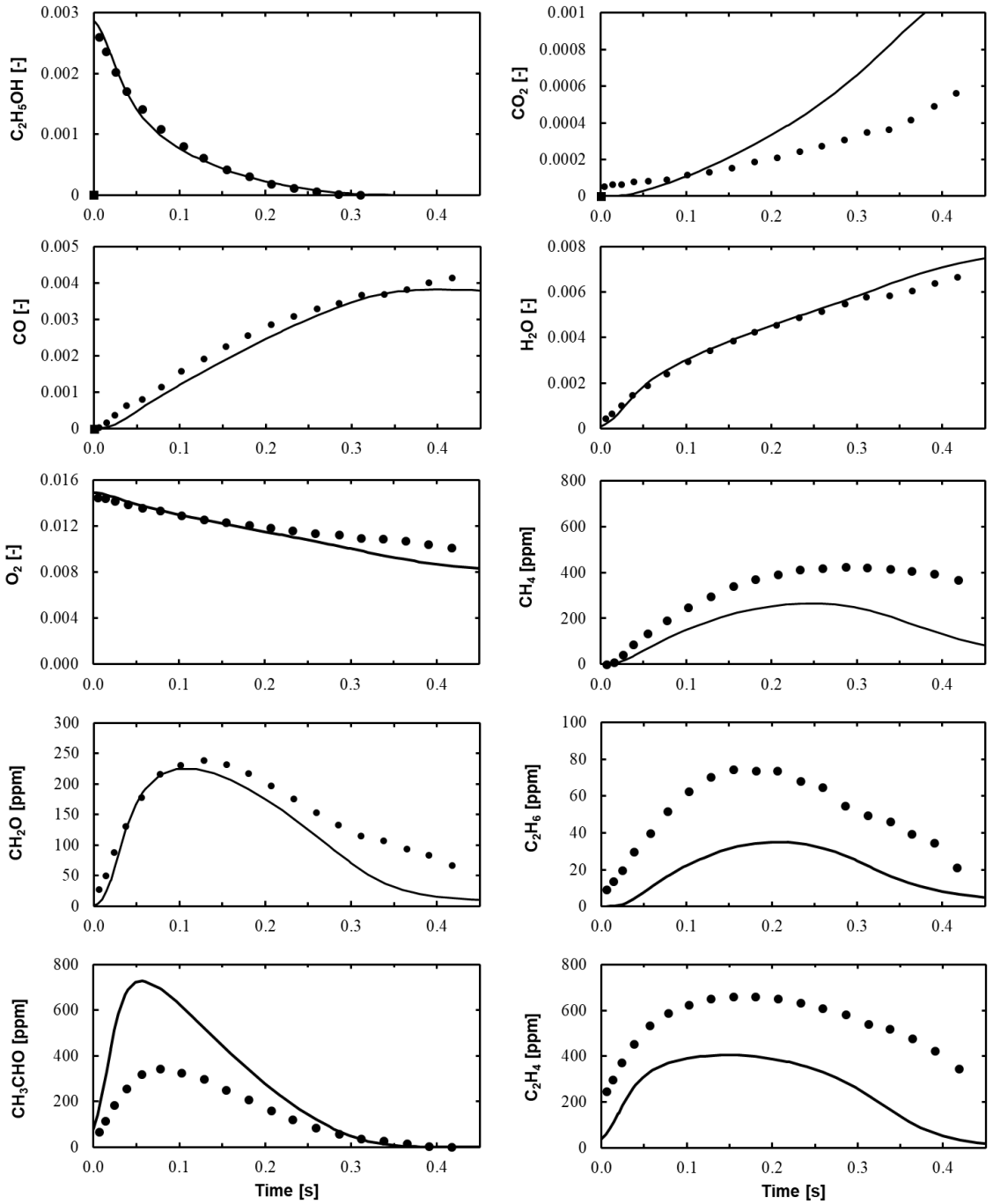

Fig. C.1. Simulated and measured intermediate species of mixture of ethanol/Air (N_2: 98.2%, C_2H_5OH: 0.3%, O_2: 1.5%) at gas pressure of 3 atm, gas temperature of 950 K, and equivalence ratio of 0.6. The mole fraction is shown by non-dimensional unit, [-], e.g., y-axis of O_2. Simulation results were shifted in time to the left by 40 ms to match the modeled and measured ethanol 50% conversion. The measured data is from [29].

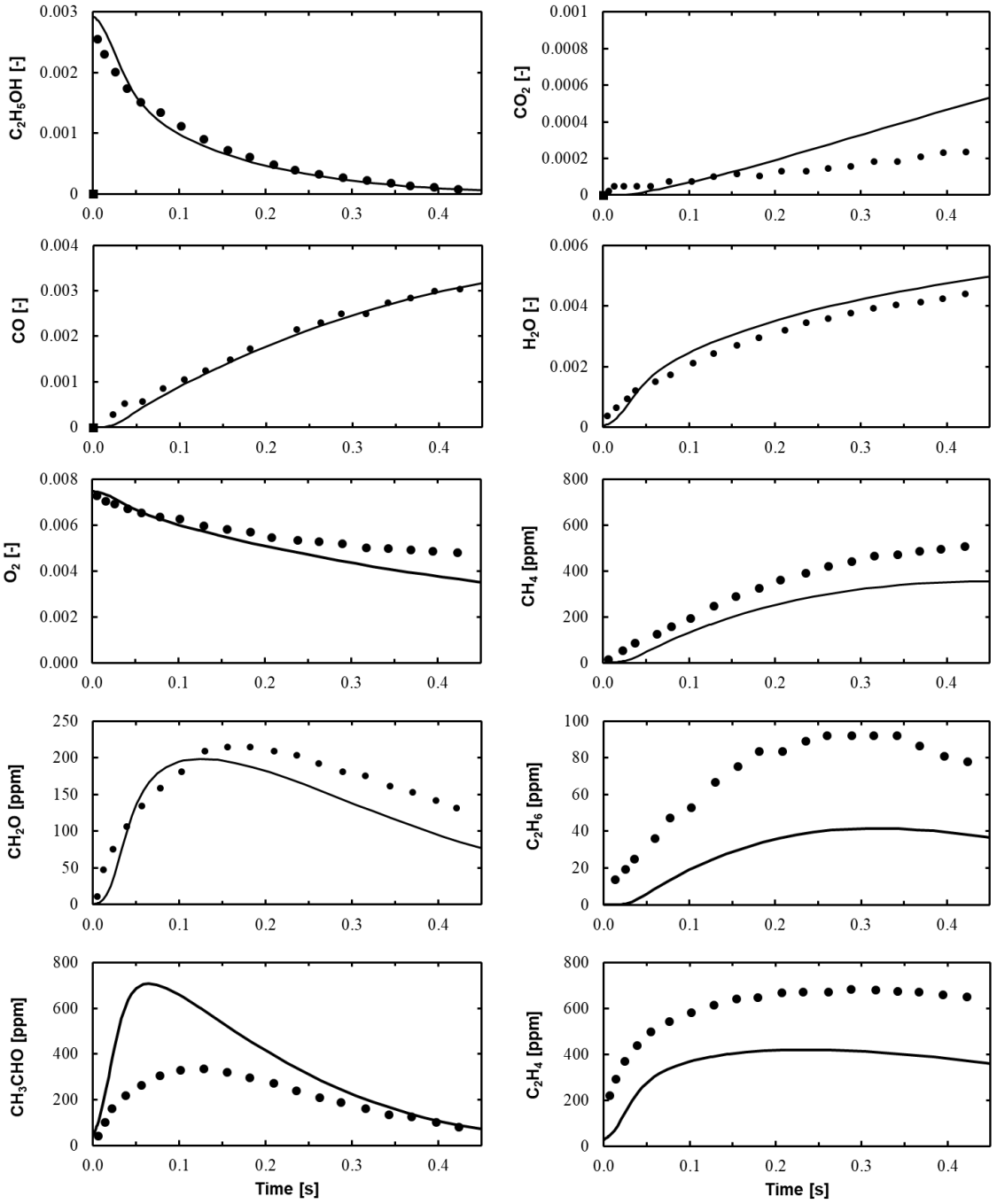

Fig. C.2. Simulated and measured intermediate species of mixture of ethanol/Air (N_2: 98.95%, C_2H_5OH: 0.3%, O_2: 0.75%) at P = 3 atm, T = 950 K and equivalence ratio of 1.2. The mole fraction is shown by non-dimensional unit, [-], e.g., y-axis of O_2. Simulation results were shifted in time to the left by 35 ms to match the modeled and measured ethanol 50% conversion. The measured data is from [29].

APPENDIX D

Python syntax. The input file (input.py) for ethanol mechanism generation in RMG. Explanations for each option in the syntax are commented by '#' throughout the syntax and do not participate in the modeling run.

```
# Data sources
database(
        # if thermo libraries are selected, it overrides the thermos calculations by RMG
        # In case of existing multiple libraries for the same species,
        # the first library in the order will define that species thermo data
    thermoLibraries = ['DFT_QCI_thermo', 'primaryThermoLibrary', 'thermo_DFT_CCSDTF12_BAC', 'USC-Mech-ii', 'Narayanaswamy', 'NISTThermoLibrary', 'KlippensteinH2O2', 'GRI-Mech3.0-N', 'GRI-Mech3.0', 'Fulvene_H', 'Chernov', 'CN', 'CHON', 'CHO', 'CHN', 'CH', 'CBS_QB3_1dHR', 'C3', 'C10H11', 'bio_oil'],
        # if reaction libraries are selected, it overrides the kinetics calculations by RMG
    reactionLibraries = [],
        # a seed mechanism can be used to include an entire sub-mechanism to the final model.
        # It is made of a list of species and reactions the user can provide in RMG.
        # then, RMG adds additional species and reactions to the model.
        # without seed mechanism the RMG generates more reaction paths but results in worse
        # results.
    seedMechanisms = ['GRI-Mech3.0'],
        # default is used usually.
    kineticsDepositories = 'default',
        # default uses the RMG families included in Table 3.1, otherwise it can be specified.
    kineticsFamilies = 'default',
        # This is the only option the RMG offers for calculating the reactions rates.
    kineticsEstimator = 'rate rules',)

# List of species
        # Input initial species in addition to the expected in the core engine.
        # It can be selected if the species is reactive or inert.
        # the structure for a certain species can be found in the RMG and listed here.
species(
    label = 'C2H5OH',
    reactive = True,
    structure = adjacencyList(
"""
1 C u0 p0 c0 {2,S} {4,S} {5,S} {6,S}
2 C u0 p0 c0 {1,S} {3,S} {7,S} {8,S}
3 O u0 p2 c0 {2,S} {9,S}
4 H u0 p0 c0 {1,S}
5 H u0 p0 c0 {1,S}
6 H u0 p0 c0 {1,S}
7 H u0 p0 c0 {2,S}
8 H u0 p0 c0 {2,S}
9 H u0 p0 c0 {3,S}
```

```
"""),
)

species(
    label = 'O2',
    reactive = True,
    structure = adjacencyList(
"""
1 O u1 p2 c0 {2,S}
2 O u1 p2 c0 {1,S}
"""),
)

species(
    label = 'N2',
    reactive = False,
    structure = adjacencyList(
"""
1 N u0 p1 c0 {2,T}
2 N u0 p1 c0 {1,T}
"""),
)

# Reaction Systems
        # only fixed conditions can be used in the RMG homogeneous batch reactors.
        # no transient temperature and pressure are available at this moment using the RMG.
        # for different conditions, multiple reactor can be added.
        # using the same used labels in the species above, the mole fraction can be specified.
        # the termination time for this modeled reactor is 2 s.
        # only one termination criterion can be specified.
simpleReactor(
    temperature = (850,'K'),
    pressure = (15,'bar'),
    initialMoleFractions={
        "C2H5OH": 0.025,
        "N2": 0.900,
        "O2": 0.075,
    },
    terminationTime = (2,'s'),
)
simpleReactor(
    temperature = (900,'K'),
    pressure = (15,'bar'),
    initialMoleFractions={
        "C2H5OH": 0.025,
        "N2": 0.900,
        "O2": 0.075,
    },
```

```
    terminationTime = (2,'s'),
)
simpleReactor(
    temperature = (950,'K'),
    pressure = (15,'bar'),
    initialMoleFractions={
        "C2H5OH": 0.025,
        "N2": 0.900,
        "O2": 0.075,
    },
    terminationTime = (2,'s'),
)
simpleReactor(
    temperature = (1000,'K'),
    pressure = (15,'bar'),
    initialMoleFractions={
        "C2H5OH": 0.025,
        "N2": 0.900,
        "O2": 0.075,
    },
    terminationTime = (2,'s'),
)
simpleReactor(
    temperature = (850,'K'),
    pressure = (30,'bar'),
    initialMoleFractions={
        "C2H5OH": 0.025,
        "N2": 0.900,
        "O2": 0.075,
    },
    terminationTime = (2,'s'),
)
simpleReactor(
    temperature = (900,'K'),
    pressure = (30,'bar'),
    initialMoleFractions={
        "C2H5OH": 0.025,
        "N2": 0.900,
        "O2": 0.075,
    },
    terminationTime = (2,'s'),
)
simpleReactor(
    temperature = (950,'K'),
    pressure = (30,'bar'),
    initialMoleFractions={
        "C2H5OH": 0.025,
        "N2": 0.900,
```

```
        "O2": 0.075,
    },
    terminationTime = (2,'s'),
)
simpleReactor(
    temperature = (1000,'K'),
    pressure = (30,'bar'),
    initialMoleFractions={
        "C2H5OH": 0.025,
        "N2": 0.900,
        "O2": 0.075,
    },
    terminationTime = (2,'s'),
)
simpleReactor(
    temperature = (900,'K'),
    pressure = (10,'bar'),
    initialMoleFractions={
        "C2H5OH": 0.06542056,
        "N2": 0.7383178,
        "O2": 0.1962617,
    },
    terminationTime = (2,'s'),
)
simpleReactor(
    temperature = (1000,'K'),
    pressure = (10,'bar'),
    initialMoleFractions={
        "C2H5OH": 0.06542056,
        "N2": 0.7383178,
        "O2": 0.1962617,
    },
    terminationTime = (2,'s'),
)
simpleReactor(
    temperature = (1100,'K'),
    pressure = (10,'bar'),
    initialMoleFractions={
        "C2H5OH": 0.06542056,
        "N2": 0.7383178,
        "O2": 0.1962617,
    },
    terminationTime = (2,'s'),
)
simpleReactor(
    temperature = (1200,'K'),
    pressure = (10,'bar'),
    initialMoleFractions={
```

```
        "C2H5OH": 0.06542056,
        "N2": 0.7383178,
        "O2": 0.1962617,
    },
    terminationTime = (2,'s'),
)
simpleReactor(
    temperature = (1400,'K'),
    pressure = (10,'bar'),
    initialMoleFractions={
        "C2H5OH": 0.06542056,
        "N2": 0.7383178,
        "O2": 0.1962617,
    },
    terminationTime = (2,'s'),
)

simpleReactor(
    temperature = (900,'K'),
    pressure = (40,'bar'),
    initialMoleFractions={
        "C2H5OH": 0.06542056,
        "N2": 0.7383178,
        "O2": 0.1962617,
    },
    terminationTime = (2,'s'),
)
simpleReactor(
    temperature = (1100,'K'),
    pressure = (40,'bar'),
    initialMoleFractions={
        "C2H5OH": 0.06542056,
        "N2": 0.7383178,
        "O2": 0.1962617,
    },
    terminationTime = (2,'s'),
)

simpleReactor(
    temperature = (1300,'K'),
    pressure = (40,'bar'),
    initialMoleFractions={
        "C2H5OH": 0.06542056,
        "N2": 0.7383178,
        "O2": 0.1962617,
    },
    terminationTime = (2,'s'),
)
```

```
simpleReactor(
    temperature = (850,'K'),
    pressure = (40,'bar'),
    initialMoleFractions={
        "C2H5OH": 0.06542056,
        "N2": 0.7383178,
        "O2": 0.1962617,
    },
    terminationTime = (2,'s'),
)

simpleReactor(
    temperature = (900,'K'),
    pressure = (5,'bar'),
    initialMoleFractions={
        "C2H5OH": 0.06542056,
        "N2": 0.7383178,
        "O2": 0.1962617,
    },
    terminationTime = (2,'s'),
)

simpleReactor(
    temperature = (1100,'K'),
    pressure = (5,'bar'),
    initialMoleFractions={
        "C2H5OH": 0.06542056,
        "N2": 0.7383178,
        "O2": 0.1962617,
    },
    terminationTime = (2,'s'),
)

simpleReactor(
    temperature = (1300,'K'),
    pressure = (5,'bar'),
    initialMoleFractions={
        "C2H5OH": 0.06542056,
        "N2": 0.7383178,
        "O2": 0.1962617,
    },
    terminationTime = (2,'s'),
)

simpleReactor(
    temperature = (850,'K'),
    pressure = (10,'bar'),
```

```
    initialMoleFractions={
        "C2H5OH": 0.0338295,
        "N2": 0.763194,
        "O2": 0.202977,
    },
    terminationTime = (2,'s'),
)

simpleReactor(
    temperature = (1000,'K'),
    pressure = (10,'bar'),
    initialMoleFractions={
        "C2H5OH": 0.0338295,
        "N2": 0.763194,
        "O2": 0.202977,
    },
    terminationTime = (2,'s'),
)

simpleReactor(
    temperature = (1200,'K'),
    pressure = (10,'bar'),
    initialMoleFractions={
        "C2H5OH": 0.0338295,
        "N2": 0.763194,
        "O2": 0.202977,
    },
    terminationTime = (2,'s'),
)

simpleReactor(
    temperature = (850,'K'),
    pressure = (10,'bar'),
    initialMoleFractions={
        "C2H5OH": 0.095057,
        "N2": 0.714829,
        "O2": 0.190114,
    },
    terminationTime = (2,'s'),
)

simpleReactor(
    temperature = (1000,'K'),
    pressure = (10,'bar'),
    initialMoleFractions={
        "C2H5OH": 0.095057,
        "N2": 0.714829,
        "O2": 0.190114,
```

```
    },
    terminationTime = (2,'s'),
)

simpleReactor(
    temperature = (1200,'K'),
    pressure = (10,'bar'),
    initialMoleFractions={
        "C2H5OH": 0.095057,
        "N2": 0.714829,
        "O2": 0.190114,
    },
    terminationTime = (2,'s'),
)

# Simulator tolerance
simulator(
        # optional absolute tolerance for the ODE solver, usually in the range of 1e15 – 1e-25.
    atol = 1e-16,
        # optional relative tolerance for the ODE solver, usually in the range of 1e4 – 1e-8.
    rtol = 1e-08,
        # default values for both relative and absolute sensitivities.
    sens_atol = 1e-06,
    sens_rtol = 0.0001,
)

# Model tolerance
model(
        # to control the satisfied flux of a species to be added to the core.
        # 0.1 is good enough for the current mechanism.
        # it could be a smaller number that produces a larger mechanism.
    toleranceMoveToCore = 0.1,
        # This feature work removes unnecessary species from the model to reduce memory.
    toleranceKeepInEdge = 0.0,
        # recommended to have the same value as the “toleranceMoveToCore”
    toleranceInterruptSimulation = 0.1,
        # determine the number of needed species in the edge.
    maximumEdgeSpecies = 100000,
    minCoreSizeForPrune = 50,
    minSpeciesExistIterationsForPrune = 2,
    filterReactions = False,
)

# Species constrains
        # this block put limits to the RMG output, e.g., the number of the maximum carbon atoms
        # needed in the model.
generatedSpeciesConstraints(
    allowSingletO2 = False,
```

```
    allowed = [],
    maximumCarbonAtoms = 4,
    maximumSiliconAtoms = 0,
    maximumSulfurAtoms = 0,
)

# Miscellaneous options
options(
    units = "si",
        # draw species pictures, but consume a lot of memory.
    generateOutputHTML = False,
        # unnecessary option for the process statistics.
    generatePlots = False,
        # save the species concentration in a file.
    saveSimulationProfiles = False,
        # save the species in the edge for further analysis.
    saveEdgeSpecies = False,
        # set time limit to terminate the job.
    keepIrreversible = None,
)
```

REFERENCES

[1] Samimi Abianeh, O., Chen, C. P., and Cerro, R. L. "Batch distillation: the forward and inverse problems." *Industrial and Engineering Chemistry Research* Vol. 51 No. 38 (2012): pp. 12435-12448.

[2] Samimi Abianeh, O., Chen, C-P, and Mahalingam, S. "Numerical modeling of multi-component fuel spray evaporation process." *International Journal of Heat and Mass Transfer* Vol. 69 (2014): pp. 44-53.

[3] Mehl, M., Chen, J-Y., Pitz, W. J., Sarathy, S. M., and Westbrook, C. K. "An approach for formulating surrogates for gasoline with application toward a reduced surrogate mechanism for CFD engine modeling." *Energy and Fuels* Vol. 25 No. 11 (2011): pp. 5215-5223.

[4] Samimi Abianeh, O., Oehlschlaeger, M. A., and Sung, C-J. "A surrogate mixture and kinetic mechanism for emulating the evaporation and autoignition characteristics of gasoline fuel." *Combustion and Flame* Vol. 162 No. 10 (2015): pp. 3773-3784.

[5] U.S. Department of Energy. “U.S. Production, Consumption, and Trade of Ethanol”. 30-3-2016. [Online]. Available:, https://afdc.energy.gov/data/10323.

[6] Heywood, J. B. "Internal combustion engine fundamentals." McGraw Hill, New York, NY, 1988.

[7] Lee, C., Vranckx, S., Heufer, K. A., Khomik, S. V., Uygun, Y., Olivier, H., and Fernandez, R. X. "On the chemical kinetics of ethanol oxidation: shock tube, rapid compression machine and detailed modeling study." *Zeitschrift für Physikalische Chemie* Vol. 226 No. 1 (2012): pp. 1-28.

[8] Mittal, G., Burke, S. M., Davies, V. A., Parajuli, B., Metcalfe, W. K., and Curran, H. J. "Autoignition of ethanol in a rapid compression machine." *Combustion and Flame* Vol. 161 No. 5 (2014): pp. 1164-1171.

[9] Barraza-Botet, C. L., Wagnon, S. W., and Wooldridge, M. S. "Combustion chemistry of ethanol: ignition and speciation studies in a rapid compression facility." *The Journal of Physical Chemistry A* Vol. 120 No. 38 (2016): pp. 7408-7418.

[10] Natarajan, K. and Bhaskaran, K. A. "High temperature combustion kinetics of ethanol. " *Thirteenth Intl. Symp. On Shock Waves* (1982): pp. 834-842.

[11] Dunphy, M. P. and Simmie, J. M. "High-temperature oxidation of ethanol. Part 1.-Ignition delays in shock waves." *Journal of the Chemical Society, Faraday Transactions* Vol. 87 No. 11 (1991): pp. 1691-1696.

[12] Cancino, L. R., Fikri, M., Oliveira, A. A., Schulz, C. "Measurement and chemical kinetics modeling of shock-induced ignition of ethanol− air mixtures." *Energy and Fuels* Vol. 24 No. 5 (2010): pp. 2830-2840.

[13] Heufer, K. A. and Olivier, H. "Determination of ignition delay times of different hydrocarbons in a new high pressure shock tube." *Shock Waves* Vol. 20 No. 4 (2010): pp. 307-316.

[14] Heufer, K. A., Uygun, Y., Olivier, H., Vranckx, S., Lee, C., Fernandes, R. X. "Experimental study of the high-pressure ignition of alcohol based biofuels." In *Proceeding of the European Combustion Meeting* 2011.

[15] Egolfopoulos, F. N., Du, D. X., and Law, C. K. "A study on ethanol oxidation kinetics in laminar premixed flames, flow reactors, and shock tubes." In *Symposium (international) on combustion* Vol. 24 No. 1 (1992): pp. 833-841.

[16] Veloo, P. S., Wang, Y. L., Egolfopoulos, F. N., and Westbrook, C. K. "A comparative experimental and computational study of methanol, ethanol, and n-butanol flames." *Combustion and Flame* Vol. 157 No. 10 (2010): pp. 1989-2004.

[17] Van Lipzig, J. P. J., Nilsson, E. J. K., De Goey, L. P. H., and Konnov, A. A. "Laminar burning velocities of n-heptane, iso-octane, ethanol and their binary and tertiary mixtures." *Fuel* Vol. 90 No. 8 (2011): pp. 2773-2781.

[18] Gülder, Ö. L. "Laminar burning velocities of methanol, ethanol and isooctane-air mixtures." In *Symposium (international) on combustion* Vol. 19 No. 1 (1982): pp. 275-281.

[19] Hara, T. and Tanoue, K. "Laminar flame speeds of ethanol, n-heptane, iso-octane air mixtures." Technical Report, International Federation of Automotive Engineering Societies (FISITA) 2006; F2006SC40.

[20] Liao, S. Y., Jiang, D. M., Huang, Z. H., Zeng, K., and Cheng, Q. "Determination of the laminar burning velocities for mixtures of ethanol and air at elevated temperatures." *Applied Thermal Engineering* Vol. 27 No.2-3 (2007): pp. 374-380.

[21] Beeckmann, J., Cai, L., and Pitsch, H. "Experimental investigation of the laminar burning velocities of methanol, ethanol, n-propanol, and n-butanol at high pressure." *Fuel* Vol. 117 (2014): pp. 340-350.

[22] Hinton, N., Stone, R., Cracknell, R., and Olm, C. "Aqueous ethanol laminar burning velocity measurements using constant volume bomb methods." *Fuel* Vol. 214 (2018): pp. 127-134.

[23] Mittal, G. and Sung, C-J. "Aerodynamics inside a rapid compression machine." *Combustion and flame* Vol. 145 No. 1-2 (2006): pp. 160-180.

[24] Petersen, E. L., Lamnaouer, M., De Vries, J., Curran, H., Simmie, J., Fikri, M., Schulz, C., and Bourque, G. "Discrepancies between shock tube and rapid compression machine ignition at low temperatures and high pressures." In *Shock Waves* (pp. 739-744). Springer, Berlin, Heidelberg, 2009.

[25] Dunphy, M. P., Patterson, P. M., and Simmie, J. M. "High-temperature oxidation of ethanol. Part 2.-Kinetic modelling." *Journal of the Chemical Society, Faraday Transactions* Vol. 87 No. 16 (1991): pp. 2549-2559.

[26] Westbrook, C. K. and Dryer, F. L. "Comprehensive mechanism for methanol oxidation." *Combustion Science and Technology* Vol. 20 No. 3-4 (1979): pp. 125-140.

[27] Marinov, N. M. "A detailed chemical kinetic model for high temperature ethanol oxidation." *International Journal of Chemical Kinetics* Vol. 31 No. 3 (1999): pp. 183-220.

[28] Saxena, P., and Williams, F. A. "Numerical and experimental studies of ethanol flames." *Proceedings of the Combustion Institute* Vol. 31 No. 1 (2007): pp. 1149-1156.

[29] Li, J., Kazakov, A., Chaos, M., and Dryer, F. L. "Chemical kinetics of ethanol oxidation." In *5th US combustion meeting* C26: pp. 25-28. University of California at San Diego, San Diego, CA, 2007.

[30] Li, J., Chaos, M., Kazakov, A., Dryer F. L., and Haas F. M. Personal communication: Ethanol Model v1.0, Princeton University, December 2009.

[31] Konnov, A. A. "Implementation of the NCN pathway of prompt-NO formation in the detailed reaction mechanism." *Combustion and Flame* Vol.156 No. 11 (2009): pp. 2093-2105.

[32] Metcalfe, W. K., Burke, S. M., Ahmed, S. S., and Curran, H. J. "A hierarchical and comparative kinetic modeling study of C1− C2 hydrocarbon and oxygenated fuels." *International Journal of Chemical Kinetics* Vol. 45 No. 10 (2013): pp. 638-675.

[33] Kéromnès, A., Metcalfe, W. K., Heufer, K. A., Donohoe, N., Das, A. K., Sung, C-J., Herzler, J., Naumann, C., Griebel, P., Mathieu, O., and Krejci, M. C. "An experimental and detailed chemical kinetic modeling study of hydrogen and syngas mixture oxidation at elevated pressures." *Combustion and Flame* Vol. 160 No. 6 (2013): pp. 995-1011.

[34] Li, Y., Zhou, C-W., Somers, K. P., Zhang, K., and Curran, H. J. "The oxidation of 2-butene: A high pressure ignition delay, kinetic modeling study and reactivity comparison with isobutene and 1-butene." *Proceedings of the Combustion Institute* Vol. 36 No. 1 (2017): pp. 403-411.

[35] Zhou, C-W., Li, Y., O'Connor, E., Somers, K. P., Thion, S., Keesee, C., Mathieu, O., Petersen, E. L., DeVerter, T. A., Oehlschlaeger, M. A., and Kukkadapu, G. "A comprehensive experimental and modeling study of isobutene oxidation." *Combustion and Flame* Vol. 167 (2016): pp. 353-379.

[36] Burke, S. M., Metcalfe, W., Herbinet, O., Battin-Leclerc, F., Haas, F. M., Santner, J., Dryer, F. L., and Curran, H. J. "An experimental and modeling study of propene oxidation. Part 1: Speciation measurements in jet-stirred and flow reactors." *Combustion and Flame* Vol. 161 No. 11 (2014): pp. 2765-2784.

[37] Burke, S. M., Burke, U., Mc Donagh, R., Mathieu, O., Osorio, I., Keesee, C., Morones, A., Petersen, E. L., Wang, W., DeVerter, T. A., and Oehlschlaeger, M. A. "An experimental and modeling study of propene oxidation. Part 2: Ignition delay time and flame speed measurements." *Combustion and Flame* Vol. 162 No. 2 (2015): pp. 296-314.

[38] Burke, U., Metcalfe, W. K., Burke, S. M., Heufer, K. A., Dagaut, P., and Curran, H. J. "A detailed chemical kinetic modeling, ignition delay time and jet-stirred reactor study of methanol oxidation." *Combustion and Flame* Vol. 165 (2016): pp. 125-136.

[39] Olm, C., Varga, T., Valkó, É., Hartl, S., Hasse, C., and Turányi, T. "Development of an ethanol combustion mechanism based on a hierarchical optimization approach." *International Journal of Chemical Kinetics* Vol. 48 No. 8 (2016): pp. 423-441.

[40] Allen, C. M. "Advanced rapid compression machine test methods and surrogate fuel modeling for bio-derived jet and diesel fuel autoignition." PhD dissertation. Michigan State University, Lansing, MI. 2012.

[41] Coleman, H. W. and Steele, W. G. "General uncertainty analysis: planning an experiment and application in validation." Experimentation, validation, and uncertainty analysis for engineers. John Wiley & Sons. 2009.

[42] Samimi-Abianeh, O., Piehl J. A., Zyada, A., Al-Sadoon, M., and Bravo, L. "Effect of Argon and Helium on Autoignition Process by Using Rapid Compression Machine." Under-review, (2019).

[43] Tanaka, S., Ayala, F., and Keck, J. C. "A reduced chemical kinetic model for HCCI combustion of primary reference fuels in a rapid compression machine." *Combustion and flame* Vol. 133 No. 4 (2003): pp. 467-481.

[44] Mittal, G. and Sung, C-J. "Autoignition of toluene and benzene at elevated pressures in a rapid compression machine." *Combustion and Flame* Vol. 150 No. 4 (2007): pp. 355-368.

[45] Goyal, T., Trivedi, D., and Samimi-Abianeh, O. "Autoignition and flame spectroscopy of propane mixture in a rapid compression machine." *Fuel* Vol. 233 (2018): pp. 56-67.

[46] He, X., Donovan, M. T., Zigler, B. T., Palmer, T. R., Walton, S. M., Wooldridge, M. S., and Atreya, A. "An experimental and modeling study of iso-octane ignition delay times under homogeneous charge compression ignition conditions." *Combustion and Flame* Vol. 142 No. 3 (2005): pp. 266-275.

[47] Zyada, A. and Samimi-Abianeh, O. "Ethanol Kinetic Model Development and Validation at Wide Range of Mixture Temperature, Pressure and Equivalence Ratio." Under-review, (2019).

[48] Desgroux, P., Gasnot, L., and Sochet L. R. "Instantaneous temperature measurement in a rapid-compression machine using laser Rayleigh scattering." *Applied Physics B* Vol.61, No. 1 (1995): pp. 69-72.

[49] CHEMKIN-PRO 15131, Reaction Design: San Diego, 2013.

[50] Song, J. "Building robust chemical reaction mechanisms: next generation of automatic model construction software." PhD dissertation. Massachusetts Institute of Technology, Cambridge, MA. 2004.

[51] Harper, M. R., Van Geem, K. M., Pyl, St. P., Marin, G. B., and Green, W. H. "Comprehensive reaction mechanism for n-butanol pyrolysis and combustion." *Combustion and Flame* Vol. 158 No. 1 (2011): pp. 16-41.

[52] Magoon, G. R., Aguilera-Iparraguirre, J., Green, W. H., Lutz, J. J., Piecuch, P., Wong, H-W., and Oluwole, O. O. "Detailed chemical kinetic modeling of JP-10 (exo-tetrahydrodicyclopentadiene) high-temperature oxidation: Exploring the role of biradical species in initial decomposition steps." *International Journal of Chemical Kinetics* Vol. 44 No. 3 (2012): pp.179-193.

[53] Gao, C. W., Allen, J. W., Green, W. H., and West, R. H. "Reaction Mechanism Generator: Automatic construction of chemical kinetic mechanisms." *Computer Physics Communications* Vol. 203 (2016): pp. 212-225.

[54] Westbrook, C. K., Pitz, W. J., Curran, H. C., Boercker, J., and Kunrath, E. "Chemical kinetic modeling study of shock tube ignition of heptane isomers." *International Journal of Chemical Kinetics* Vol. 33 No. 12 (2001): pp. 868-877.

[55] Sarathy, S. M., Westbrook, C. K., Mehl, M., Pitz, W. J., Togbe, C., Dagaut, P., Wang, H., Oehlschlaeger, M.A., Niemann, U., Seshadri, K., Veloo, P.S., Ji, C., Egolfopoulos, F.N., and

Lu, T. "Comprehensive chemical kinetic modeling of the oxidation of 2-methylalkanes from C 7 to C 20." *Combustion and flame* Vol.158 No. 12 (2011): pp. 2338-2357.

[56] Benson, S. W. and Buss, J. H. "Additivity rules for the estimation of molecular properties. Thermodynamic properties." *The Journal of Chemical Physics* Vol. 29 No. 3 (1958): pp. 546-572.

[57] Magoon, G. R. and Green, W. H. "Design and implementation of a next-generation software interface for on-the-fly quantum and force field calculations in automated reaction mechanism generation." *Computers and Chemical Engineering* Vol. 52 (2013): pp. 35-45.

[58] Susnow, R. G., Dean, A. M., Green, W. H., Peczak, P., and Broadbelt, L. J. "Rate-based construction of kinetic models for complex systems." *The Journal of Physical Chemistry A* Vol. 101 No. 20 (1997): pp. 3731-3740.

[59] Smith, G. P., Golden, D. M., Frenklach, M., Moriarty, N. W., Eiteneer, B., Goldenberg, M., Bowman, C. T., Hanson, R. K., Song, S., Gardiner Jr., William C., Lissianski, V. V., and Qin, Z. "GRI-Mech3.0", [Online]. Available: http://www.me.berkeley.edu/gri_mech/.

[60] Slack, M., Grillo, A. "High temperature rate coefficient measurement of CO+O chemiluminescence." *Combustion and Flame* Vol. 59 (1985): pp. 189-196.

[61] Guiberti, T. F., Durox, D., and Schuller, T. "Flame chemiluminescence from CO2-and N2-diluted laminar CH4/air premixed flames." *Combustion and Flame* Vol. 181 (2017): pp. 110-122.

[62] Sivaramakrishnan, R., Su, M-C., Michael, J. V., Klippenstein, S. J., Harding, L. B., and Ruscic, B. "Rate constants for the thermal decomposition of ethanol and its bimolecular reactions with OH and D: reflected shock tube and theoretical studies." *The Journal of Physical Chemistry A* Vol. 114 No. 35 (2010): pp. 9425-9439.

[63] Baulch, D. L., Cobos, C., Cox, R. A., Esser, C., Frank, P., Just, T., Kerr, J. A., Pilling, M. J., Troe, J., Walker, R. W., and Warnatz, J. "Evaluated kinetic data for combustion modelling." *Journal of Physical and Chemical Reference Data* Vol. 21 No. 3 (1992): pp. 411-734.

[64] Harding, L. B. and Klippenstein, S. J. "Roaming radical pathways for the decomposition of acetaldehyde." *The Journal of Physical Chemistry A* Vol. 114 No. 2 (2010): pp. 765-777.

[65] Li, J. PhD dissertation, Princeton University, Princeton, NJ, 2004.

[66] Gupte, K. S., Kiefer, J. H., Tranter, R. S., Klippenstein, S. J., and Harding, L. B. "Decomposition of acetaldehyde: Experiment and detailed theory." *Proceedings of the Combustion Institute* Vol. 31 No. 12 (2007): pp. 167-174.

[67] Taylor, Philip H., Rahman, M. Sm, Arif, M., Dellinger, B., and Marshall, P. "Kinetic and mechanistic studies of the reaction of hydroxyl radicals with acetaldehyde over an extended temperature range." In *Symposium (International) on Combustion* Vol. 26 No. 1 (1996): pp. 497-504.

[68] Xu, Z. F., Park, J., Lin, M. C. "Thermal decomposition of ethanol. III. A computational study of the kinetics and mechanism for the CH_3+ C_2H_5OH reaction." *The Journal of chemical physics* Vol. 120 No. 14 (2004): pp. 6593-6599.

[69] Jasper, A. W., Klippenstein, S. J., and Harding, L. B. "Theoretical rate coefficients for the reaction of methyl radical with hydroperoxyl radical and for methylhydroperoxide decomposition." *Proceedings of the Combustion Institute* Vol. 32 No. 1 (2009): pp. 279-286.

ABSTRACT

ETHANOL AUTOIGNITION MODELING AND VALIDATION AT WIDE RANGES OF MIXTURE TEMPERATURES, PRESSURES, AND EQUIVALENCE RATIOS

by

ANTOWAN ZYADA

May 2019

Advisor: Dr. Omid Samimi-Abianeh

Major: Mechanical Engineering

Degree: Doctor of Philosophy

A new ethanol detailed kinetic model with 107 species and 1795 reactions was developed by using the reaction mechanism generator (RMG) and a thorough reaction path analysis. The mechanism model was extensively evaluated against measured ignition delay times, laminar flame speeds, and time-resolved species concentrations. The ignition delay experiments were conducted at pressures of 15, 20, and 30 bar, a temperature range of 850 to 1000 K, and equivalence ratios of 0.5, 1.0 and 2.0 using an optically accessible rapid compression machine (RCM). The effect of oxygen concentration on the ignition delay at a fixed equivalence ratio was also measured and studied using the new kinetic model. High speed camera was used to investigate the autoignition process and chemiluminescence emission at low to intermediate temperatures. Different combustion behaviors with respect to the chemiluminescence color and intensity were identified during the autoignition of ethanol mixture. The new combustion kinetic model predicts the measured data from this research and those available in the literature very well.

AUTOBIOGRAPHICAL STATEMENT

Antowan Zyada received his Bachelor of Science in Mechanical Engineering and Master of Science in Automotive Engineering from Damascus University, Syria. He joined the Mechanical Engineering Department of Wayne State University to purse a Ph.D with a focus on the combustion process and modeling. He will be working as an engine development scientist on a mixed-mode homogenous charge compression ignition engine in Hyundai America Technical Center (HATCI).